

https://dspace.org/

Improvement of the V-1 characteristic of zinc oxide (ZnO) based metal oxide varistors (MOVs) using Silicon Telluride (SiTe2) and Lanthanum Hexaboride (LaB6) materials

Hove, Miidzo

2009-06-29T08:12:43Z
http://hdl.handle.net/10539/7047

Downloaded from a DSpace repository. https://dspace.org/

IMPROVEMENT OF THE V-I CHARACTERISTIC OF ZINC OXIDE (ZnO) BASED METAL OXIDE VARISTORS (MOVs) USING SILICON TELLURIDE ($SiTe_2$) AND LANTHANUM HEXABORIDE (LaB_6) MATERIALS

Miidzo Hove

A thesis submitted to the Faculty of Engineering and the Built Environment, University of Witwatersrand, Johannesburg, in fulfilment of the requirements for the degree of Doctor of Philosophy in Engineering

Johannesburg, 2006

DECLARATION

I declare that this thesis is my own, unaided work. It is being submitted for the Degree of Doctor of Philosophy in the University of Witwatersrand, Johannesburg. It has not been submitted before for any degree or examination in any other University.

(Signature of candidate)

day of (year)

ABSTRACT

A study to improve the V-I characteristic of the ZnO-based commercial MOV using a characterised chalcogenide material, Silicon Telluride ($SiTe_2$), and a field-emissive material, Lanthanum Hexaboride (LaB_6), has been conducted. The need arises in that the current commercial ZnO-based metal oxide varistors (MOVs) have a V-I characteristic that departs substantially from that of the ideal one. As a result of this shortcoming, they do not offer ideal clamping action, and the consequence of this is that the protection they are supposed to offer is compromised. The problem behind this shortcoming is the microstructure, which is not ideal. An ideal microstructure to constitute an ideal device is not known yet, hence the problem.

Based on a model, a prototype MOV was fabricated using conventional sintering techniques. The phases and microstructure of this prototype MOV were studied using XRD and SEM with EDS facility. The V-I characteristic was studied using the two point probe method, and the clamping action was studied using an impulse generator.

A prototype MOV with a near ideal V-I characteristic, with improvements in the leakage, active (breakdown) and up-turn regions was developed. In the leakage region, leakage currents were reduced by 1.0 %. In the active region, the rate of breakdown was increased and discharge currents were increased by on average 4 times those of a dimensionally comparable commercial MOV. The instability responsible for the breakdown was found to be field dependent. The up-turn region was removed. The corresponding surge clamping action of the prototype MOV was identical to that that of the studied commercial MOV, but with lower surge current. The improvements are attributed to the usage of characterised powders and new additives, as well as the process method, in the development of the prototype MOV.

One other related major finding is that the pyrochlore phase, $Bi_2Zn(Zn_{4/3}\ Sb_{2/3})O_6$, and the spinel phase, $Zn(Zn_{4/3}\ Sb_{2/3})O_4$ are not the only phases that can give rise to the varistor property which gives rise to the non-linear V-I characteristic in a ZnO-based commercial MOV. This is contrary to current know-how.

A prototype ZnO-based MOV with near ideal V-I characteristic can be developed.

ACKNOWLEDGEMENTS

First and foremost, I would like to heartily thank my Supervisor, Professor I. R. Jandrell, for his guidance in carrying out this research. It is through his vision and expertise that I got to this academic platform. I cherish his words of wisdom

I am also indebted to the School of Electrical and Information Engineering, the academic and administrative staff who contributed directly and indirectly to the success of this research. The same goes to the academic and administrative staff of associate schools of the University for access to their laboratories and facilities as well as assistance rendered.

I would like to thank the University of Witwatersrand for affording me the opportunity of being part of its research community, and for financial support received from the University, through its Post Graduate Award, NRF and Eskom via the TESP programme. Without this support, the research would have been impossible.

Last but not least, to S and M, *" handina rekureva*".

CONTENTS Page

DECLARATION ii

ABSTRACT iii

ACKNOWLEDGEMENTS iv

CONTENTS v

LIST OF FIGURES ix

LIST OF TABLES xiii

LIST OF SYMBOLS xiv

LIST OF ACRONYMS xvi

1 INTRODUCTION 1

2 LITERARURE REVIEW 4

2.1 What is a MOV? 4

2.2 Manufacture and Microstructure of a ZnO- based Commercial MOV 8

2.2.1 Manufacture of a ZnO-based Commercial MOV 8

2.2.2 Microstructure and Phases of a ZnO-based Commercial MOV 9

2.3 The Relationship between the Microstructure and the V-I Characteristic of a ZnO-based Commercial MOV 12

2.4 Microstructure-Equivalent Circuit Relationship 13

2.4.1 Operation of the ZnO-based Commercial MOV 14

2.5 Conduction Mechanism in a ZnO-based Commercial MOV 16

2.6 The Ideal Surge Protective Device (SPD) 22

2.7 S-type and N-type Instabilities 26

2.8 Problems Pertaining to ZnO-based Commercial MOV 28

3 THE HYPOTHESIS AND MODEL 30

3.1 The Hypothesis 31

3.2 The Model 32

3.2.1 Theory of the Model 33

4 EXPERIMENTAL PROCEEDURES 37

4.1 Powder Characterisation 37

4.2 Fabrication of Prototype MOVs 41

4.3 Electrical Testing of Prototype MOV 42

4.3.1 Determination of the V-I Characteristic 44

4.3.2 Determination of Surge Voltage Clamping Action 46

4.4 Microstructure and Phase Analysis 48

5 RESULTS 50

5.1 The V-I Characteristic 51

5.2 Surge Clamping Action 53

5.3 Microstructure and Phases of Prototype MOV 59

5.3.1 Microstructure 59

5.3.2 Phases 65

6 DISCUSSION 67

6.1 The V – I Characteristic of the Prototype MOV 67

6.1.1 The Improvements and Benefits 69

6.1.2 Explaining the Improvements in the V-I Characteristic of the Prototype MOV 76

6.1.3 Charge Transport Mechanism in the Prototype MOV 77

6.2 The Surge Clamping Action of the Prototype MOV 83

6.3 Microstructure and Phase Analysis of the Prototype MOV 108

6.3.1 Microstructure Analysis 108

6.3.2 Phase Analysis 113

6.3.3 Microstructure-Electrical Properties Relationship 120

6.4 The Contribution 122

7 CONCLUSIONS AND RECOMMENDATIONS 124

Conclusion 124

Recommendations for Future Work 125

APPENDIX A CALCULATION OF THE AREA UNDER THE LEAKAGE REGION OF THE V-I CHARACTERSTIC 126

APPENDIX B THE "ELECTRODE EFFECT" 130

REFERENCES 134

LIST OF FIGURES

Figure		Page
2.1	The V-I characteristic of a current commercial ZnO-based MOV	4
2.2	Surge clamping action of a typical commercial ZnO-based MOV	6
2.3	Principle of overvoltage protection by a MOV	7
2.4	Commercial ZnO-based MOV blocks as sintered, and ready to use MOVs	9
2.5	Typical microstructure of a commercial ZnO-based MOV	10
2.6	Equivalent circuit of a ZnO-based commercial MOV	14
2.7	MOV equivalent circuit in the leakage, active and up-turn regions	15
2.8	Conduction mechanism in a ZnO-based commercial MOV	16
2.9	Energy band diagram for a ZnO-based commercial MOV	18
2.10	The V-I characteristic of an ideal MOV	23
2.11	The V-I characteristic of an approximate ideal MOV	23
2.12	Typical surge clamping action of a ZnO-based commercial MOV compared to an ideal MOV	24
2.13	The j-E characteristic for NNDC (*N*-type) instability	27
2.14	The j-E characteristic for SNDC (*S*-type) instability	27
2.15	The V-I characteristic of the ZnO-based commercial MOV compared to that of the ideal device	29
3.1	Model for the development of an ideal MOV	31
3.2	Model microstructure of a ZnO-based commercial MOV	32
3.3	Model microstructure of an ideal ZnO-based MOV	33
3.4	The equivalent circuit of a modelled prototype MOV with a near ideal V-I characteristic	35
3.5	The reduced equivalent circuit of a modelled prototype MOV with a near ideal V-I characteristic	36
4.1	Test rig for electrical tests	43
4.2	Circuit used to obtain V-I data for the V-I characteristic	44

4.3	Impulse generator arrangement in the combinational mode	47
4.4	Impulse generator equivalent circuit in the combinational mode	48
5.1	Typical prototype MOV block studied. Also shown is the prototype MOV	50
5.2	The V-I characteristic of the prototype MOV	52
5.3	(a) Surge response action of prototype MOV @ 0.5 kV	54
	(b) Surge response action of prototype MOV @ 0.8 kV	55
	(c) Surge response action of prototype MOV @ 1.0 kV	56
	(d) Surge response action of prototype MOV @ 1.25 kV	57
	(e) Surge response action of prototype MOV @ 1.5 kV	58
5.4	Microstructure of the prototype MOV	59
5.5	EDS spectrum of the prototype MOV showing the elements in the grey grains	60
5.6	EDS spectrum of the grain boundary material	61
5.7	Fracture surface of the prototype MOV showing two “rod-like” structures	62
5.8	One of the “rod-like” structures in figure 5.7 at a higher magnification.	62
5.9	Fracture surface of the prototype MOV showing a free “rod-like” structure possibly snapped	63
5.10	EDS spectrum of a typical “rod-like” structure	64
5.11	Fracture surface of the prototype MOV showing a “stub-like” structure.	64
5.12	Fracture surface of the prototype MOV showing a layered phase	65
5.13	XRD pattern of the prototype MOV	66
6.1	The V-I characteristic of prototype MOV compared to that of a commercial MOV, V275K20P.	68
6.2	The V-I characteristic of prototype MOV compared to that of V275K20P in the L.V. region	70
6.3	The V-I characteristic of specimen V275K20P-c compared to V275K20P	73
6.4	Energy band diagram for the prototype MOV modelled to be a	

S-I-M-I-S for zero bias (V = 0). 78

6.5 Energy band diagram for the prototype MOV modelled to be a S-I-M-I-S device with bias (V > 0) 79

6.6 (a) Comparative surge clamping action of the prototype MOV to the acclimatized V275K20P @ V_a = 0.5 kV 85

(b) Comparative surge clamping action of the prototype MOV to the acclimatized V275K20P @ V_a =0.8 kV 86

(c) Comparative surge clamping action of the prototype MOV to the acclimatized V275K20P @ V_a = 1.0 kV 87

(d) Comparative surge clamping action of the prototype MOV to the acclimatized V275K20P @ V_a = 1.25 kV 88

(e) Comparative surge clamping action of the prototype MOV to the acclimatized V275K20P @ V_a = 1.5 kV 89

6.7 (a) Comparative surge clamping action of the prototype MOV to the acclimatised V275K20P @ V_a= 0.5 kV 91

(b) Comparative surge clamping action of the prototype MOV to the acclimatised V275K20P @ V_a= 0.8 kV 92

(c) Comparative surge clamping action of the prototype MOV to the acclimatised V275K20P @ V_a= 1.0 kV 93

(d) Comparative surge clamping action of the prototype MOV to the acclimatised V275K20P @ V_a= 1.25 kV 94

(e) Comparative surge clamping action of the prototype MOV to the acclimatised V275K20P @ V_a= 1.5 kV 95

6.8 (a) Surge clamping action of the as-received V275K20P @ 0.5 kV 97

(b) Surge clamping action of the as-received V275K20P @ 0.8 kV 97

(c) Surge clamping action of the as-received V275K20P @ 1.0 kV 98

(d) Surge clamping action of the as-received V275K20P @ 1.25 kV 98

(e) Surge clamping action of the as-received V275K20P @ 1.5 kV 99

6.9 Surge clamping action of the acclimatised commercial MOV tested (using type (i) electrode system) 103

6.10 Surge clamping action of the commercial MOV tested in the as-received state 104

6.11 Surge clamping action of the prototype MOV tested (using type (i) electrode system) 105
6.12 Surge clamping action of the as received V275K20P at 1.5 kV tested using a more attenuating current probe 106
6.13 Surge clamping action of the as received V275K20P at 5.0 kV tested using a more attenuating current probe 107
6.14 Microstructure of a MOV block, showing a "rod- like" structure inside and running across a pit 110
6.15 The "rod-like" structure in figure 6.15 at a higher magnification showing that it is anchored 111
6.16 XRD pattern of the prototype MOV compared to that of the studied commercial MOV 117
A1.1: V-I characteristic of prototype MOV compared to the commercial MOV - Calculation of the area under the leakage regions 126
B1.1: (a) Surge clamping action of V275K20P block (uncoated) (u.p.e.) compared to V275K20P (coated) (u.p.e.) @ V_a = 0.8 kV 132
(b) Surge clamping action of V275K20P block (uncoated) (u.p.e.) compared to V275K20P (coated)(u.p.e.) @ V_a =1.0 kV 133

LIST OF TABLES

Table		Page
4.1	As-received powders and their grain sizes	37
6.1	Comparative rates of breakdown of prototype MOV and a commercial MOV	71
6.2	Surge response data of the prototype MOV and acclimatised commercial MOV tested using type (i) electrode system compared to the commercial MOV tested in the as-received state	84
6.3	Surge response data of the prototype MOV and acclimatised commercial MOV tested using type (ii) electrode system compared to the commercial MOV tested in the as-received state	90
6.4	Secondary phases of the prototype MOV and the studied commercial MOV compared	118
A1	Computed areas in the leakage regions of the prototype MOV an commercial MOV	127

LIST OF SYMBOLS

Activation energy	Δ
Area	A
Boltzmann Constant	κ_β
Breakdown Voltage	V_b
Capacitance	C
Charge number density	n
Clamped Voltage	V_{cl}
Ceramic constant	κ
Current	I
Current density	j
Electrical conductivity	σ
Electrical field	**E**
Electrical current	I
Electron mobility	μ
Electron density	n
Electrical charge	e
Effective mass	m^*
Heat energy	Q
Holding voltage	V_h
Knee Voltage	V_{to}
Inductance	L
Magnetic field density	B
Magnetic flux	φ
Negative differential conductivity	σ_{diff}
Operating Voltage	V_{op}
Relaxation time	τ
Resistance	R
Resistance of Zinc Oxide grain	R_{ZnO}
Temperature	T
Time	t

Threshold voltage	V_{TH}
Voltage	V,ε
Work function	ϕ

LIST OF ACRONYMS

E-B Energy Band

NDC: Negative Differential Conductivity

NNDC: N-type Negative Differential Conductivity

SNDC S-type Negative Differential Conductivity

SPD: Surge Protective Device

ASPD: Absolute Surge Protective Device

M : A ZnO-based characterised powder such that the powder grains are μ MOVs

O : A characterised semiconducting chalcogenide glass powder composed of two phases with $SiTe_2$ as the main phase.

Q : A characterised powder which is Bi-Co-Mn-based.

1 INTRODUCTION

The objective of this investigation was to improve the V-I characteristic of the ZnO-based commercial metal-oxide varistor (MOV) so that it approximates that of the ideal device without sacrificing the surge voltage clamping action. The improvement was with respect to reducing the leakage current in the leakage region, increasing the rate of breakdown in the active region, and to remove the up-turn region. This was done by infusing *S-type* instability into the *N-type* instability as contained in the current ZnO-based commercial MOVs so as to produce a prototype MOV with an *ideal microstructure*. The instability that results from an ideal microstructure was coined *Γ-instability.* It was hypothesised that such an instability would give an ideal V-I characteristic and in turn ideal surge clamping action. The development was done through the use of characterised powders, new additives together with some traditional additives. The main powder was characterised such that the powder grains were micro-varistors (μ-MOVs) and hence N-type instability. The infusion of the S-type instability to the N-type instability was metallurgically done through the use of a characterised semiconductor chalcogenide glass, silicon telluride ($SiTe_2$), together with lanthanum hexaboride (LaB_6). In addition, other microstructure conditioning additives were used, one, a characterised Bi-based compound termed ***Q*** -additive and the other being the traditional α-bismuth oxide (α-Bi_2O_3).

This investigation was necessitated because the V-I characteristic of a ZnO-based commercial MOV departs substantially from that of the ideal device. This is because of its microstructure which deviates from that of the ideal, of which the latter is not known yet. The microstructure determines the electrical behaviour of a material, typically the V-I characteristic.

The deviation of the V-I characteristic from the ideal is in three regions: the leakage region, the active region (breakdown region) and the up-turn region. Deviation in the leakage region of the V-I characteristic means that when in

service the ZnO-based commercial MOV has higher leakage currents than the ideal device. Now leakage currents lead to degradation of the MOV V-I characteristic through I^2R loss, which eventually leads to premature MOV failure whilst in service, and thus reduces service availability. This is undesirable for the industrialist and the consumer.

In the active region, the instability responsible for the breakdown is predominantly thermal in nature and therefore the gradient of the V-I characteristic in this region is finite as opposed to that of the ideal which is zero. Thermal-based breakdown also promotes the degradation of the V-I characteristic of the MOV.

Further, the up-turned portion of the V-I characteristic implies that if the surge current is higher than the prospective, the MOV no longer offers the required protection, since the MOV voltage then rises with the current, which is not desirable.

The foregoing constitutes the problem. This investigation was therefore directed at developing a prototype MOV with a V-I characteristic with reduced leakage region, an **E**-field dependent instability in the active region and no up-turn region when compared to the commercial MOV.

The problem was investigated using a designed model based on the Principle of Superposition. Based on this model, a prototype MOV was fabricated using conventional sintering techniques. Its V-I characteristic was studied using the two-point probe method, and the surge clamping action was studied using an impulse generator. The microstructure and phases of this prototype MOV were studied using SEM and XRD techniques respectively.

The developed prototype MOV showed an improved V-I characteristic over that of the commercial MOV. In the leakage region, leakage currents were reduced by 1.0 %. In the active region, the rate of breakdown was increased and discharge

currents were increased by on average 4 times those of a dimensionally comparable commercial MOV. The instability responsible for the breakdown was found to be **E**-field dependent. The up-turn region was removed. The improvements were attributed to the use of characterised powders and new additives used as well as the processing method. The corresponding surge clamping action of the prototype MOV was identical to that that of the studied commercial, but with lower surge currents.

One other important and associated finding needs mentioning. According to current know-how, the pyrochlore phase, $Bi_2Zn(Zn_{4/3}\ Sb_{2/3})O_6$, and the spinel phase, $Zn(Zn_{4/3}\ Sb_{2/3})O_4$ are said to be responsible for the varistor property (VP), which gives rise to the non-linear V-I characteristic in a ZnO-based commercial MOV. These phases were absent in the developed prototype MOV. Thus these phases are not the only ones that are responsible for the VP.

This work has shown that a ZnO-based MOV with a near ideal V-I characteristic can be developed.

The structure of the thesis is as follows:

Chapter 2: A brief overview of what a MOV is, its manufacture, microstructure, and operation. Problems pertaining to ZnO-based commercial MOVs are reviewed and the problem under investigation is highlighted.

Chapter 3: The Hypothesis and Model used to study the problem is presented. The theory behind the model is also presented

Chapter 4: The experimental methods used to study the problem are presented

Chapter 5: Here results of the experimental study are presented

Chapter 6: The results of the experimental study are discussed and explained

A summary of findings of the research are presented in the "Conclusion", and finally "Recommendations for Further Work" is given.

2 LITERARURE REVIEW

This chapter introduces the concept of a MOV, its manufacture, microstructure, phases and use. An explanation of how it works is also given. The problems associated with ZnO-based commercial MOVs are reviewed and the problem under investigation is highlighted.

2.1 What is a MOV?

Metal Oxide Varistors (MOVs) are ceramic devices with a non-linear V-I characteristic (Matsuoka, 1971), (Harnden et al, 1981), (Van Der Merwe, 1989), (Harris Manual, 1995), (EPCOS, 2001). A typical V-I characteristic is shown in figure 2.1.

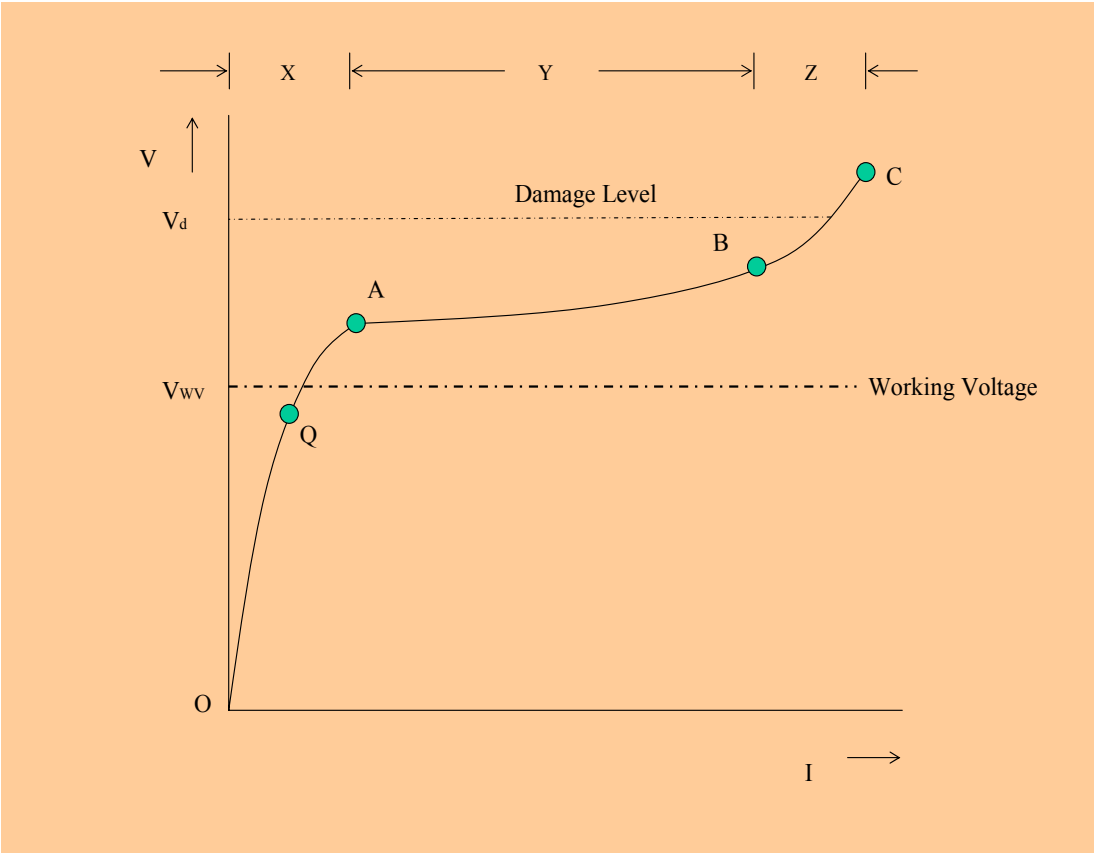

Figure 2.1: The V-I characteristic of a ZnO-based commercial MOV (Harris Manual, 1995),(SABS, NRS 039: 1995)

Note that this characteristic is the alternating current (AC) V-I characteristic as opposed to the direct current (DC) V-I characteristic; the latter is Zener-diode like (Greuter *et al*, 1989). In this work, the "V-I characteristic" refers to the AC one.

The V-I characteristic shown above has four distinct regions of operation. These are the ohmic region (OQ), pre-breakdown region (QA), breakdown region, also called the active region (AB), and the up-turn region (BC). Often these operating regions are reduced to three, marked X, Y and Z (Harris Manual, 1995). The ohmic region and pre-breakdown region are lumped into one, called the leakage region, marked X in figure 2.1. The leakage region is also called the OFF state. The active region is termed normal operating region, marked Y. The normal operating region is also called the ON state. The up-turn region is also called the high current region. It is marked Z.

State A is called the "knee" point or turn-on point; it is the point where the breakdown starts to be strong. The corresponding voltage is called turn-on voltage V_{to}, or "knee-point" point voltage.

The V-I relation of a MOV as shown in figure 2.1 is described by the Varistor Equation (Mahan, 1979) (EPCOS, 2001)

$$I = \kappa V^{\alpha}, \quad \ldots\ldots\ldots\ldots\ldots\ldots (2.1)$$

where I is the current flowing through the MOV, V is the voltage across its terminals, α is the non-linearity index, which is a measure of the degree of non-linearity of the V-I curve, and κ is a ceramic constant. For commercial ZnO – based MOVs, α is typically in the range $30 \leq \alpha \leq 100$.

The surge voltage clamping action of a typical ZnO-based commercial MOV is shown in figure 2.2. The figure shows the clamped waveform of surge voltage as well as the waveform of the surge current, that is, the current that flows through the MOV when the surge voltage is present.

Figures 2.1 and 2.2 are inter-related. The V-I characteristic is a measure of the surge voltage clamping action. That is, the more non-linear the V-I curve is as determined by α, the better the clamping action.

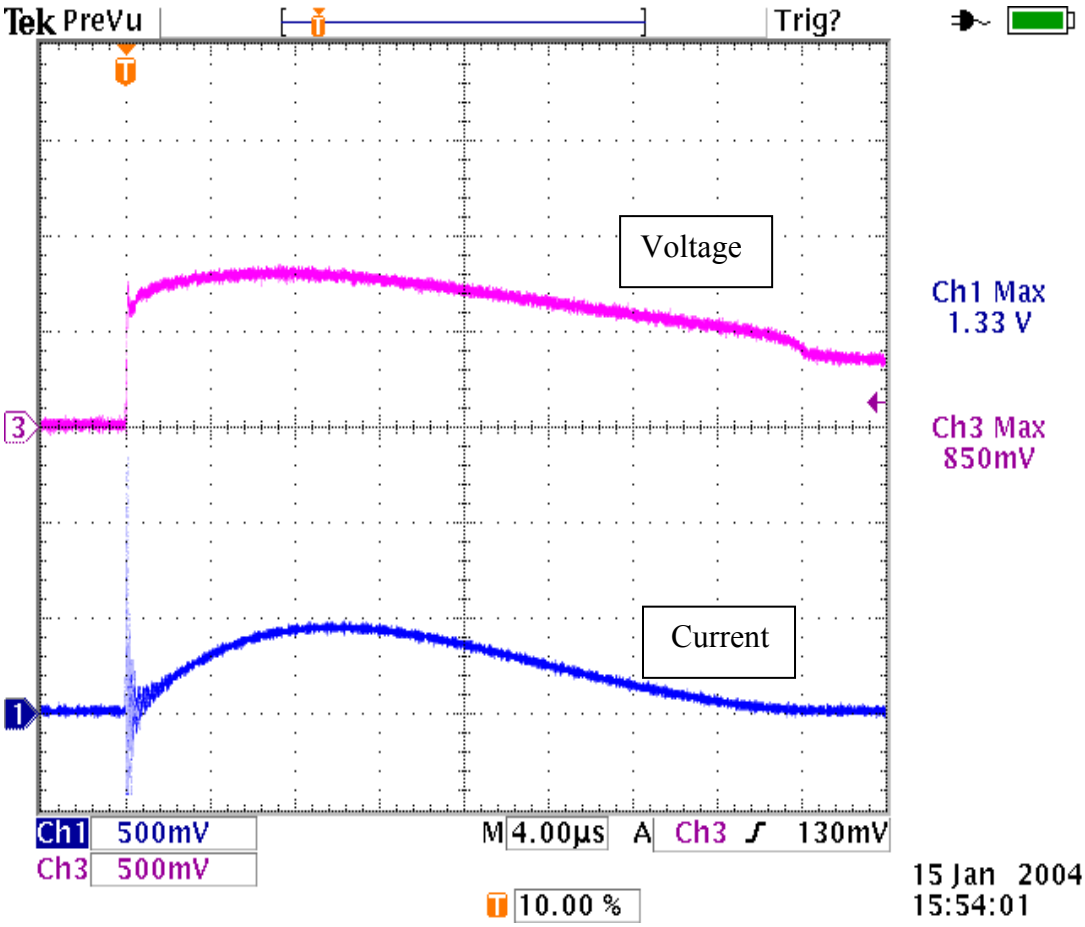

Figure 2.2: Surge clamping action of a typical commercial ZnO-based MOV.

A MOV is used to protect electrical and electronic equipment from damage due to electrical surges in power networks. It does so by clamping the surge voltage to a safe predetermined value and shunts the transient electromagnetic energy to earth. This is done by connecting the MOV in parallel with the device to be protected, see figure 2.3.

In the absence of a surge, the MOV is in the OFF-state and the voltage across the MOV is the same as that of X, the device being protected. When there is a surge,

represented by an impulse generator with source impedance, Zs, the overvoltage is superimposed on the normal mains voltage. The voltage across the MOV, V_M, is by the Voltage Division Rule

$$V_M = (Z_M/(Z_M + Z_s))V \quad , \ldots\ldots\ldots\ldots\ldots \quad (2.2)$$

where V is the applied surge voltage, Z_M is the impedance of the MOV. If $V_M \geq V_{to}$, the turn-on voltage (also termed "knee" point voltage) of the MOV, then the MOV switches from the OFF state to the ON state, thereby clamping the surge voltage to a predetermined safe value.

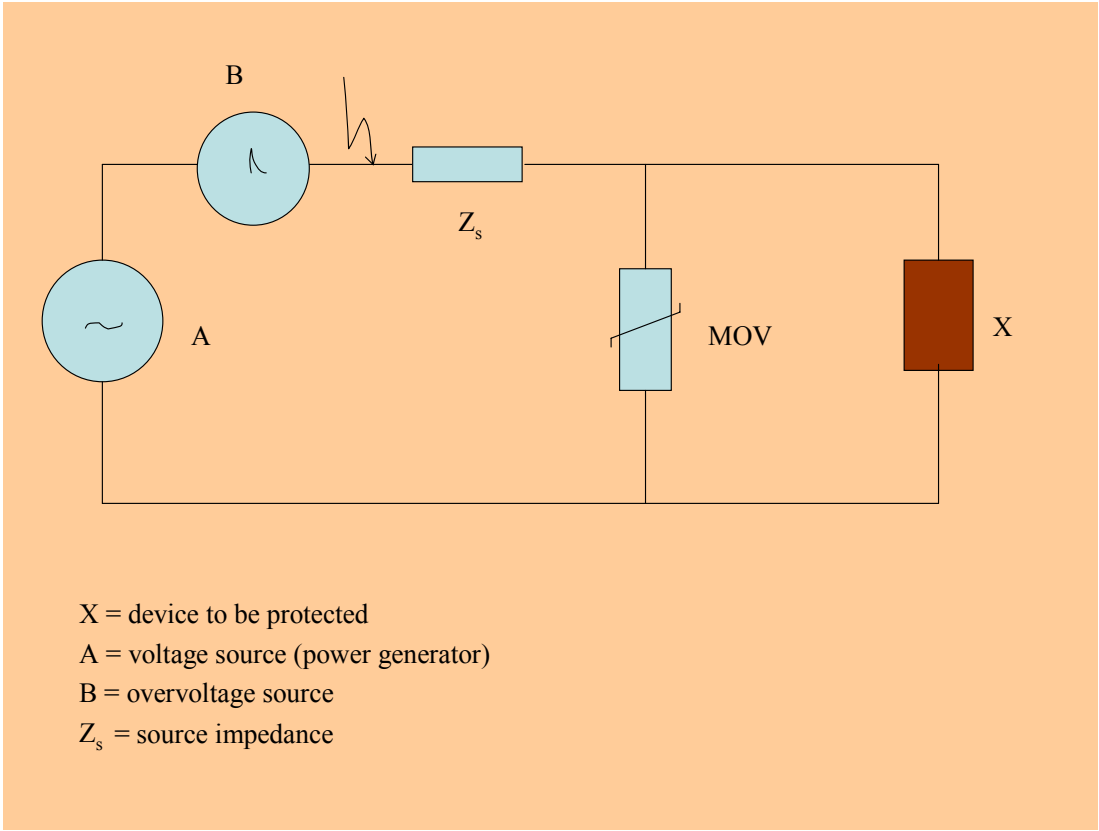

Figure 2.3: Principle of overvoltage protection by a MOV

2.2 Manufacture and Microstructure of a ZnO-based Commercial MOV

2.2.1 Manufacture of a ZnO-based Commercial MOV

The ZnO-based commercial MOV is prepared from zinc oxide (ZnO) powder as the main constituent material with smaller quantities of other oxide additives, mainly transition metal oxides (TMOs) (Matsuoka *et al,* 1970), (Clark, 1978), (Eda, 1979), (Greuter *et al*, 1989) (Mahan *et al*, 1996). As many as ten or more additives are used in the manufacture of commercial MOVs. A typical MOV composition is ZnO + 1.0 mol% Bi_2O_3 + 1.0 mol% CoO + 0.5 mol% MnO + 0.1 mol% Cr_2O_3 + 1.0 mol% Sb_2O_3. This is a typical composition for medium voltage (MV) MOVs. For high energy, high voltage (HV) MOVs, NiO if often included in the above composition, and for low voltage (LV) MOVs, TiO_2 is often included (Cordaro, *et a*l, 1986).

Fabrication is mainly by conventional compaction and sintering techniques. Typical commercial ZnO-based MOV blocks before electrode mounting and resin encapsulation are shown in figure 2.4. The finished and ready to use commercial ZnO-based MOVs are also included in figure 2.4.

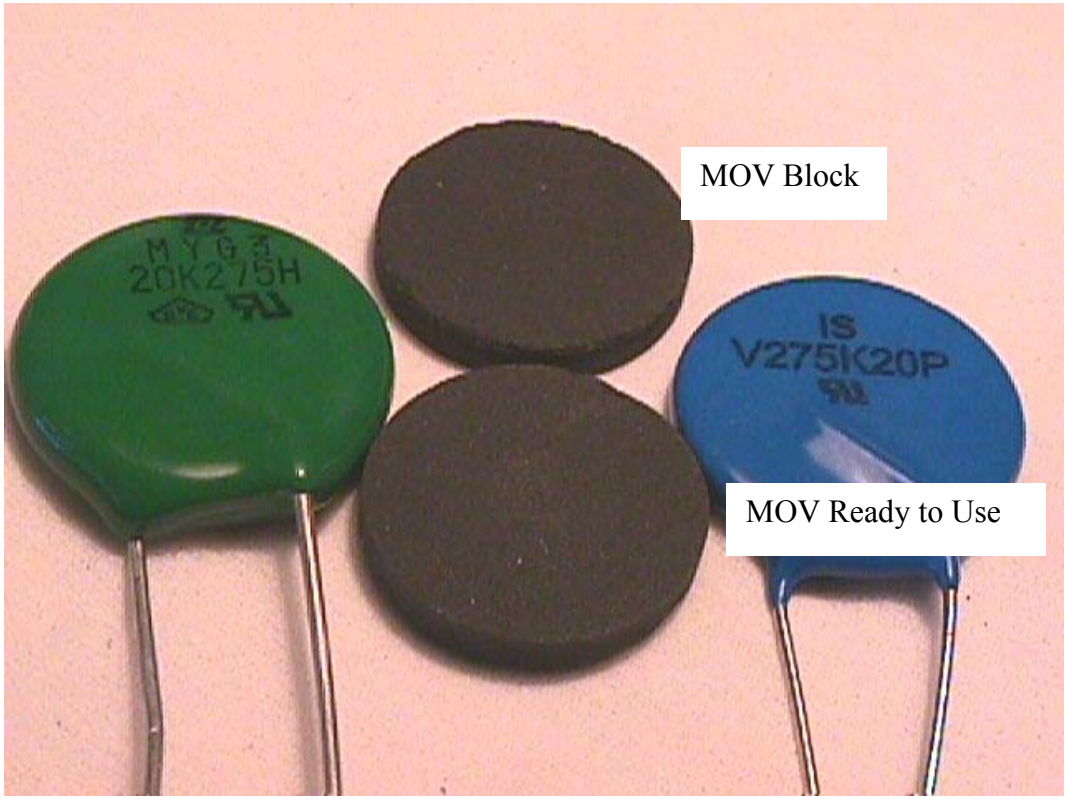

Figure 2.4: Commercial ZnO-based MOV blocks as sintered, and ready to use MOVs

2.2.2 Microstructure and Phases of a ZnO-based Commercial MOV

The microstructure of a ZnO-based commercial MOV is shown in figure 2.5.

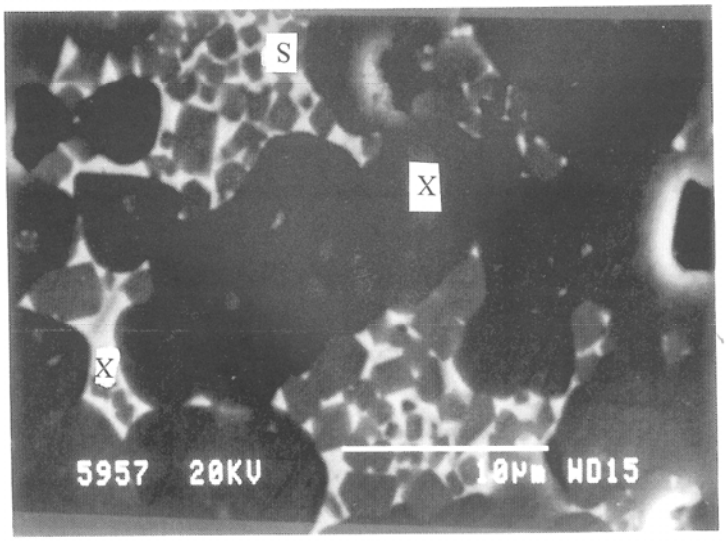

Fig 2.5 (a): Typical microstructure of a commercial ZnO-based MOV, showing ZnO grains (X), spinel particle (S) and inter-granular material (Z)

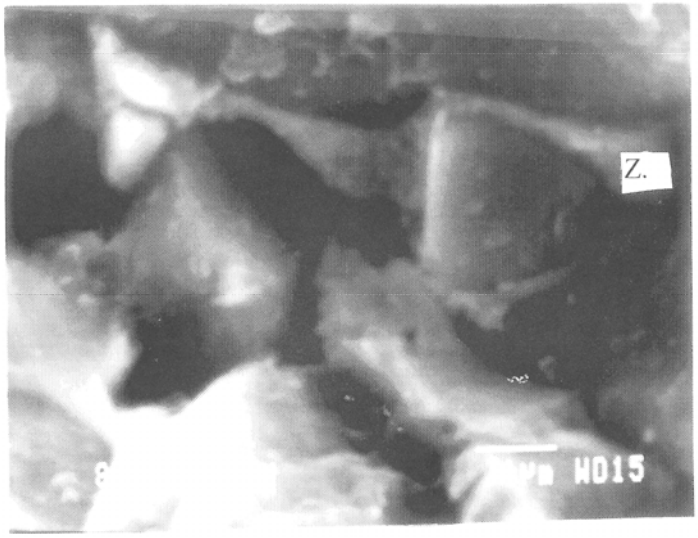

Fig 2.5 (b): Typical microstructure of a commercial ZnO-based MOV, showing the inter-granular layer (Z) at a higher magnification.

The microstructure of the polycrystalline ZnO-based MOV consists of

a) Densely compacted *N*-type semiconductive, Co^{2+}- and Mn^{2+}-doped ZnO-grains as the main phase. These grains measure on average 20 μm and resemble irregular polyhedrons, the common faces of which provide direct contact between adjacent grains (Greuter *et al*, 1989). They are separated by,
b) An inter-granular material of thickness < 0.2 μm, whose phases are a pyrochlore, $Bi_2Zn(Zn_{4/3}\ Sb_{2/3})O_6$, and a spinel phase, $Zn(Zn_{4/3}\ Sb_{2/3})O_4$ (Clarke, 1978), (Asokan *et al*, 1990), (Cho *et a*l, 1997), (Greuter *et al*, 1989). These phases are also doped with Co^{2+} and Mn^{2+}.
c) A monolayer interface between the ZnO-grain and the inter-granular layer; it is composed of Bi and O atoms.
d) porosity

The spinel phase appears as fine grains; these grains are most easily distinguished from the ZnO grains by their octahedral shape.

The monolayer is important in that it has a bearing on the varistor behaviour of the MOV - the issue of surface states, see section 2.5.

This microstructure results upon sintering the starting raw materials at a temperature usually in the range 1200° C ≤ T ≤ 1350° C. This microstructure gives a V-I characteristic (figure 2.1) that is of the *N*-type instability, see section 2.7.

2.3.2.1 Process Variables that Alter the Microstructure

The microstructure determines the electrical behaviour of the MOV. Thus the α in equation (2.1) is determined by the microstructure. The microstructure in turn is determined by the process variables. These are

a) Sintering temperature
b) Soaking time

c) Medium of sintering or sintering atmosphere
d) Rate of heating and cooling
e) Type and levels of additives
f) Forming pressure

How these process variables affect the microstructure has been outlined by Hove (1999).

2.3 The Relationship between the Microstructure and the V-I Characteristic of a ZnO-based Commercial MOV

As stated above, the microstructure of a material determines its V-I behaviour. Similarly the microstructure of the ZnO-based commercial MOV shown in figure 2.5 determines its V-I behaviour. The resistance (R) of this microstructure is a function of the applied voltage (V_a). That is, the ZnO-based commercial MOV is a *voltage dependent resistor* (VDR) (Greuter *et al*, 1989), and its resistance R can functionally be written as

$$R = R(V_a) = R_o V^{\alpha-1} \quad \text{..... (2.3).}$$

Ro is the resistance for $\alpha = 1$. This functional dependence expresses the non-ohmic V-I behaviour of the MOV. This phenomenon is called the *Varistor Effect*, also called Varistor Property (VP). This property is characterised by a reversible transition or switching process from an insulating (OFF) state to a highly conductive (ON) state at some threshold voltage, called the breakdown voltage (V_b). That is, the MOV reverts to the blocking state as soon as the voltage falls below the breakdown voltage. The switching process is extremely fast, being of the order of 25 ns or less.

The breakdown voltage, V_b, also often termed the turn-on voltage or "knee voltage", can be set to the required value typically in the range 10 volts to 10^5 volts, by careful dimensioning of the geometry of the MOV block (κ in equation (2.1)) as well as its controlled manufacture (α in equation (2.1)).

2.4 Microstructure-Equivalent Circuit Relationship

Again as stated above the microstructure of a MOV determines its V-I behaviour. The V-I behaviour in turn can be translated into an equivalent circuit. Thus the microstructure of the MOV can be represented by an equivalent circuit. The equivalent circuit of the commercial ZnO-based MOV is shown in figure 2.6.

R_{OFF} is the resistance due to the MOV when in the OFF-state electrically; it is due to the highly insulating Bi-rich inter-granular material, composed of mainly the Co^{2+} - and Mn^{2+}- doped pyrochlore phase, $Bi_2Zn(Zn_{4/3}\ Sb_{2/3})O_6$, and also the Co^{2+} - and Mn^{2+} - doped spinel phase, $(Zn_{4/3}\ Sb_{2/3})O_2$. It arises due to the scattering of charge carriers by optical phonons and accounts for the ohmic region, which is a sub-region of the leakage region in the V-I characteristic shown in figure 2.1.

R_{SE} represents the switching element at breakdown which switches the MOV from the OFF-state to the ON-state, and accounts for the active (breakdown) region in the V-I characteristic shown in figure 2.1. It too is due to the inter-granular material. It stands for the quantum mechanical double Shottky potential barriers (DSPBs) which collapse at the breakdown voltage. This is discussed later in more detail in Section 2.5.

R_{OFF} and R_{SE} can be lumped into one equivalent resistor, R_p, the effective resistance of the polycrystalline material.

R_{ZnO}, represents the resistance of the n-type semiconductive ZnO grains. C_p is the effective capacitance between the ZnO grains.

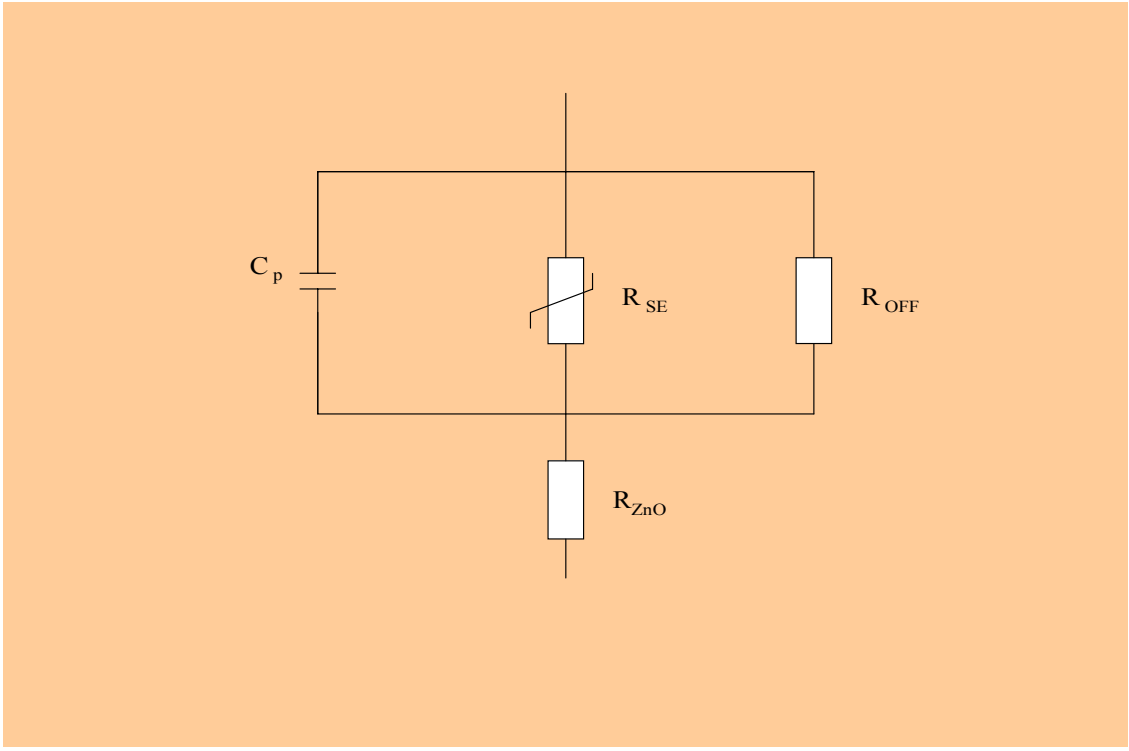

Figure 2.6: Equivalent circuit of a ZnO-based commercial MOV (Wong, 1973), (Harris Manual, 1995), (EPCOS, 2001)

2.4.1 Operation of the ZnO-based Commercial MOV

The operation of the ZnO-based MOV can be understood using the equivalent circuit of the device. This is described below.

In the OFF-state (no surge, but mains ON), $R_{ZnO} < R_{OFF} << R_{SE} = \infty$. The reactance X_c due to C_p is such that $X_c >> R_{SE}$. Therefore R_{OFF} determines the electrical behaviour of the MOV. R_{OFF} is finite and constant and hence accounts for the ohmic behaviour of the MOV in the ohmic region, which is part of the leakage region. The equivalent circuit reduces to that shown in figure 2.7 (a).

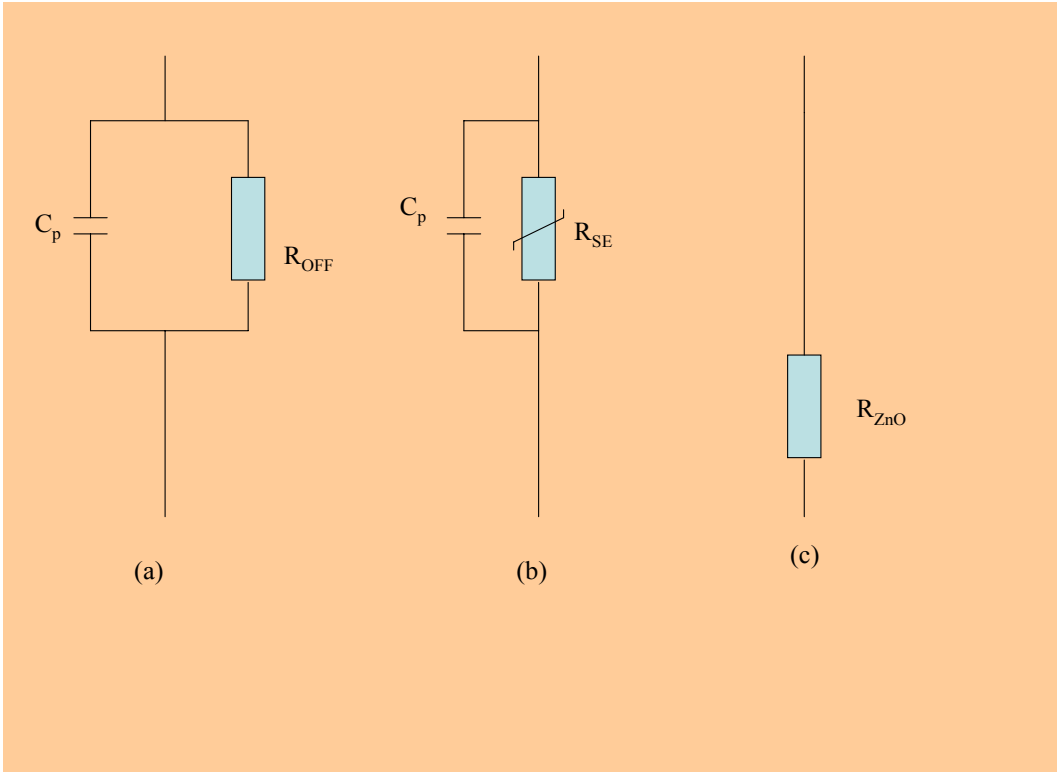

Figure 2.7: MOV equivalent circuit in the leakage region (a), active (breakdown down) region (b), and in the up-turn region (c). C_p = capacitance of the grain boundary material, R_{ZnO} = resistance of ZnO grains, R_{OFF} = resistance of the grain boundary material ($\rho = 10^{12} - 10^{13}$ Ωcm), R_{SE} = resistance of the switching element (part of the grain boundary material) ($0 - \infty$ Ω).

In the ON-state (with surge present and mains ON), $R_{ZnO} < R_{SE} << R_{OFF}$. Again X_c is such that $X_c >> R_{SE}$, and thus R_{SE} determines the electrical behaviour of the MOV. The MOV switches from the leakage region to the active region (breakdown region), and the equivalent circuit reduces to that shown in figure 2.7 (b).

If the surge voltage is such that the surge current is higher than expected then the MOV goes into the up-turn region, also called the high current region or super-ohmic region. Here $R_{SE} < R_{OFF} < R_{ZnO}$, hence R_{ZnO} determines the electrical behaviour in this region. The behaviour is ohmic, often termed super-ohmic and the equivalent circuit reduces to that shown in figure 2.7 (c).

If the surge voltage is such that state C in figure 2.1 is exceeded, then the MOV fails catastrophically. At and below state C, it can recover to its original state, if the surge voltage is removed.

Note that the two ohmic regions, one for the leakage and the other for the up-turn are due to different media, hence different scattering mechanism. The former is due to the insulating grain boundary material, whereas the latter is due to the n-type semiconductive ZnO grains. This also explains why the slopes of these two linear regions are different in figure 2.1. It should also be noted that the above indirectly explains the nature of the V-I characteristic shown in figure 2.1

2.5 Conduction Mechanism in a ZnO-based Commercial MOV

The conduction mechanism of a ZnO-based commercial MOV can be understood by using a model for the microstructure (Santhanam *et a*l, 1979), (EPCOS, 2001), see figure 2.8.

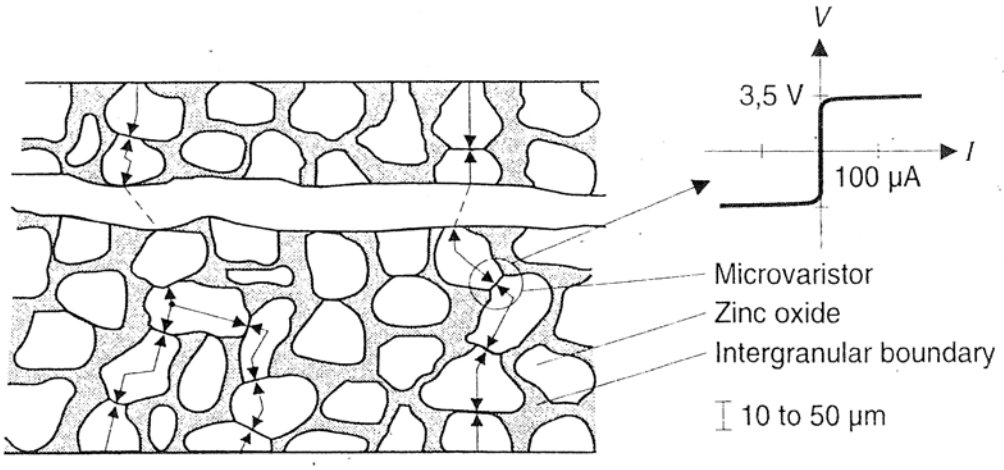

Figure 2.8: Conduction mechanism in a ZnO-based commercial MOV

The ZnO-grains typically 20µm in size, are semiconducting. They have a resistivity value typically of the order of 1.0 Ωcm or less. The matrix, of average thickness of 0.2 µm is highly resistive, with a resistivity value of the order $\geq 10^{12}$ Ωcm. Each single boundary between two adjacent ZnO-grains constitute a micro-

varistor (μ-MOV), with a V-I (DC) curve as shown in the insert and a V-I (AC) curve, the area of focus in this work, as shown in figure 2.1 (Levinson, 1975), (Greuter *et al*, 1989), (EPCOS, 2001). The breakdown voltage of these μ-MOVs is about 3.5 V. The ceramic body as a whole is therefore nothing other than a Voronoi network (Mahan *et al*, 1996) of these small μ-MOVs. The electrical behaviour of the MOV then is just a series and parallel connections of these μ-MOVs connected together. It follows therefore that the observed electrical properties are controlled by the physical dimensions of the MOV block, namely

- twice the ceramic thickness produces twice the protection level because then twice as many μ-MOVs are arranged in series.
- twice the area produces twice the current handling capability because then twice the number of current paths are arranged in parallel.
- twice the volume produces almost twice the energy absorption capability because then there are twice as many μ-MOV absorbers in the form of ZnO-grains.

Having presented the model, the conduction mechanism is explained; this is done below.

Current theory regards the Varistor Property in the ZnO-based commercial MOV as being a grain boundary phenomenon, predominantly thermal in origin with quantum tunnelling superimposed. That is, upon surge, the grains conduct and because there is current flow, there is a heating effect at the grain boundary layer, releasing thermal electrons, which assisted by quantum tunnelling flow from the MOV block to earth, thus diverting the surge (Greuter *et al*, 1989).

When a voltage is applied to the MOV, all the voltage drop takes place solely at the grain boundaries, for the ZnO grains are good conductors relative to the grain boundary. This is because the ZnO grains have a relatively high electrical conductivity. At each ZnO grain-grain boundary material interface, there is a localised electrostatic potential barrier. This potential barrier is called a Schottky barrier. Thus in moving from one ZnO grain to the nearest neighbour ZnO grain,

there are two Schottky barriers. These Schottky barriers control the transfer of charge carriers from one grain to another. The control is through their heights and thicknesses, the latter being a measure of the transparency of the barriers against quantum tunnelling. Thus the non-linear V-I behaviour, and hence the VP of a ZnO-based commercial MOV is due to the double Schottky potential barriers (DSPBs) (Cordaro *et al*, 1986).

The DSPBs arise from interface states, also called trap states, see figure 2.9. These interface states are a kind of electronic defects that are found in ZnO-based MOVs (Cordaro *et al*, 1986). They are caused by lattice defects of ZnO, O-vacancies acting as donors and Zn-vacancies that act as acceptors. The O-vacancies are predominant inside the ZnO grain and constitute what are called bulk traps. The Zn-vacancies are predominant in a thin region at the ZnO grain-grain boundary material interface. These defects in turn are controlled by the presence of an extrinsic donor found in the monolayer (section 2.2.2) as well as by diffusion during cooling of the MOV block from the sintering temperature.

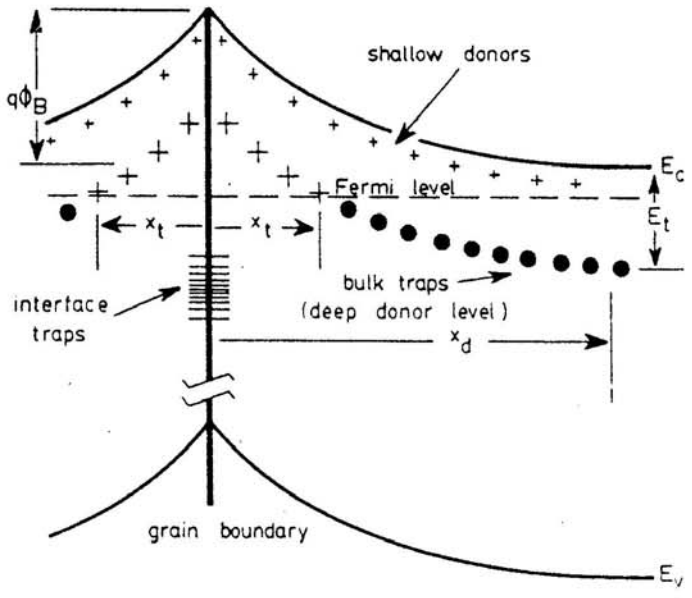

Figure 2.9: Energy band diagram for a ZnO-based commercial MOV (Schwing, *et al*, 1985), (Cordaro *et al*, 1986), (Greuter *et al*, 1989) showing the DSB due to interface traps. Also shown are bulk traps.

It was mentioned in section 2.1 that the V-I curve has 3 regions. In the leakage region, which accounts for low and medium voltages, the aforesaid DSPBs are very high, typically in the range of 0.6-0.8 eV (Kingery, *et al*, 1979), and very thick such that they prevent charge flow. That is, the barriers are so high and so thick such that neither surmounting the potential barriers by carriers due to thermal excitation, nor quantum tunnelling, is possible. The carriers do not have sufficient energy to do either. They just "fall into" trap states at the grain boundaries. However the charge carriers are bosons, hence obey Boltzmann distribution. As a result, they are few charge carriers that will have sufficiently high energy to overcome these potential barriers. These constitute the experimentally observed leakage current in the leakage region.

Again as mentioned in section 2.1, the leakage region comprises of the ohmic region and pre-breakdown region. The ohmic region arises because the few electrons that are energetic enough to overcome the potential barriers and become available for conduction are scattered by optical phonons in the lattice of the MOV. This scattering is constant. Because scattering is a measure of resistance and it is constant, Ohm's Law holds. Put differently, the linearity observed in the ohmic region of the V-I characteristic arises because the optical phonons are absorbing as much energy as the electrons are giving out energy to the lattice. The electrons get energy from the electromagnetic field, hence their excitation.

The above explains the V-I characteristic in figure 2.1 from state O to state Q, the ohmic region. The V-I curve "knees off" from Q to A giving the locus QA, accounting for the pre-breakdown region. This indicates the filling up of trap states. It is characterized by that any increase in the applied voltage, V_a, and hence **E**, the electric field, does not produce a proportionate current. This marks the onset of non-linearity and defines the pre-breakdown region.

The effective resistance experienced by charge carriers in the leakage region corresponds to the circuit element R_{OFF} in figure 2.6.

When the applied voltage is increased such that the breakdown voltage is reached, corresponding to high **E**-fields, typically of the order of 10^4 Vm^{-1}, the DSPBs collapse. That is, the matrix undergoes a breakdown. The collapse of DSPBs implies a collapse in the resistance of the MOV; the resistance collapses to some low finite value, depending on the rating of the MOV. This collapse is the switching process from the highly insulating (OFF) state represented by R_{OFF} in figure 2.6, to the highly conducting (ON) state represented by R_{SE}. This switching process is characterised by a large current flowing. It is also characterised by that a small change in voltage gives rise to a large change in current. As a result the voltage across the low resistance is maintained at practically a constant level, hence the clamping action.

The instabilities that are responsible for the breakdown are of two kinds which are inter-related. One is the Zener breakdown and the other one is avalanche breakdown. The collapse of DSPBs results in an avalanche of charge carriers across the grain boundaries, some flowing into nearest neighbour ZnO grains and others circumventing them to the next nearest neighbour grains. This gives the series-parallel aspect of the equivalent circuit shown in figure 2.6. Because there is a "sea" of electrons available for conduction as a result of the breakdown, the current flows virtually unhindered. This can be seen from the following relations:

$$\sigma = \boldsymbol{ne}\,\mu_{\boldsymbol{e}} \qquad \ldots\ldots\ldots\ldots\ldots\ldots \quad (2.4)$$

$$\boldsymbol{I} = \sigma \boldsymbol{E} \qquad \ldots\ldots\ldots\ldots\ldots\ldots \quad (2.5),$$

where σ is the electrical conductivity of the medium composed of n-type grains and grain boundary material under breakdown, *n,* is the electron density, *e*, is the charge of an electron, μ_e is electron mobility, *I* is the current flowing and ***E*** is the electric field intensity. The observed large current flowing during breakdown as given in equation (2.5) arises from the large *n* in equation (2.4), with ***E*** and hence the voltage V, almost constant. This accounts for the active (breakdown) region, the so-called non-linear region AB in the V-I characteristic shown in figure 2.1 and explains how the clamping action is effected by the MOV as shown in figure 2.2.

The transition from the active region to the up-turn region is better understood in energy terms. In the breakdown state, large current flowing gives rise to heat, i.e. high phonon generation. The avalanching electrons constitute an electron gas. This gas experiences some weak scattering from phonons and hence some resistance. This small resistance is represented by the circuit element R_{SE} in figure 2.6. It also accounts for the low slope of AB in figure 2.1. How the electron gas experiences some weak scattering is explained as presented below.

In the breakdown state accounting for the active region AB in figure 2.1, there is an energy balance between the electron gas and the lattice (the grains). This is expressed by the following relation (Omar, 1975):

$$eE\nu - \frac{\overline{E}(\tau_e) - \overline{E}(\tau)}{\tau_e} = 0 \quad \text{..... (2.6)}$$

where e is the charge of an electron, $\boldsymbol{E}$ is the applied **E**-field, ν is the mean velocity of the electrons, $\overline{E}(\tau_e)$ and $\overline{E}(\tau)$ are the mean fields in the electron gas and the lattice respectively. The first term in equation (2.6) represents the supplied electromagnetic energy, and the second expresses the difference in energies between that of the electron gas and the lattice.

The balance expressed by equation (2.6) means that the scattering of electrons by optical phonons is a constant. The scattering of electrons is a measure of the resistance. Because the scattering is constant and hence constant resistance, this implies ohmic relation. Certainly this region (AB) can be represented by a near straight line (EPCOS, 2001).

For voltages higher than the turn-on voltage, that is higher than $V_A \approx V_B$ in figure 2.1, the current and hence heat due to the avalanching electrons, will be high enough such that the dynamic balance in energy exchange between hot electrons (avalanching electrons constituting the electron gas) and phonons as expressed by equation (2.6) no longer exits. That is, the electromagnetic energy supplied to the avalanching electrons does not balance with the energy absorbed and then

dissipated by the ZnO-grains. The result is that the ZnO polycrystalline lattice temperature, T_l, "picks up" because the ZnO grains can not cope to dissipate the energy from the hot electrons. This means that the atoms forming the ZnO crystal undergo violent harmonic oscillations, i.e. acoustic phonon generation. The result is an increase in acoustic phonon generation, and hence an increase in hot electron- phonon (acoustic) scattering, and hence resistance. It is this resistance that manifest itself as R_{ZnO} in the equivalent circuit. This marks the up-turn region, BC, in figure 2.1. This also explains why R_{ZnO} is said to be responsible for the up-turn region in the V-I characteristic. R_{ZnO}, represents the resistance of the n-type semiconductive ZnO grains.

The preceding sections described what a MOV is, its function, microstructure charge transport mechanism and applications. The question that arises is: What makes a good MOV? The answer to this question lies in defining first what an ideal surge protective device (SPD) is. This then will be reduced to the ZnO-based MOV. This is presented in the following subsection.

2.6 The Ideal Surge Protective Device (SPD)

An ideal surge protective device is one whose V-I characteristic is Heaviside-step-function-like, see figure 2.10, (Van Der Merwe, 1989) and is approximated by that shown in figure 2.11, typically due to the Zener diode (Harris Manual, 1995). Its surge clamping action is shown and compared to that of a ZnO-based commercial MOV in figure 2.12.

An ideal device is characterised by (Harris Manual, 1995): a) Zero to low leakage current, b) Zero or no follow current, c) Low clamping level, d) High energy handling capability, e) Low/high capacitance, f) Fast response time, and g) Low cost.

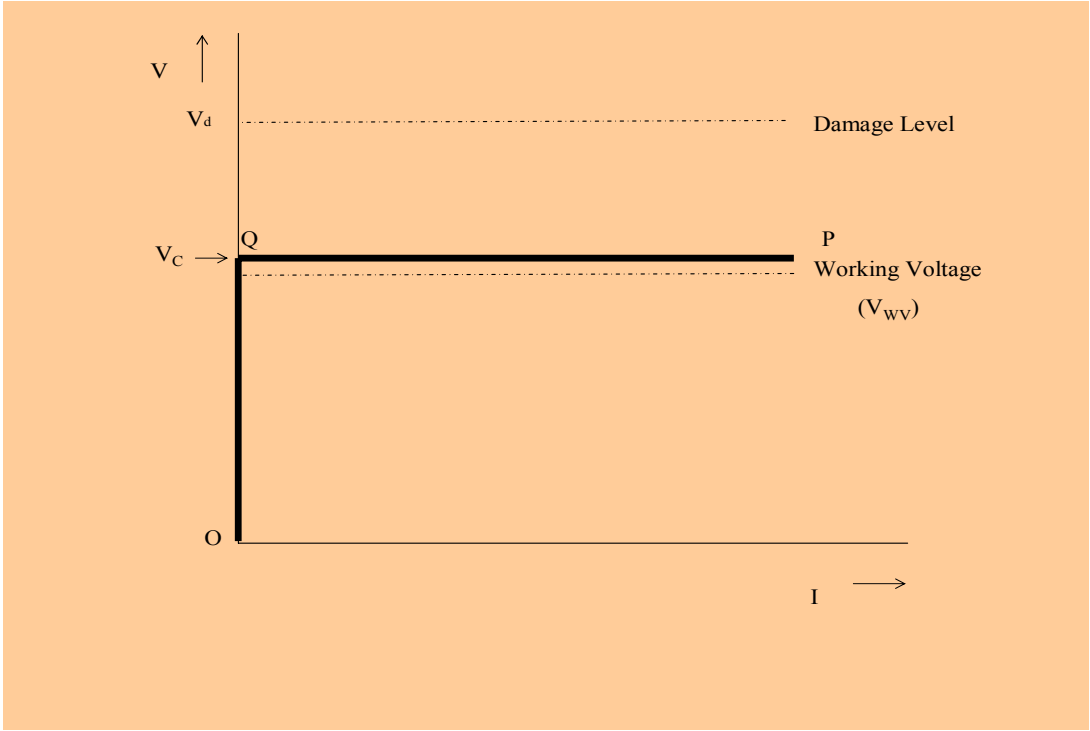

Figure 2.10: The V-I characteristic of an ideal MOV (Van Der Merwe, 1989)

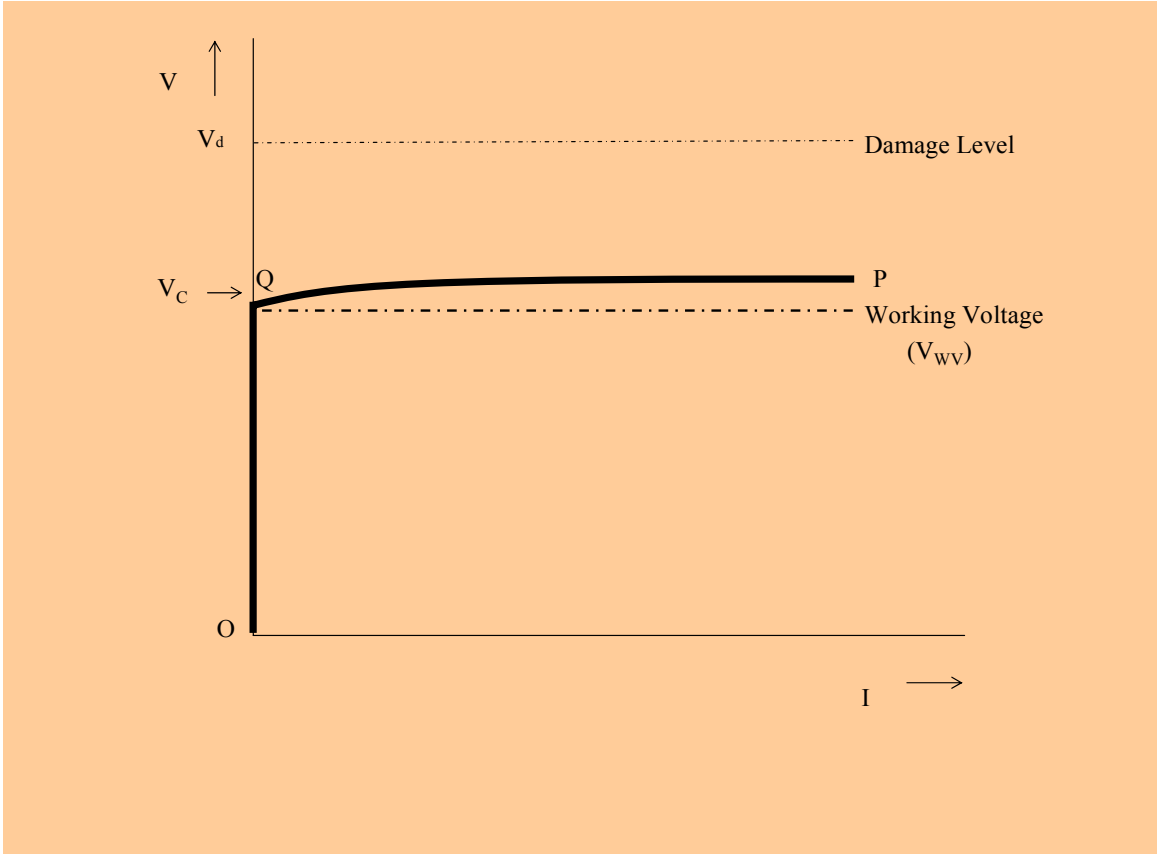

Figure 2.11: The V-I characteristic of an approximate ideal MOV (Harris Manual,1995)

In figures 2.10 and 2.11, the working voltage (V_{WV}) refers to the rated operating voltage of the electrical or electronic equipment to be protected by the MOV, V_c is the clamping level of the MOV and damage level (V_d) refers to the voltage at which the MOV catastrophically fails.

In figure 2.12, the waveform labelled "1.2/50 µs applied surge voltage" is the typical lightning waveform. If this surge voltage is applied to the ZnO-based commercial MOV, the MOV clamps it to a lower pre-determined level, giving a waveform labelled "classical clamping". The current through the MOV, called surge current, is large and its waveform is denoted by " 8/20 µs surge current".

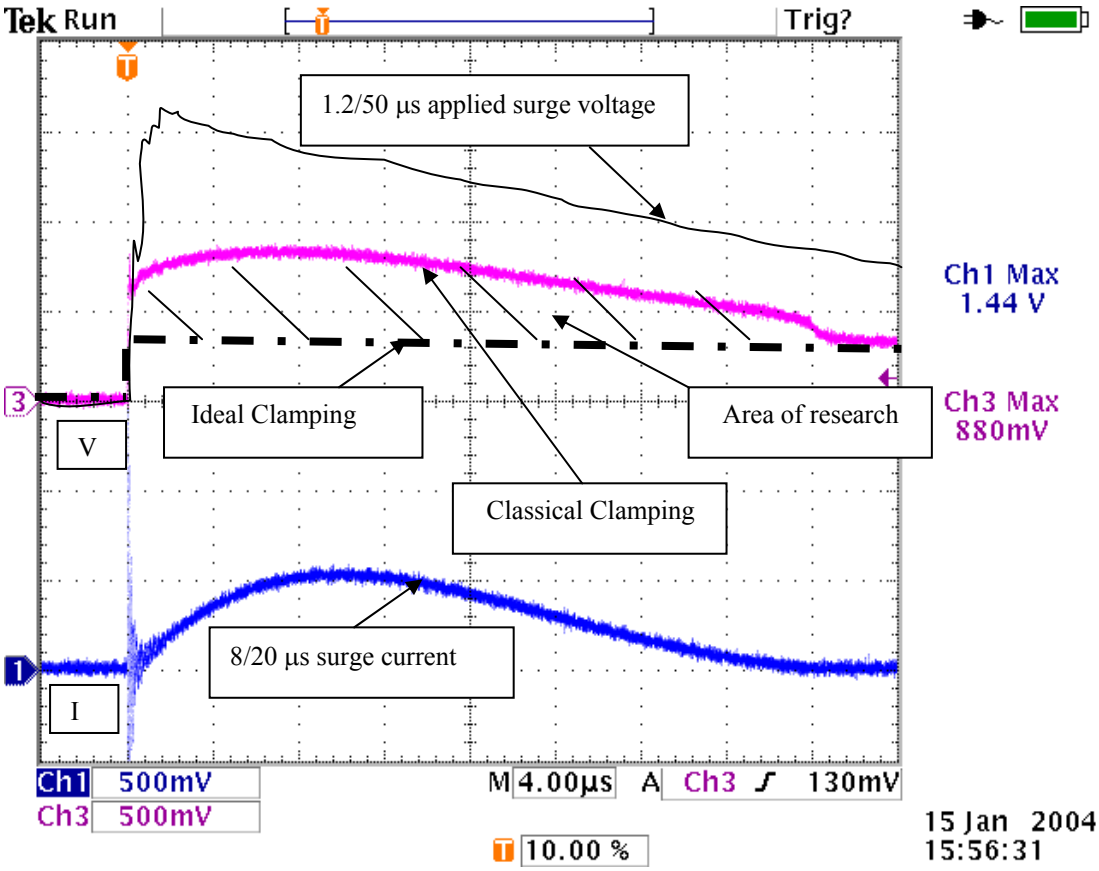

Figure 2.12 Typical surge clamping action of a ZnO-based commercial MOV compared to an ideal MOV, showing the deviation from ideal behaviour.

If the same surge voltage is applied to an ideal device, it clamps it giving a waveform depicted as “ideal clamping”. The associated surge current is similar in waveform to that of the ZnO-based commercial MOV.

It is clear from the foregoing that these two SPDs, the ideal device and the ZnO-based commercial MOV differ in performance with respect to surge clamping action. The shaded region in figure 2.12 is a measure of the deviation of the V-I characteristic of the ZnO-based commercial MOV from that of the ideal device (see also figure 2.15) and constitutes the area of research in this work. It must be reduced to zero, hence the problem.

From the foregoing, a good MOV is one with a V-I characteristic with negligible leakage current in the OFF state, sharp and very fast transition from the OFF state to the ON state, near infinite rate of breakdown when it conducts such that the amplitude of the clamped surge voltage is finite and time independent or a constant. To get the ZnO-based commercial MOV behave this way requires that the instability at breakdown be electronic in nature, field-dependent, thermal-free and be very high. There area a number of breakdown mechanisms that occur in materials, including the ZnO-based commercial. The most common ones are thermal breakdown, Zener breakdown, avalanche breakdown, and field emission, also called Frenkel-Poole breakdown (Walther *et al*, 1971). These are often classified as N-type or S-type instability. This is the subject of review in the following sub-section.

2.7 S-type and N-type Instabilities

When a semiconductor is under sufficiently strong excitation conditions such as large electric or magnetic fields, strong optical irradiation, or high current injection, it will in general exhibit transport properties which deviate substantially from linear V-I relations. This leads in many cases to instabilities like current runaway, current oscillations, discontinuities in the current and/or voltage, switching, and hysteretic V-I characteristics (Schöll, 1987). Although these instabilities have a detrimental effect upon the performance of solid state devices, they have been used intentionally in a number of semiconductor devices, typically for the fabrication of fast electronic switches.

The I-V (equivalently j-E) behaviour of a semiconductor material is determined by the microscopic properties of that semiconductor material, that is, the microstructure. If the j-**E** characteristic has a regime of *negative differential conductivity* (NDC), σ_{diff}, that is such that

$$\sigma_{diff} = \frac{dj}{dE} < 0 , \quad \ldots\ldots\ldots (2.7)$$

that is, if the current density (**j**) decreases with increasing electric field (**E**), or vice versa, then the corresponding time-independent states are generally unstable (Schöll, 1987).

Negative differential conductivity (NDC) can be classified as NNDC, also called *N*-type, or SNDC, also called *S*-type, depending upon the shape of the j-**E** characteristic, which may resemble the letter N or S respectively (Schöll, 1987), (Roy, 1976). Figures 2.13 and 2.14 show the j-**E** characteristics for the NNDC and SNDC instabilities respectively. NNDC and SNDC are associated with voltage- and current-controlled instabilities respectively. In the NNDC case, j is a single-valued function of E, but E is multi-valued. The $j(E)$ relation has three branches in a certain range of j. The SNDC case is complimentary in the sense that E and j are interchanged.

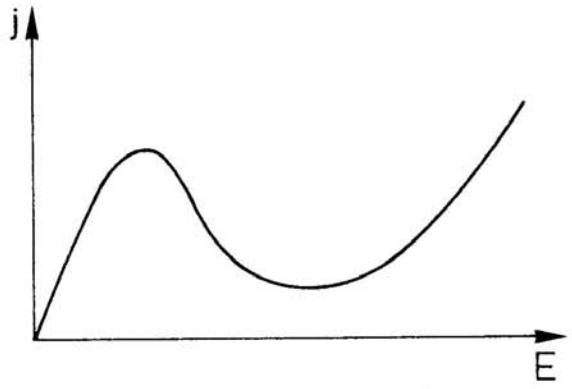

Figure 2.13: The j-E characteristic for NNDC (*N*-type) instability

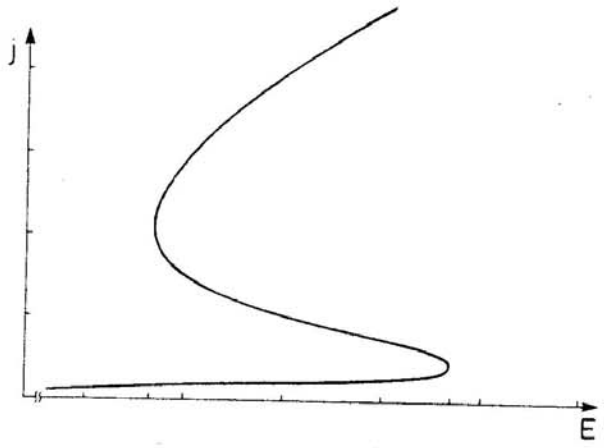

Figure 2.14: The j-E characteristic for SNDC (*S*-type) instability

Combinations of SNDC and NNDC can occur. In this case, regimes of SNDC and NNDC may follow one another on the static j-**E** characteristic as the E-field is increased. The characteristics may evolve from SNDC to NNDC as time goes on, or the characteristics may have a more complicated shape than the simple *N* or *S*, and being multi-valued in both *j* and *E*.

The V-I curve of the ZnO-based commercial MOV falls under N-type instability (NNDC). A typical material that gives the S-type instability is the chalcogenide glass of composition 65.5 wt% Te + 24.3 wt% As + 2.9 wt% Si + 7.3 wt% Ge Deis *et al* (1970).

2.8 Problems Pertaining to ZnO-based Commercial MOV

The current commercial ZnO-based MOV suffers from two problems that are inter-related:

a) The V-I characteristic (both reported and determined in this work) shows substantial departure from that of the ideal one, see figure 2.15.
b) It suffers from electrical degradation, also called aging (Greuter *et al*, 1989)

The first problem is due to the microstructure, for the microstructure determines the V-I behaviour. The second is thermal in nature, and is mainly due to the fact that when the MOV becomes active, it transforms the electromagnetic energy of the surge into heat mainly. This energy has to be dissipated by the MOV, and in the process it degrades the Varistor Property. The other contribution to "aging" comes from the relatively high I^2R losses of the MOV when in the OFF state. The leakage currents give rise to these watt losses. These thermal related processes cause a shift in the power-temperature characteristic towards higher losses. This makes the MOV to be leakier with time.

The first problem constitutes the research problem of this work. The areas to be minimised ideally to zero are shown in figure 2. 15; they are marked S1 and S2.

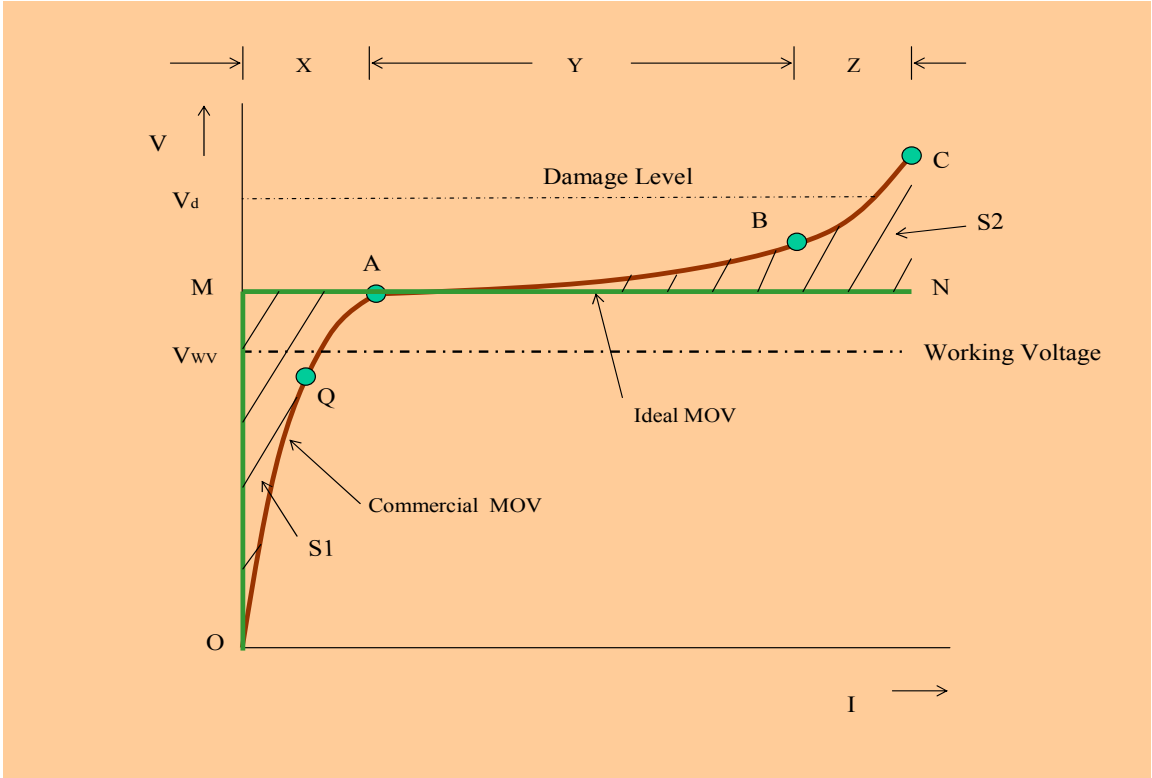

Figure 2.15: The V-I characteristic of the ZnO-based commercial MOV compared to that of the ideal device showing the regions to be improved.

Now that the background and research problem have been presented, in the next chapter, a hypothesis and a model to be used in an attempt to solve the problem will be presented.

3 THE HYPOTHESIS AND MODEL

From the preceding chapter, it was highlighted that the current ZnO-based commercial MOV has a V-I characteristic that deviates from that of the ideal device. The deviation is a result of the microstructure of the MOV block. Now ceramic processing variables determine the microstructure. The microstructure determines the conduction mechanisms, which in turn determine the nature of the V-I characteristic and therefore the surge clamping action. It follows therefore that by appropriately characterising the microstructure, theoretically an ideal microstructure and hence ideal electrical behaviour can be obtained. In order to come up with an ideal microstructure, a model was developed on the basis of a hypothesis. This chapter gives the hypothesis and model used to try and solve the problem. The theory of the model is also presented.

.

3.1 The Hypothesis

Define the instability that is responsible for ideal V-I behaviour as *Γ-type instability*. Then

$$\Gamma - instability = N - instability + S - instability$$

In V-I terms,

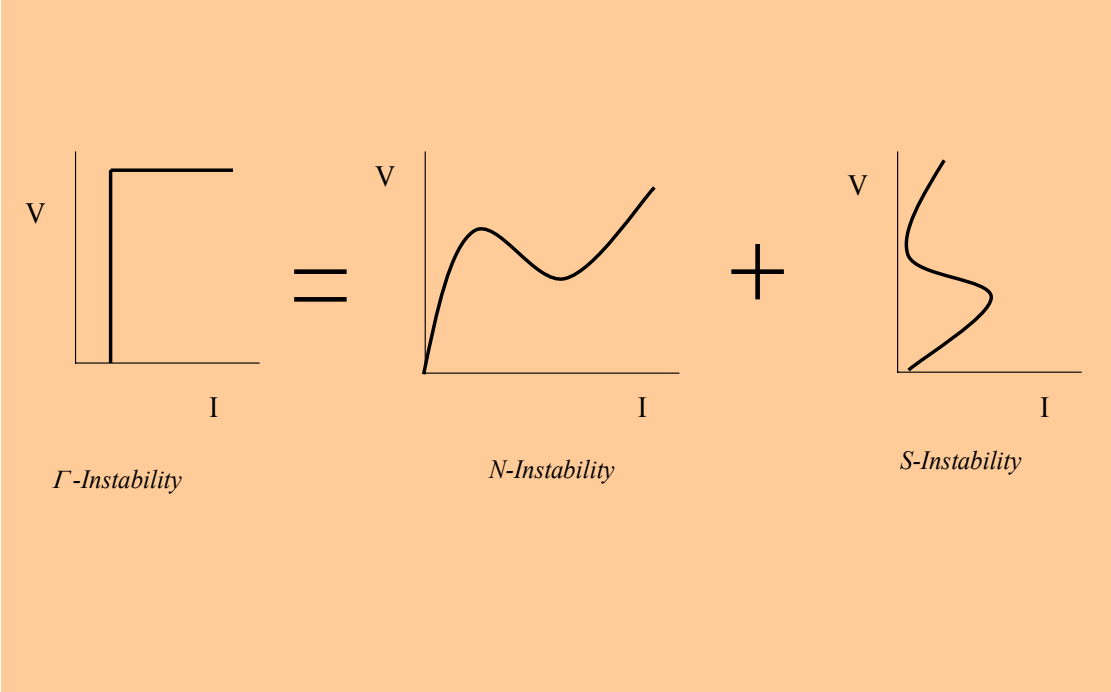

Figure 3.1: Model for the development of an ideal MOV

The above hypothesis is saying that in order to get an ideal V-I characteristic, see figure 2.10, let us suppose that the instability response is called Γ-type. Then this instability is by the Superposition Principle, a hybridization or an infusion of the N-type instability plus S-type instability.

Experimentally the N-type instability is provided by characterised powder, called the ***M*** -powder, prepared from a powder mixture of the form: 93.23 wt% ZnO + 5.47 wt% Bi_2O_3 + 0.88 wt% CoO + 0.42 wt% MnO. Because such a composition is typical for MOVs, the powder grains of this powder are micro-MOVs. The S-type instability is provided by a chalcogenide glass powder, $SiTe_2$ and is enhanced

by a field-emission material, LaB_6. The $SiTe_2$ is prepared from a STAG (Silicon, Tellurium, Arsenic, Germanium) composition of the form 65.5 wt% Te + 24.3 wt% As + 2.9 wt% Si + 7.3 wt% Ge. In order to promote reactivity amongst these powders so as to get a ceramic with a microstructure with the Γ-type instability, other conditioning additives will be used. This is detailed in Chapter 4.

3.2 The Model

The microstructure of the ZnO-based commercial MOV is shown in figure 2.5. It is modeled to be as shown in figure 3.2 (Greuter *et al*, 1989).

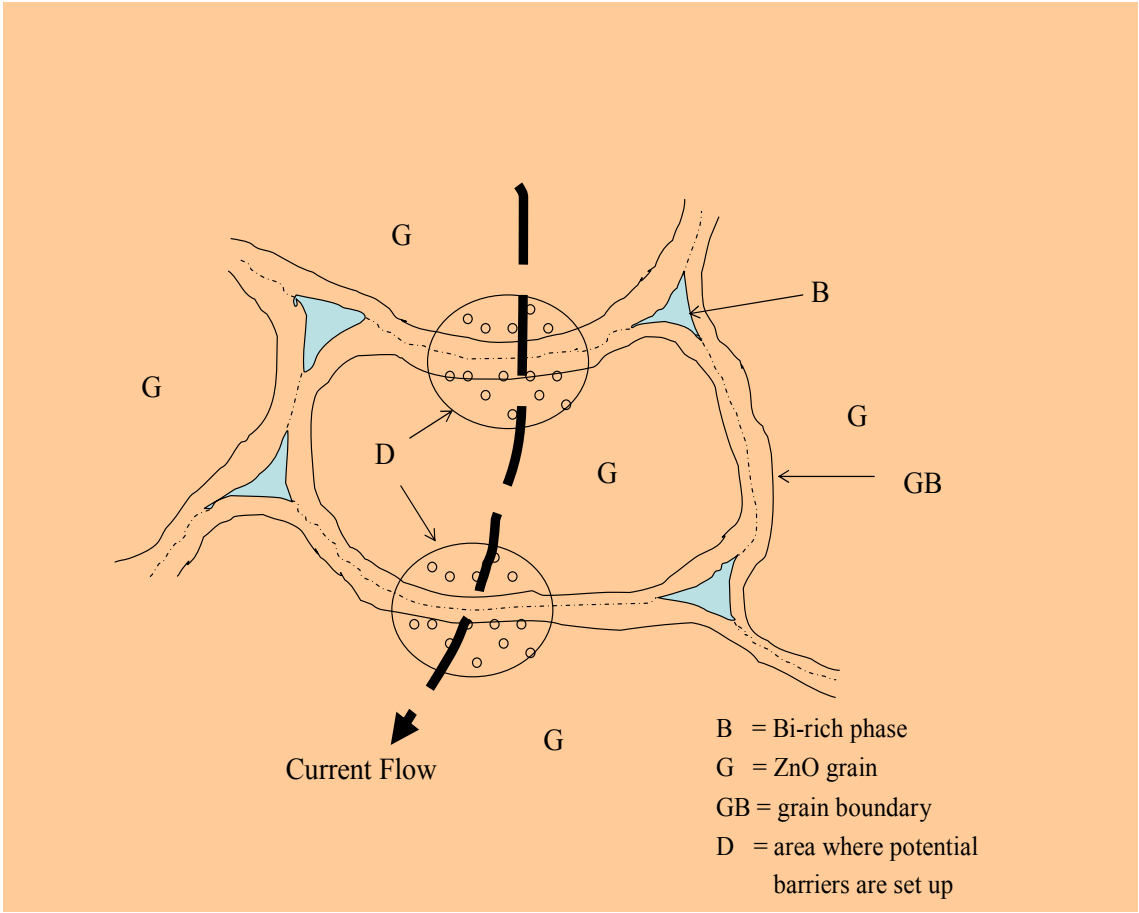

Figure 3.2: Model microstructure of a ZnO-based commercial MOV. Typical composition is ZnO +1.0 mol% Bi_2O_3 +1.0 mol% CoO + 0.5 mol% MnO + 1.0 mol% Sb_2O_3. The grain boundary contains Bi-related phases, $Bi_2Zn(Zn_{4/3}\ Sb_{2/3})O_6$ and $Zn(Zn_{4/3}\ Sb_{2/3})O_4$

The hypothetical microstructure proposed by the above hypothesis is shown in figure 3.3.

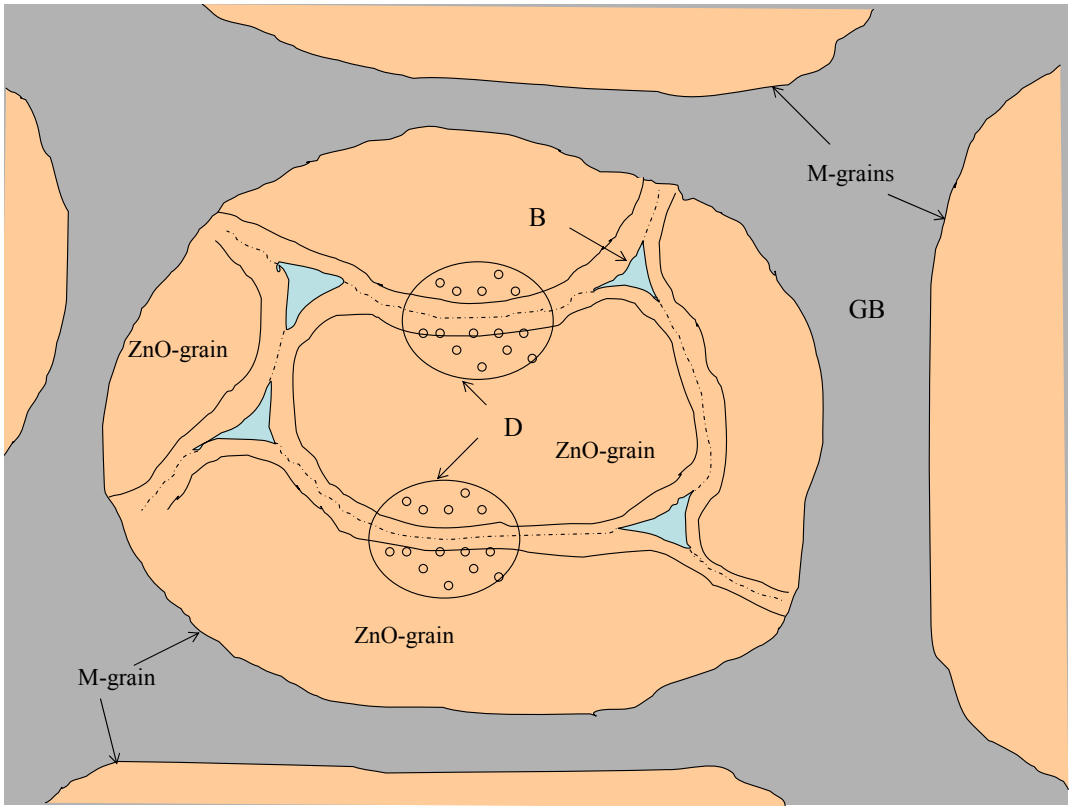

Figure 3.3: Model microstructure of an ideal ZnO-based MOV. B = a localised region in the sub-grain boundary between 2 adjacent ZnO grains rich in Bi-based phases, GB = grain boundary, D = area where potential barriers are set up. The grain boundary (GB) contains Bi-related phases **plus** LaB_6 and $SiTe_2$.

3.2.1 Theory of the Model

As mentioned in section 2.3, the ZnO-based commercial MOV is a VDR. That is, its microstructure shown in figure 2.5 and modelled as in figure 3.2 has a resistance R which is a function of the applied voltage. Thus R can be written as

$$R = R(V_a) = R_o V^{1-\alpha} \quad \ldots\ldots\ldots\ldots\ldots\ldots (3.1)$$

This expression translates to the equivalent circuit shown in figure 2.6.

Now to effect ideal V-I behaviour in the current ZnO-based commercial MOV, it requires that the effective resistance of the ideal MOV, R, must be some function of the applied voltage, V_a, as to be Heaviside's step-function-like, i.e.

$$R = R_{0,m} // R_{o.bg.b}\theta(V - V_{TH}) = R_{0,m} \times R_{0,g.b}\theta(V - V_{TH}) \Big/ \{R_{0,m} + R_{0,g.b}\theta(V - V_{TH}\} \quad \ldots\ldots\ldots\ldots\ldots\ldots (3.2)$$

with $\theta(V\text{-}V_{TH})$ defined thus

$$\theta(V\text{-}V_{TH}) = \begin{cases} 1 & : \ V < V_{TH} \\ 0 & : \ V > V_{TH} \end{cases} \quad \ldots\ldots\ldots\ldots\ldots\ldots (3.3)$$

Just as equation (3.1) translates to an equivalent circuit shown in figure 2.6, similarly equation (3.2) translates to some other equivalent circuit. Let this equivalent circuit be as shown in figure 3.4. This circuit can be reduced to that shown in figure 3.5, with $R_M = R_{o,m}$, and $R_{AD} = R_{o.g.b}\theta(V\text{-}V_{TH})$.

Figure 3.5 expresses the fact that the equivalent circuit of an ideal MOV is a parallel circuit of the resistance of the μ-MOVs, R_M, which is voltage controlled, and the resistance of a new switching element, R_{AD}, which is current controlled. This switching element will be called a *Bi-directional Current Controlled Zener Diode* (BCCZD). It is a kind of an avalanche diode (AD), and therefore can be represented in the circuit as an active device of resistance R_{AD}. From a microstructure point of view, this element is introduced by the characterisation process of powders used in the manufacture of the prototype MOV.

The theory of operation of the circuit in figure 3.4 and hence figure 3.5 is very similar to that of the commercial MOV (figure 2.6). The difference is the presence of R_{AD}, the resistance of BCCZD. BCCZD is highly insulating below and up to some threshold voltage. At the threshold voltage, it switches into a highly conducting state, where the current flowing becomes independent of the voltage.

The switching process of R_{AD} in figure 3.4 by-passes R_{ZnO}, and therefore removes the up-turn region of the V-I characteristic shown in figure 2.1, for R_{ZnO} is known

to be responsible for the up-turn region. This models how the up-turn region is removed.

The switching process of R_{AD} is due to some instability responsible for the breakdown. This instability has been coined the Γ-type instability. When the ceramic with this instability goes into breakdown, the rate of breakdown is so high such that the slope of the active region shown in figure 2.1 is close to zero. That is, a very small change in the applied voltage (ΔV) produces a very large change in the current flowing (ΔI). This makes the active region of the V-I characteristic due to the modelled prototype MOV shift towards the ideal case, namely, zero gradient.

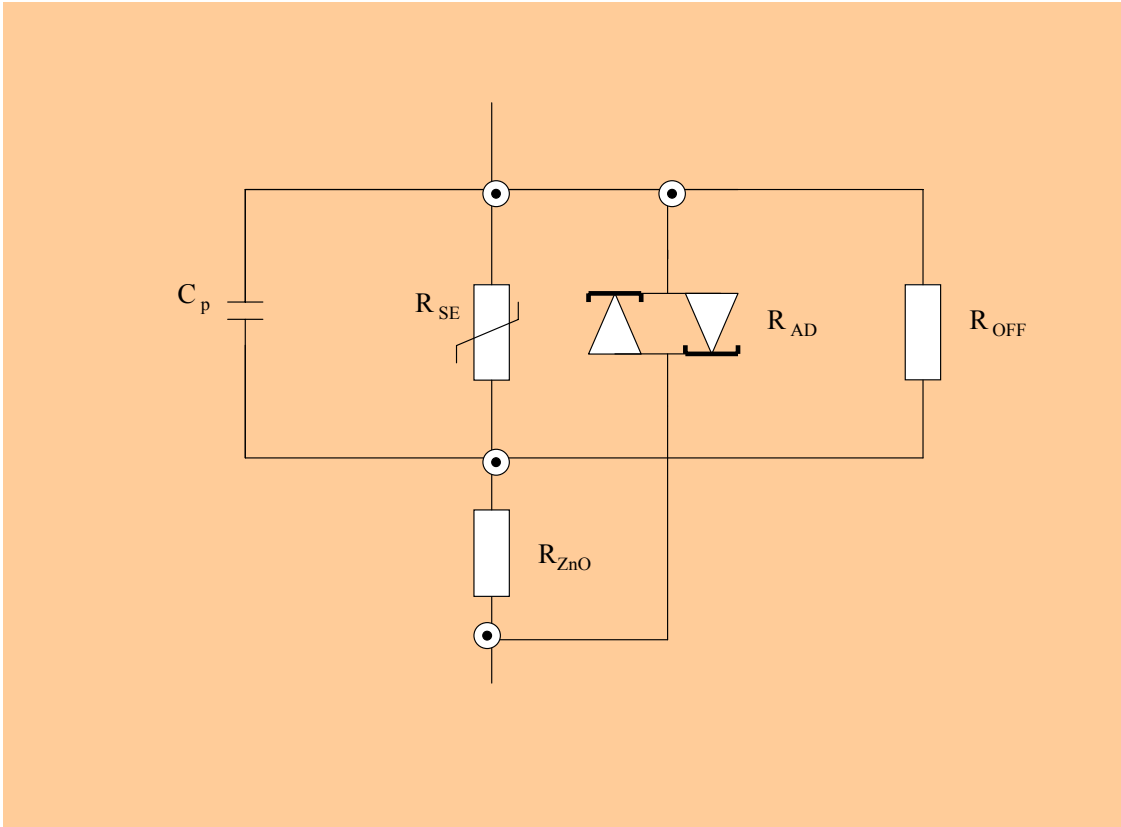

Figure 3.4: The equivalent circuit of a modelled prototype MOV with a near ideal V-I characteristic

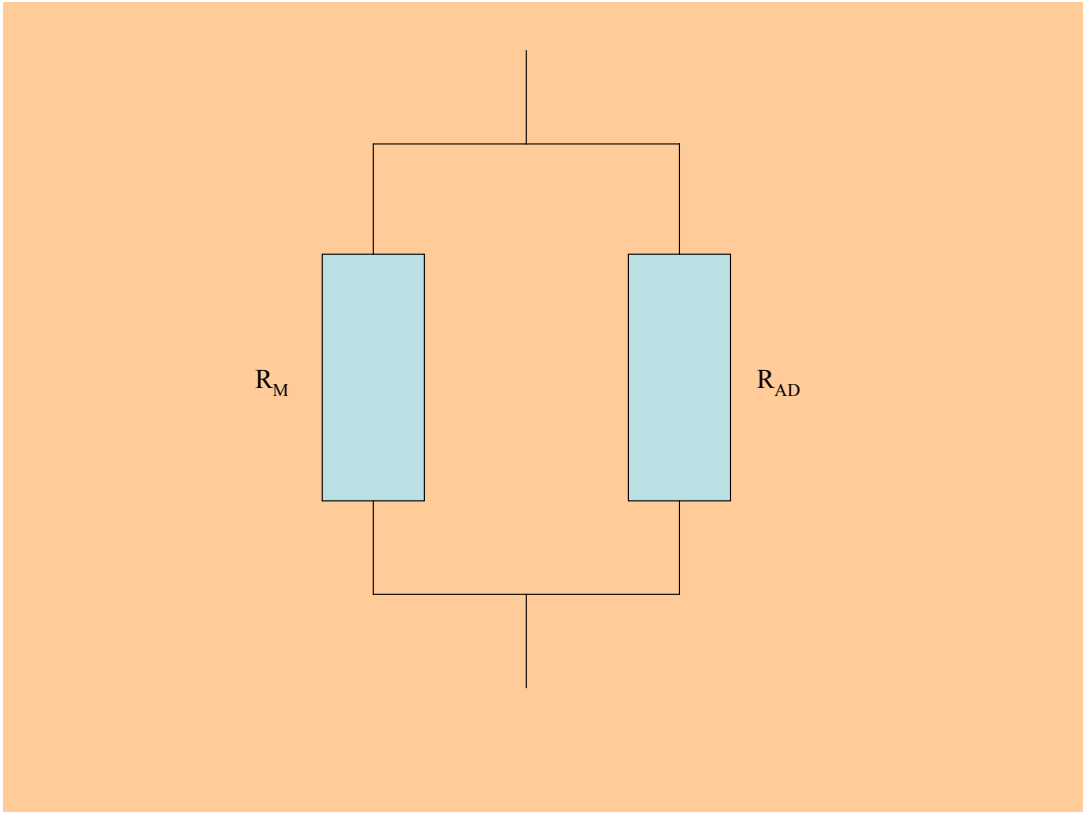

Figure 3.5: The reduced equivalent circuit of a modelled prototype MOV with a near ideal V-I characteristic

Although in figures 2.6 and 3.4, there is a circuit component denoted by R_{OFF}, its values are different in the two circuits. It is much higher in figure 3.4 than in figure 2.6. This makes the leakage current in the leakage region of the V-I characteristic due to the modelled prototype MOV shift towards ideal levels.

A ZnO-based MOV with a microstructure as modelled in figure 3.3, with a corresponding equivalent circuit as shown in figure 3.4 should give a near ideal V-I characteristic, see figure 2.11. The next chapter presents experimental procedures to get such a device using the above model.

4 EXPERIMENTAL PROCEEDURES

In the previous chapter a hypothesis and a model to be used to improve the leakage, active and up-turn regions of the V-I characteristic of a ZnO-based commercial MOV was presented. This chapter presents experimental procedures used to fabricate a prototype MOV with lower leakage currents, improved active region and no up-turn region of the V-I characteristic. It also presents methods used to test the prototype and how the phases and microstructures were studied.

According to the model, it was necessary to characterise some of the powders before fabrication could be done in order to obtain desired electrical characteristics in the product.

4.1 Powder Characterisation

The as-received powder types and their grain sizes are given in Table 4.1.

Table 4.1: As-received powders and their grain sizes

Powder Name	**Powder grain size (μm)**
Zinc Oxide (ZnO)	< 1
Bismuth (III) Oxide (Bi_2O_3)	< 10
Cobalt Oxide (CoO)	44
Manganese (II) Oxide (MnO)	250 - 88
Nickel Oxide (NiO)	44
Lanthanum Hexaboride (LaB_6)	< 10
Tellurium (Te)	74
Arsenic (As)	150
Silicon (Si)	44
Germanium (Ge)	150

From some of the as-received powders, characterised powders were prepared on the basis of the model presented in Chapter 3. These are:

(i) the $\boldsymbol{M}$ -powder

(ii) the $\boldsymbol{Q}$ -powder and

(iii) the $\boldsymbol{O}$ -powder

The characterisation of powder $\boldsymbol{M}$ was in respect of the varistor property and hence N-type instability. That is, the powder grains were to be macro-MOVs as per model. To ensure that they retained the varistor property, the grain size of the powder was set to $\leq$ 53 μm. Larger grain sizes retain the varistor property but results in a leaky product after sintering, and this is undesirable. There is also a lower limit in grain size upon which the varistor property can still be maintained.

The $\boldsymbol{M}$ -powder was prepared according to the following composition: 93.23 wt% ZnO + 5.47 wt% Bi_2O_3 + 0.88 wt% CoO + 0.42 wt% MnO. This is a typical composition that will produce the needed varistor property in the powder grains. It is also a typical composition for low and medium energy commercial MOVs. The powder was prepared thus: The respective powders were weighed out according to the above proportions and milled for six hours in a planetary mill using 20 mm tungsten carbide (WC) balls. The powder mixture was then weighed out in 5 g batches into petri-dishes, followed by granulation. Distilled water was used for granulation and to act as a binder. The granulated 5 g batches were bi-directionally compacted using a 20 mm diameter die and a press. The compaction pressure was 50 MPa. The compacted blocks measuring 20 mm in diameter and 5 mm in thickness were then dried at 100 °C for 1 hour. They were then sintered at 1250 °C in static air for 1 hour and furnace cooled to room temperature. The as-sintered blocks measured on average 19 mm in diameter and 4 mm in thickness. These blocks were V-I tested as well as impulse tested to ensure that their electrical behaviour was similar to that of a commercial MOV. That is, to ensure that they had the varistor property (VP).

The as-sintered blocks were milled using the Sieb technique mill and sieved to obtain a powder of grain size of ≤ 53 μm. Because the milled blocks had the varistor property, the powder grains were considered to be small varistors or micro-varistors (μ-MOVs).

The powder denoted by ***Q*** was prepared in like manner. The differences were in the composition of the starting powders, total mass of the powder mixture, sintering temperature and method of cooling. The powder was prepared according to the following composition: 71.57 wt% Bi_2O_3 + 11.51 wt% CoO + 5.45 wt% MnO + 11.47 wt% NiO. The green compacts had a mass of 4.0 g. The sintering temperature was 800 °C, and after the 1 hour soaking time, the as-sintered blocks were air quenched. Its grain size after milling and sieving as mentioned above was also ≤ 53 μm.

The characterisation of the ***Q*** -powder was in respect of avalanche instability and energy handling capability. It is known that direct addition of powders CoO, MnO and NiO in the presence of Bi_2O_3 in the fabrication of ZnO-based commercial MOVs promotes thermally assisted avalanche instability and enhances energy handling capability. In this investigation, strong **E**-field instability, reduced thermally assisted avalanche instability and enhanced energy handling capability were need, hence indirect addition was done. Why this approach is because in direct addition preferential reactions occur than in indirect addition. As outlined in Chapter 2, the commercial ZnO-based MOV has a strong thermally assisted avalanche instability, which promotes MOV degradation mechanically as well as its V-I characteristic electrically. Thus the ***Q*** -powder when used in the fabrication of the prototype MOV, the resulting ceramic would have reduced thermally assisted avalanche breakdown, and that it would be able to handle large amounts of heat from the surge before it fails.

The characterisation of powder denoted by $\boldsymbol{O}$ was in respect of the S-type instability as required in the model. It was prepared according to the following formula: 65.5 wt% Te + 24.3 wt% As + 2.9 wt% Si + 7.3 wt% Ge (Deis *et al*, 1970). As before the respective powders were weighed out according to the above proportions. The powder mixture was loaded into a glass ampoule and sealed under vacuum. The ampoule was tumbled on a tumble roller for 1 hour to homogenise the powder. Thereafter, the homogenised powder mixture was heat treated at 900°C in static air for 24 hours, after which the ampoule was ice-water quenched. By breaking the glass, the heat treated contents were extracted from the ampoule. Two phases were produced. One was a glassy, silvery clinker and was code-named silvery phase (*s-phase)*. The other was a black phase, amorphous in character. It was likewise code-named black phase (*b-phase)*. Both phases were V-I tested. The s-phase gave a V-I curve similar to that reported by Deis *et al* (1970). The b-phase was found to be highly insulating for the voltage range used. As mentioned earlier in Chapter 2, the above composition is one among many other silicon-tellurium-arsenic-germanium compositions, the so-called STAG compositions, that posses S-type instability, when heat treated typically as above. Such instability was first reported Ovshinsky (1968) using a similar composition. Thus the s-phase was the desired one. It is the phase that produces the S-type instability when subjected to an electric field.

To obtain the powder, the clinker of the s-phase was milled as mentioned above and sieved to grain size of ≤ 63 μm. The characterisation was in respect of its electrical behaviour and grain size. This grain size was chosen to ensure that the characterisation was not destroyed.

Because the b-phase was 'discarded', the $\boldsymbol{O}$ -powder refers to the s-phase henceforth.

Powders $\boldsymbol{Q}$ and $\boldsymbol{O}$ served as characterised additives in the fabrication of prototype MOVs. From XRD studies, the s-phase was found to be $SiTe_2$ and the $\boldsymbol{Q}$ was found to be a Bi-Co-Mn-Ni-based compound.

4.2 Fabrication of Prototype MOVs

After a series of trial runs, a prototype MOV of composition

$\boldsymbol{M}$ + 2.8 wt % $SiTe_2$ + 1.4 wt % Bi_2O_3 + 2.8 wt % $\boldsymbol{Q}$ + 1.4 wt% LaB_6

was fabricated. The prototype MOVs were fabricated using characterised as well as as-received powders. Conventional compaction and sintering techniques were employed. The process used for fabricating the prototype MOV is described below.

The powders were weighed out separately in the required proportions so as to give a powder mixture of total mass of 4 g. This was the total mass needed to form one green compact. Then all the additives were blended together, loaded into poly-top bottles and homogenised separately from the $\boldsymbol{M}$ - powder. The homogenisation was done by tumbling on a tumble roller for 1 hour. Thereafter the $\boldsymbol{M}$ -powder was introduced to the homogenised composite additive powder mixture. The total powder mixture was then homogenised as before. Thereafter the homogenised powder mixture forming the above compositions was weighed out in 4 g batches for compaction. Compaction was done at 50 MPa as described before.

A set of nine (9) such green compacts measuring on average 19 mm in diameter and 4 mm in thickness were prepared. After drying for 1 hour in a drying oven, the green compacts were heated in static air to 850 °C at a rate of 20 °C min^{-1}. They were soaked for 1 hour at 850 °C and then air quenched. The as-sintered prototype MOV blocks weighed on average 3.90 g and measured on average 17.00 mm in diameter and 3.65 mm in thickness.

The nine as-sintered MOV blocks were distributed as follows: three (3) were used for electrical testing, another three were used for XRD studies and the last three were used for SEM studies. These are described in the following sub-sections.

It is noteworthy that several such runs were made to ensure repeatability.

4.3 Electrical Testing of Prototype MOV

The as-sintered prototype MOV blocks were V-I tested to determine the nature of the V-I characteristic, and they were impulse tested to determine the surge clamping action. In order to carry out these electrical tests, it was necessary to mount wire electrodes onto the opposite faces of the as-sintered blocks using colloidal silver paste. The MOV blocks with the affixed electrodes were then mounted onto an in-house fabricated test rig (figure 4.1) for testing.

Due to what I later termed as the "*electrode effect*" (see Discussion), one other prototype MOV block had its opposite faces coated to about 90% with the modified In/Ga alloy and tested using pressure electrodes. That is, the coated block was positioned between the two brass rods shown in figure 4.1 and then pressure applied by "screwing in" the threaded brass rods and then tested. This was done so as to compare results of prototype MOVs tested using silver paste mounted wire electrodes.

From the foregoing prototype MOVs were tested using two types of electrode systems:

(i) silver paste mounted electrode wires;

(ii) In/Ga coated blocks using pressure electrodes (u.p.e.).

Henceforth these were termed type (i) and type (ii) electrode systems.

For the "In/Ga coated blocks using pressure electrodes (u.p.e.)", a modified indium/gallium (In/Ga) eutectic liquid was used as the coating material. It was modified because the as-received alloy had very low viscosity, i.e., it was watery and ran off the MOV block surfaces. Indium powder was used to increase the viscosity of the liquid alloy.

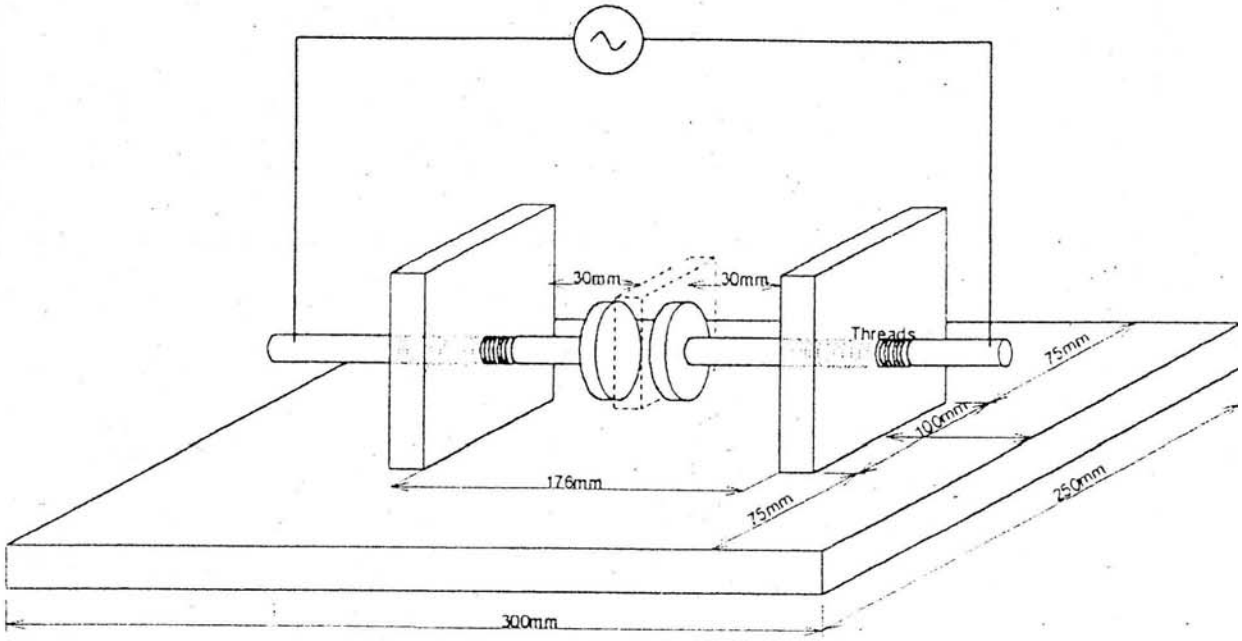

Figure 4.1: Test rig for electrical tests.

To make comparative tests, a commercial MOV of comparable dimensions, V275K20P, was first tested as received. It was then brought to the same conditions as the fabricated prototype MOV, that is, "acclimatised" and then tested as above. The "acclimatisation" was done as follows: Two as-received V275K20P MOVs had their resin coating stripped, electrode wires pulled off and the electrode mounting and coating material ground off so that they were similar to the as-sintered prototype MOV blocks. Thereafter, one of these blocks had about 90% of its faces coated with the modified In/Ga alloy. It was code-named "V275K20P block (coated) (In.Ga)(u.p.e.)", that is type (ii) electrode system. To the other one, wire electrodes were mounted using silver paste, thus acclimatising

the V275K20P MOV block to type (i) electrode system. It was code-named "V275K20P block (acclimatised)".

4.3.1 Determination of the V-I characteristic

The V-I characteristic was determined by the two-point electrode method, see figure 4.2. Only prototypes using the silver paste mounted electrode wires were tested; those using pressure electrodes gave unsatisfactory results. Data was obtained by varying the voltage (V) and recording the corresponding current (I). The V-I characteristics were plotted using Excell.

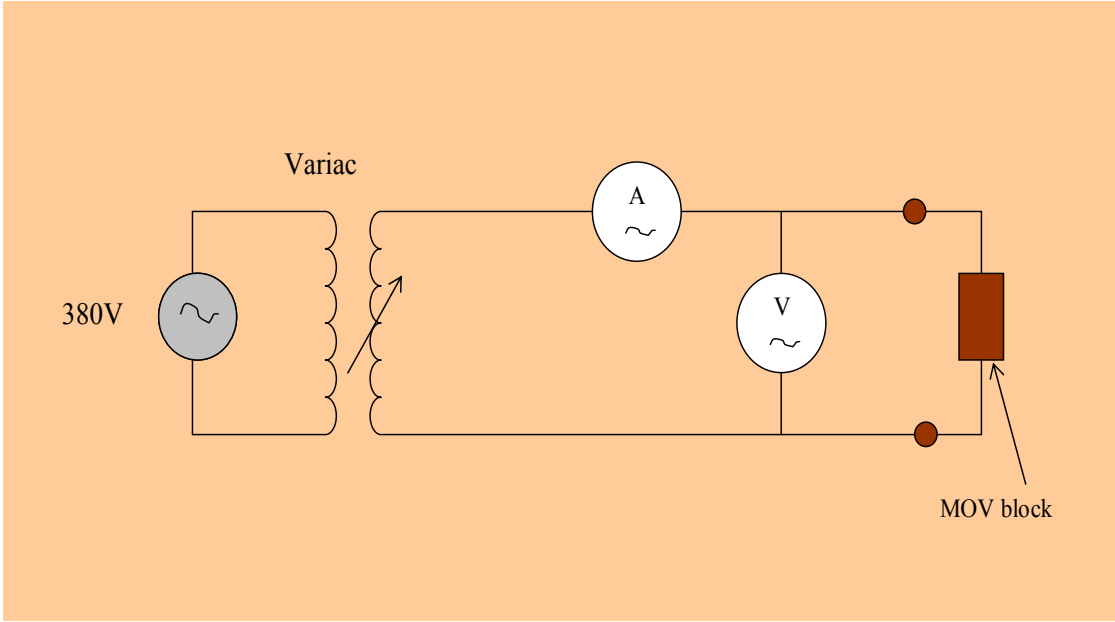

Figure 4.2: Circuit used to obtain V-I data for the V-I characteristic.

From Chapter 2, Section 2.1, it was pointed out that the V-I characteristic of a commercial MOV has three (3) regions, namely the leakage, the active and the up-turn regions. In order to quantify the degree of improvement in the leakage region, it was necessary to compute the area under the curve of the V-I characteristics of the prototype MOV as well as that of the experimentally determined V-I characteristic of the as-received commercial MOV.

4.3.1.1 Determination of the area of the leakage region of the V-I characteristic

Referring to figure 2.15, the method used to determine the area under the V-I curve defined by the leakage region is described below.

a) Determine the point where the curves start to leave the V-axis, that is, the tangent to the curve, call it P_1. $P_1 = (I_1,V_1) = O$

b) The V-I curve in the active region is generally horizontal. Draw a line coincident with the active region. Where it makes a tangent with the curve, call it P_2. $P_2 = (I_{12},V_2) = A$

c) The locus defined by points P_1 P_2 is generally hyperbolic and defines the ohmic region *plus* the pre-breakdown region. The I-V relation of the pre-breakdown region is generally given by Varistor Equation (equation 2.1) with $\alpha = 2$, i.e. Childs Law,

$$I = \kappa V^2, \quad \text{..... (4.1)}$$

d) The area, S_1, under the curve bounded by the curve, points P_1, M and P_2 is determined from

$$S_1 = \int_{I1}^{I2} V dI = \tfrac{2}{3}\frac{1}{\kappa'} I^{3/2} + C \Big|_{I1}^{I2} \quad \text{..... (4.2)}$$

For simplicity, since the κ' is a constant, and the specimens were of the same composition and same dimensions, κ' is taken to be unity.

4.3.1.2 Determination of the α

The degree of non-linearity, that is the degree of flatness in the active or breakdown regions of the V-I curves of prototype MOVs, is measured by the non-linearity index, α. The larger it is, the nearer the active region is towards the ideal active region ($\alpha = \infty$). The α-values for the determined V-I characteristics were determined from the V-I data and calculated using equation 4.3, which is derived from equation (2.1) (Matsuoka *et al*, 1970), (Matsuoka, 1971), (Morris, 1973), (Wong *et al,* 1974), (Wong, 1980), (EPCOS, 2001).

$$\alpha = \frac{\log I_2 - \log I_1}{\log V_2 - \log V_1} = \frac{1}{\log(V_2/V_1)} \quad \text{..... (4.3)}$$

where V_1 is the voltage across the MOV block when the current flowing through it, I_1, is 1 mA. V_2 is the voltage when the current flowing I_2, is 10 mA (Eda, 1979).

4.3.2 Determination of Surge Voltage Clamping Action

In order to determine the surge voltage clamping capability of the fabricated prototype MOVs, the prototype MOVs were impulse tested using an impulse generator in the combinational mode, see figure 4.3. The standard lightning waveforms, namely 1.2/50μs for the voltage and 8/20μs for the current, were used. A 1000:1 high voltage probe and 100:1 Rogowski coil were used to measure voltage and current respectively. The prototype MOV blocks were impulse tested using both electrode systems. The applied impulse voltages were in the range 0.5 - 1.5 kV. Higher voltages were avoided due to surface flashovers across MOV blocks due to ionisation and subsequent breakdown of the surrounding air.

Again for comparative purposes, the commercial MOV, V275K20P, was also impulse tested first in the as-received state and then with types (i) and (ii) electrode systems.

Figure 4.3 shows the generator arrangement in the combinational mode while figure 4.4 gives the equivalent circuit.

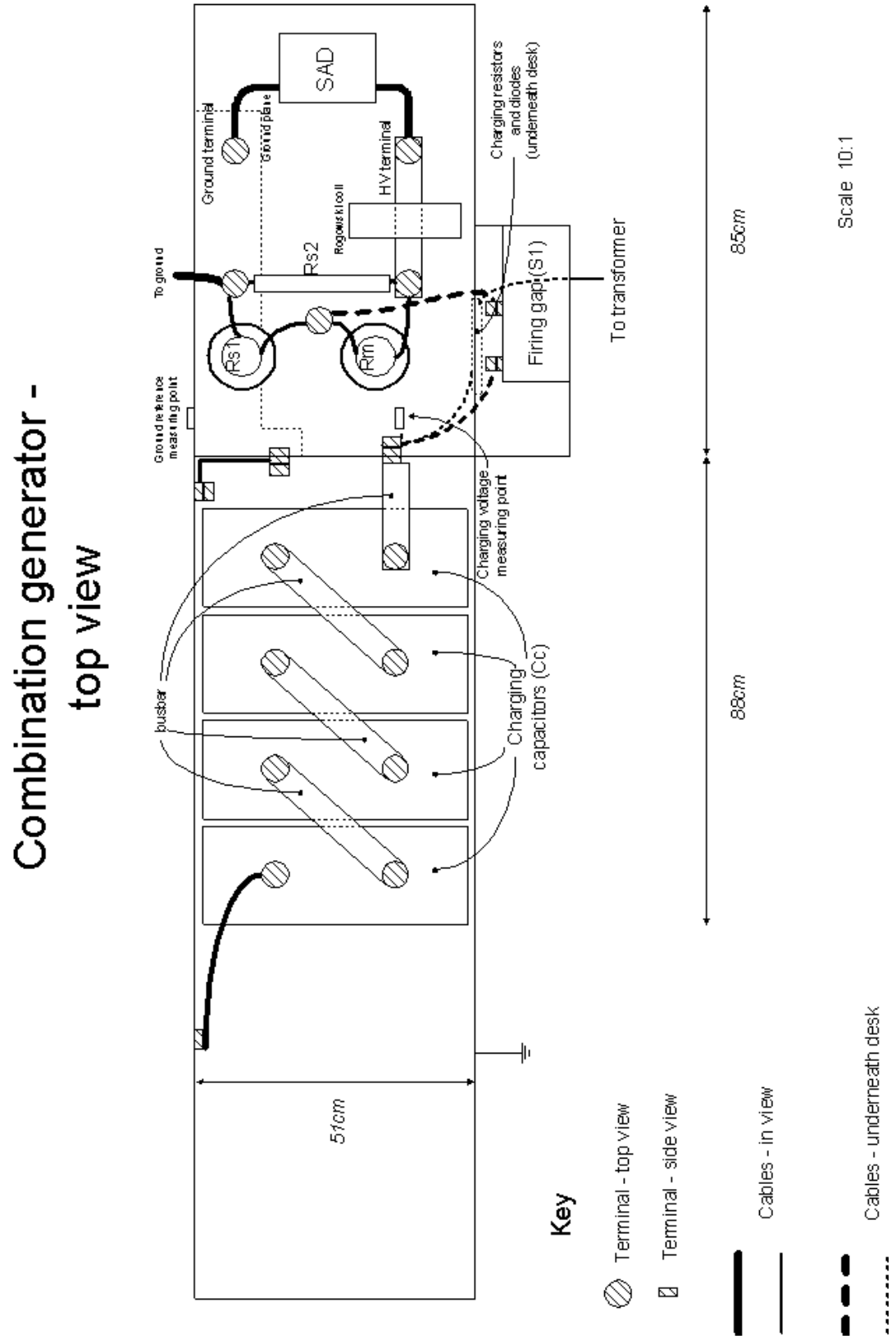

Figure 4.3: Impulse generator arrangement in the combinational mode (Beutel, 2000), S = sample

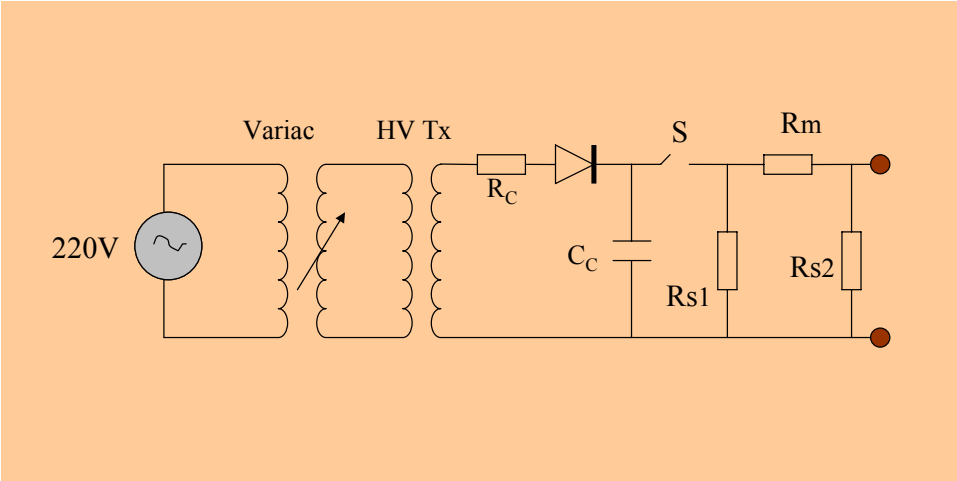

Figure 4.4: Impulse generator equivalent circuit in the combinational mode

In the above circuit, R_c is the charging resistor, C_c is the bank of capacitors, S is the trigger switch, R_m, R_{s1} and R_{s2} are wave-shaping elements. The test piece mounted on the test rig was then connected to the output of the impulse generator.

4.4 Microstructure and Phase Analysis

Since the microstructure determines the electrical behaviour of a material, in this case the V-I characteristics and surge clamping action, it was necessary to study the microstructures and phases of the fabricated prototype MOVs to establish the correlation. For comparative analysis, the microstructures and phases of V275K20P was studied too.

The microstructures were studied using a Joel JSM 840 Scanning Electron Microscope that had an Energy Dispersive Spectroscopy (EDS) facility. The phases were studied using a Bruckner AXS D8 Advance XRD machine.

In order to uniquely identify the phases present in the prototype MOV as well as the commercial MOV studied, the phases present in the as-received powders ZnO, Bi_2O_3, CoO, MnO and NiO were individually studied. The phases were then determined by "peak-matching" the d-peaks of the experimentally determined

XRD patterns with those from the database of the XRD machine. Published data by was also used as an aid in the identification of phases. The XRD data of Te, As, Si and Ge was obtained from the database of the XRD machine. These phases were then related to those obtained in the XRD pattern of the prototype MOV as well as the studied commercial MOV.

.

Having outlined the experimental procedures used to fabricate, test, and study the phases and microstructures of prototype MOVs, the results are presented in the next chapter.

5 RESULTS

In the previous chapter the experimental procedures used to fabricate, test, and study the phases and microstructure of a prototype MOV were presented. In this chapter the V-I characteristic of the ZnO-based prototype MOV with improvements in the leakage, active and up-turn regions over that of a dimensionally comparable commercial ZnO-based MOV are presented. The surge clamping action of the studied prototype MOV is also presented and so is the microstructure and phases.

Figure 5.1 shows a typical prototype MOV block as well as the ready to use prototype MOV studied.

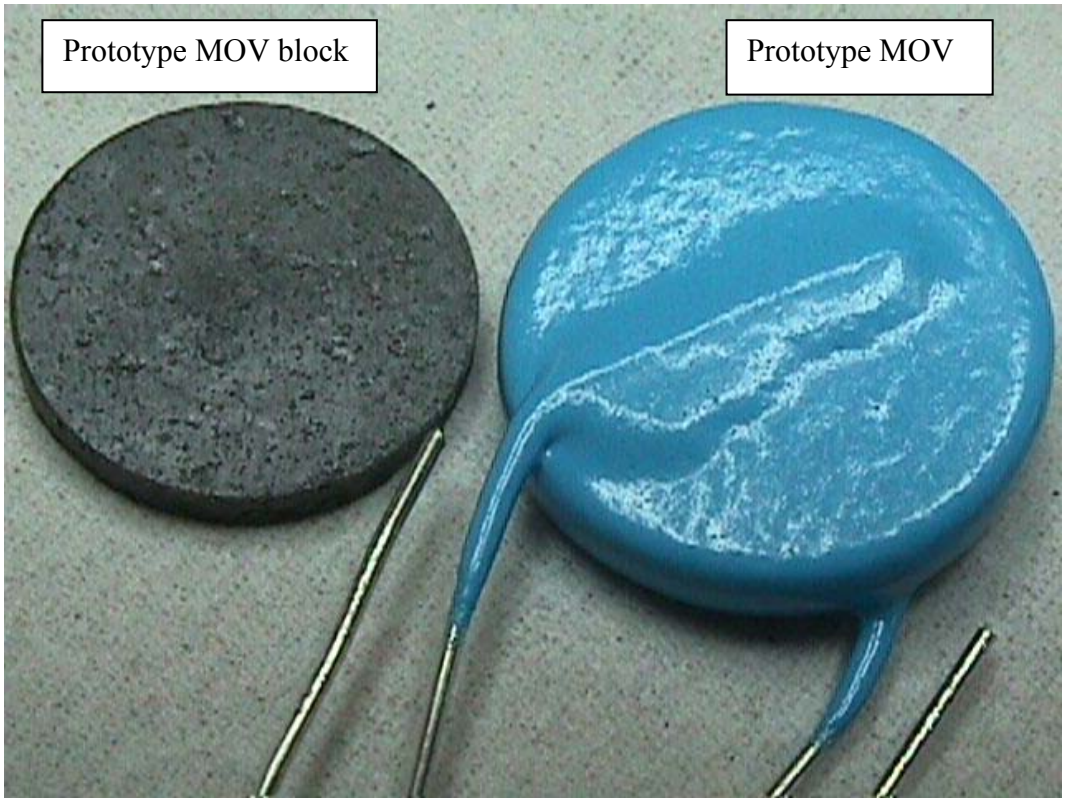

Figure 5.1: Typical prototype MOV block studied. Also shown is the prototype MOV

5.1 The V-I Characteristic

Only the V-I characteristic of the prototype MOV block tested using type (i) electrode system is presented; the one that was tested using type (ii) electrode system gave an unsatisfactory curve.

The V-I characteristic of the prototype MOV is shown in figure 5.2. Using equation (4.3), the α-value of the characteristic was found to be 30.02. This value is comparable to α-values of typical medium energy ZnO-based commercial MOVs. Of significance is the fact that the characteristic has two (2) regions, namely the leakage and active regions. This is unlike the studied commercial ZnO-based MOV, V275K20P, which has three (3) regions, both determined from this study and known from literature. As will be presented in Chapter 6, the above V-I characteristic is near ideal and is an improvement over that of the studied commercial MOV. It will be shown then that the improvement is three-fold: a) the leakage region was reduced by 1%, b) the rate of breakdown in the active region was increased and discharge currents were increased by on average 4 times those of a the studied commercial MOV. The instability responsible for this breakdown was found to be field dependent instead of thermal. c) the up-turn region was removed.

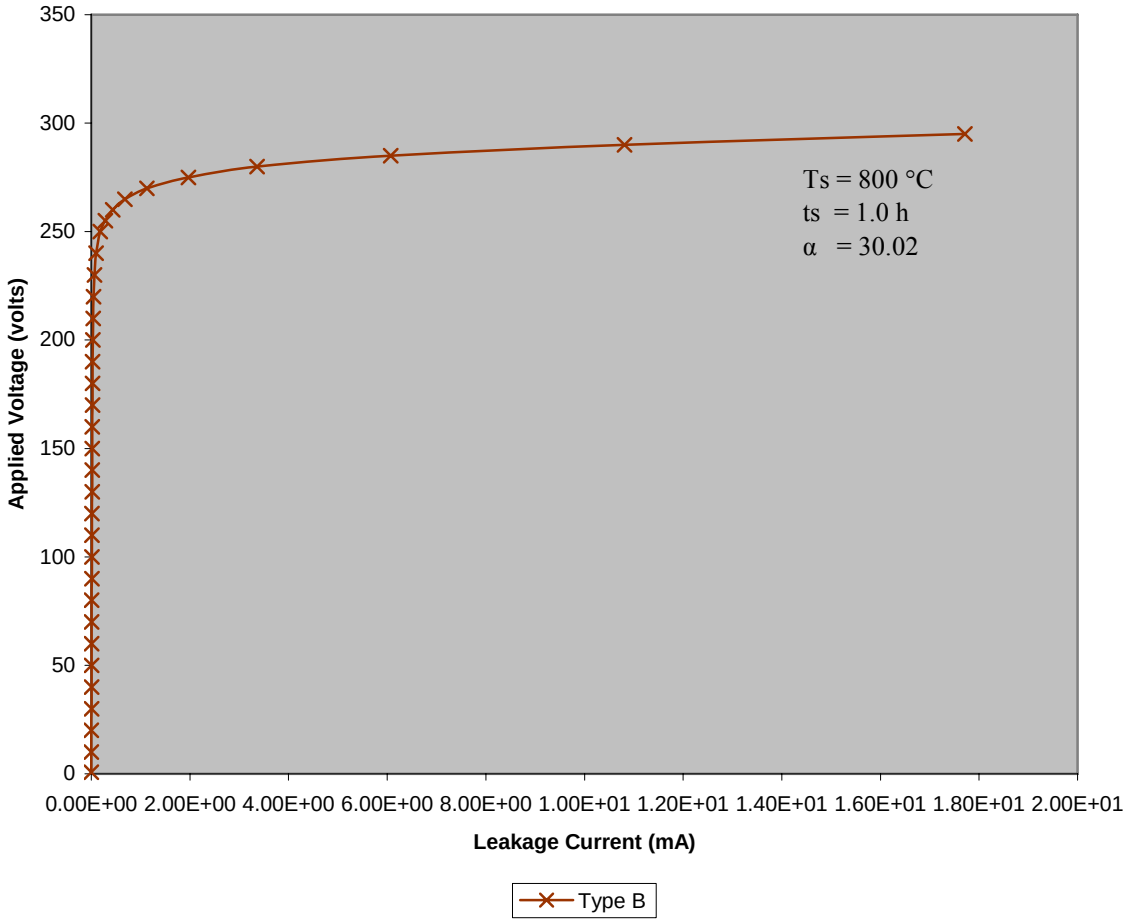

Figure 5.2: The V-I characteristic of the prototype MOV

It is noteworthy that this V-I characteristic is identical to that predicted by the model, namely, figure 2.11.

5.2 Surge Clamping Action

Since the area of focus was on the improvement of the V-I characteristic, it was sufficient to establish that the surge clamping action was not sacrificed. However it was and still is inherently believed that an improvement in the V-I characteristic should reflect an improvement in the surge clamping action. That this is so is highlighted below.

The surge clamping action of the prototype MOV is shown in figure 5.3 for applied surge voltages in the range of 0.5 -1.5 kV. The results obtained using type (i) electrode system are shown as figure 5.3 (a1)-(e1); those obtained using type (ii) electrode system are shown as figure 5.3 (a2)-(e2).

The results obtained using type (i) electrode system show that the prototype MOV is in the open circuit state for an applied surge voltage of 0.50 kV, figure 5.3 (a1). It starts to conduct at an applied surge voltage of 0.80 kV, see figure 5.3 (a2). For higher applied surge voltages, it is conducting. Its surge voltage response action is characterised by a voltage "hump", the amplitude of which increases with increase in the applied surge voltage. The surge current also increases with increase in the applied surge voltage. Whether it is surge clamping or not is discussed in Chapter 6.

When the prototype MOV was tested with type (ii) electrode system, its surge voltage response was similar but noticeably different to that when using type (i) electrode system. What is strikingly clear is that the surge current is much larger when using type (ii) electrode system. The voltage "hump" is also much more pronounced than when using type (i) electrode system. Further, the voltage waveform of the clamped surge voltage "tails off" to a constant level when using type (ii) electrode system, whereas in type (i) electrode system the voltage waveform "tails off" to different levels, the level of which increases with increase in the applied surge voltage. Such is the influence of the type of electrode system used.

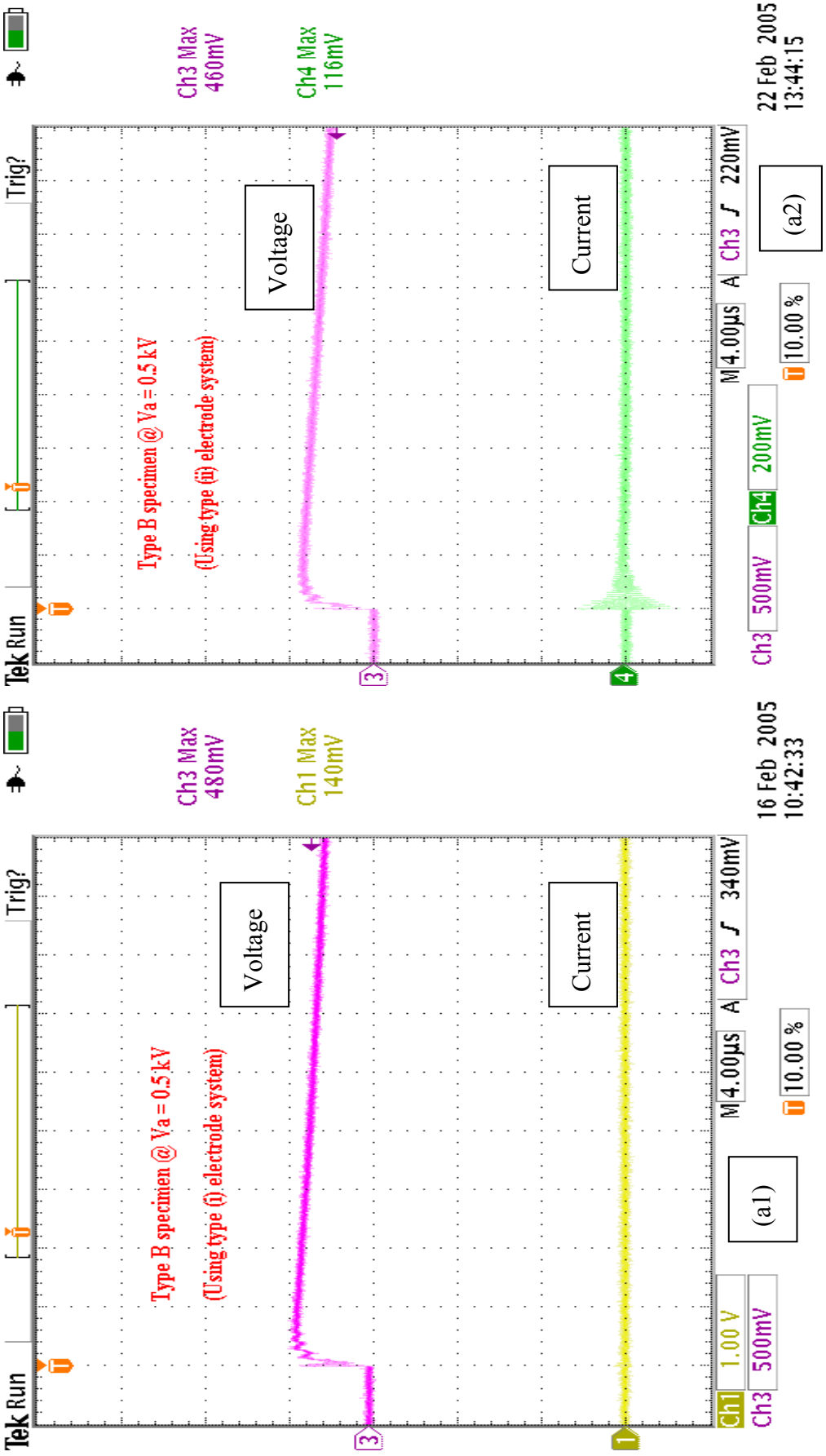

Figure 5.3 (a): Surge response action of prototype MOV @ 0.5 kV giving an open circuit condition.

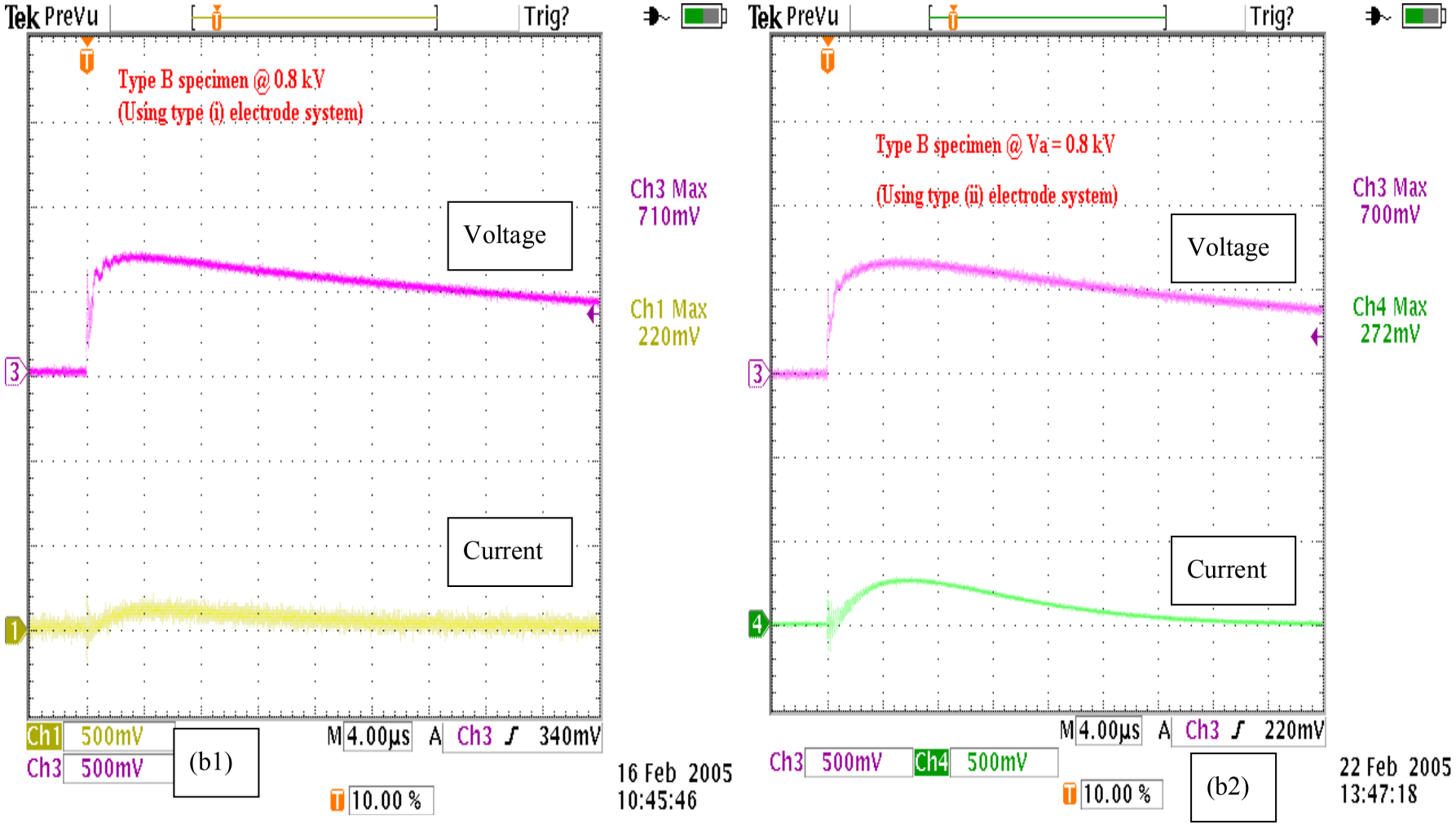

Figure 5.3 (b): Surge response action of prototype MOV @ 0.8 kV, now conducting

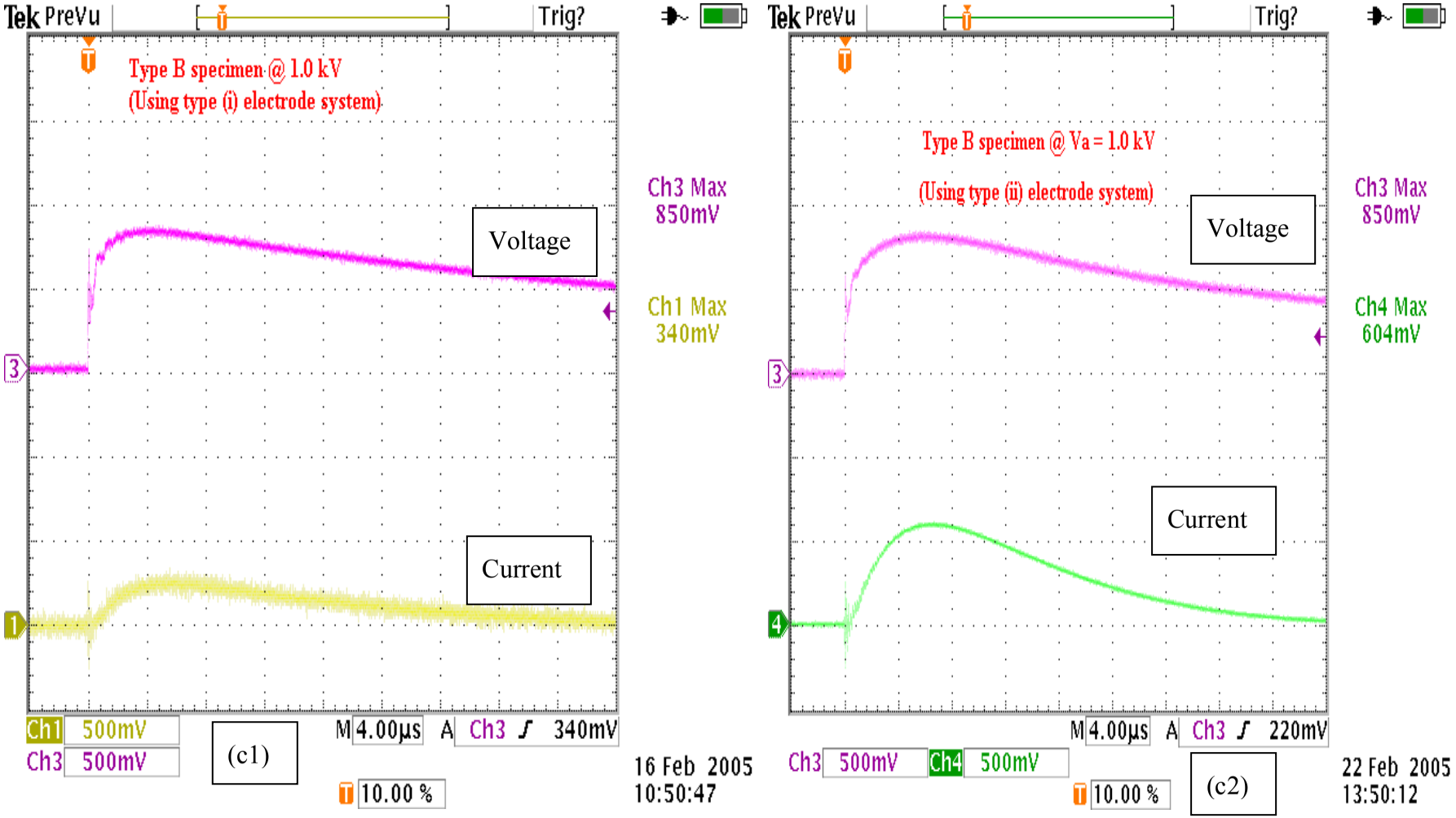

Figure 5.3 (c) : Surge response action of prototype MOV @ 1.0 kV.

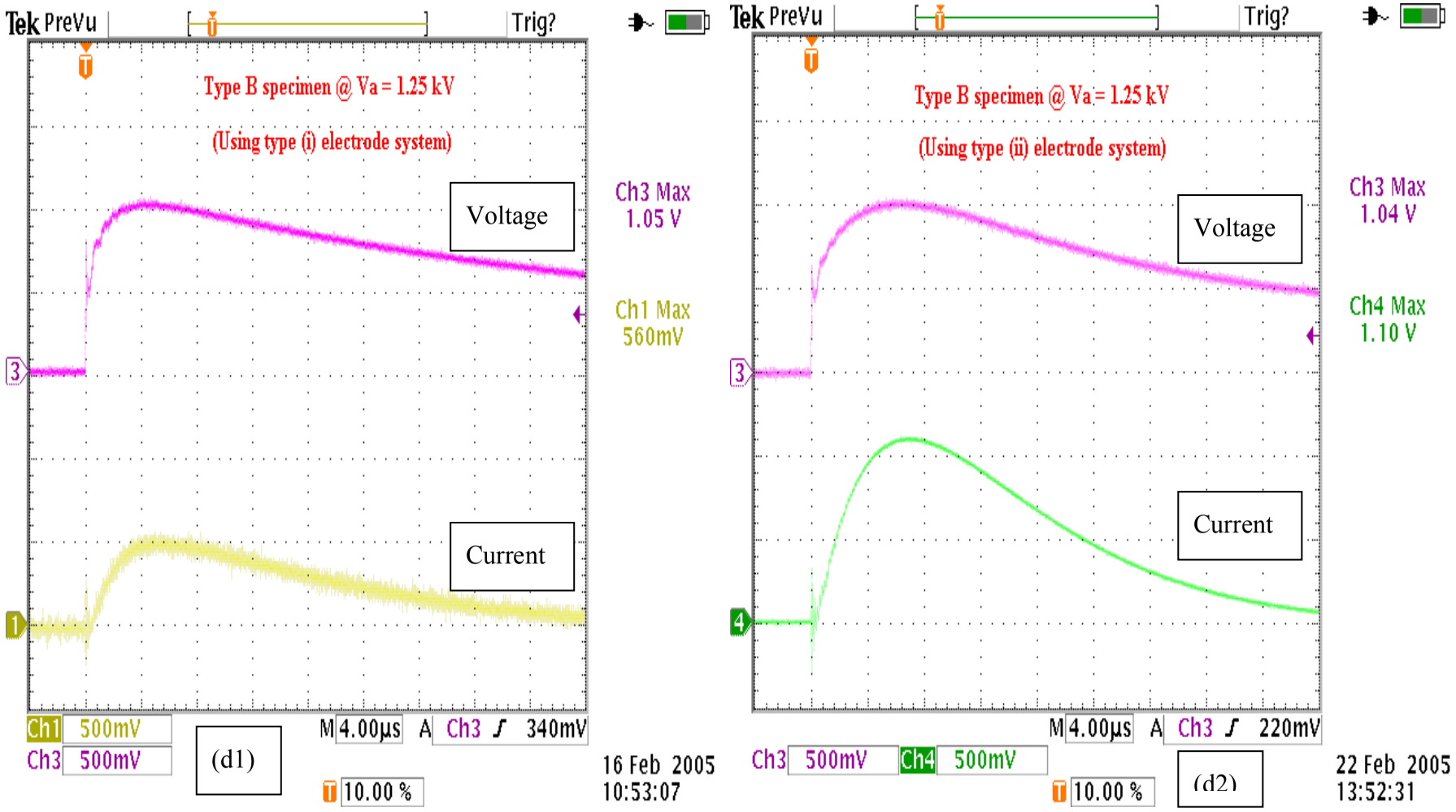

Figure 5.3 (d): Surge response action of prototype MOV @ 1.25 kV.

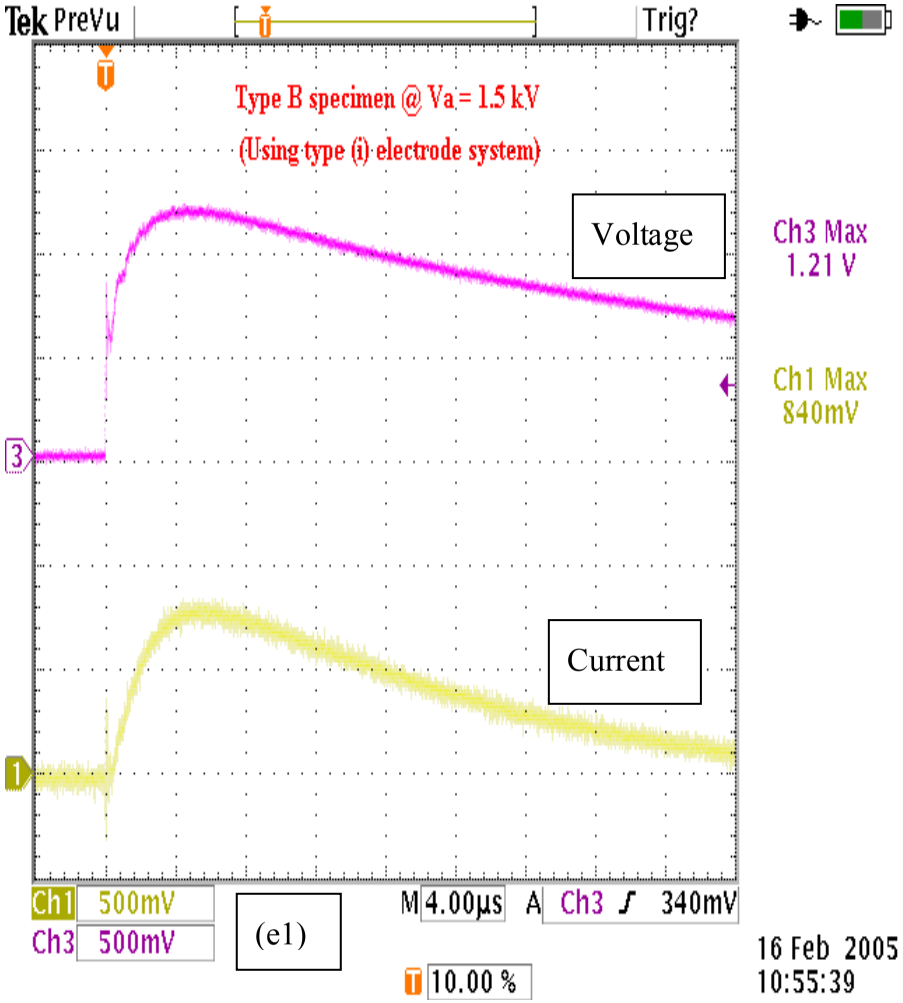

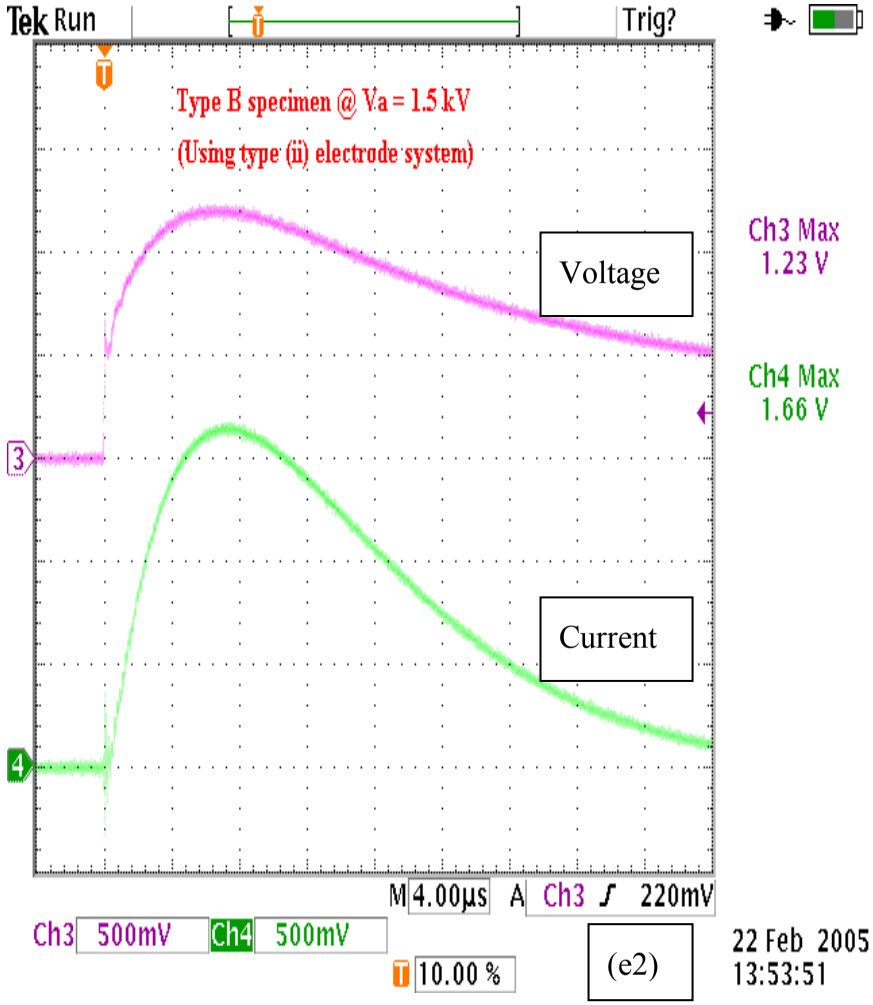

Figure 5.3 (e): Surge response action of prototype MOV @ 1.5 kV.

5.3 Microstructure and Phases of Prototype MOV

5.3.1 Microstructure

The observed electrical behaviour is due to microstructural characteristics. The microstructure of the prototype MOV is shown in figure 5.4.

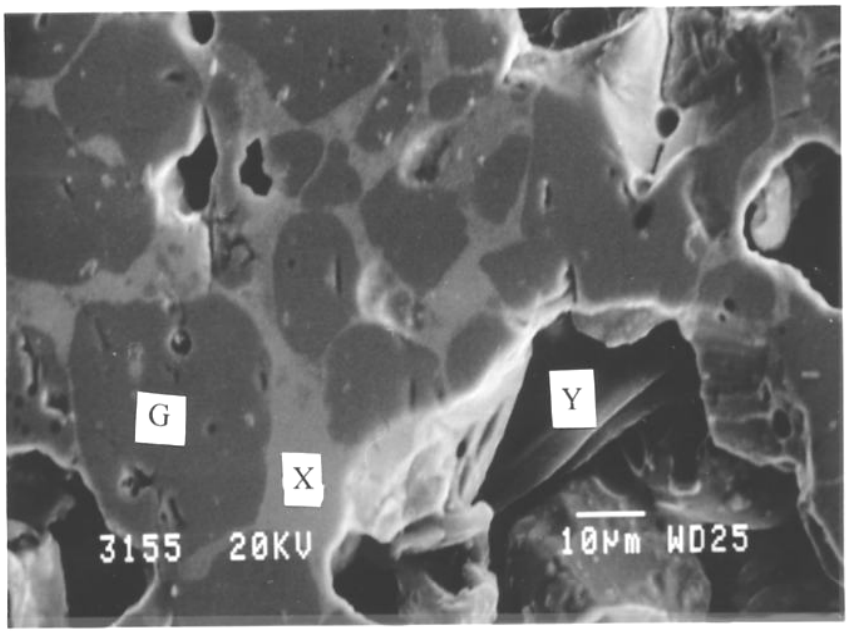

Figure 5.4: Microstructure of the prototype MOV showing a) grey grains (G), separated by b) a light-grey grain boundary material (X), and c) "rod-like structures" (Y) running across a pit

The microstructure of the prototype MOV was found to be poly-phase. It consists of large grey grains that are separated by a poly-phase inter-granular material, and "rod-like" structures that run across pores and pits. Not shown in this image are very white lumpy amorphous structures that are sparsely populated and randomly distributed. The structure is also porous.

From EDS, a spot scan analysis revealed that the grey grains were composed of Zn, Co and Mn. This is shown in the EDS spectrum in figure 5.5. An areal scan analysis showed that in addition to the above, the grains also contained Bi. Why the spot scan did not show the presence of Bi is presented in the "Discussion", section 6.3.1.

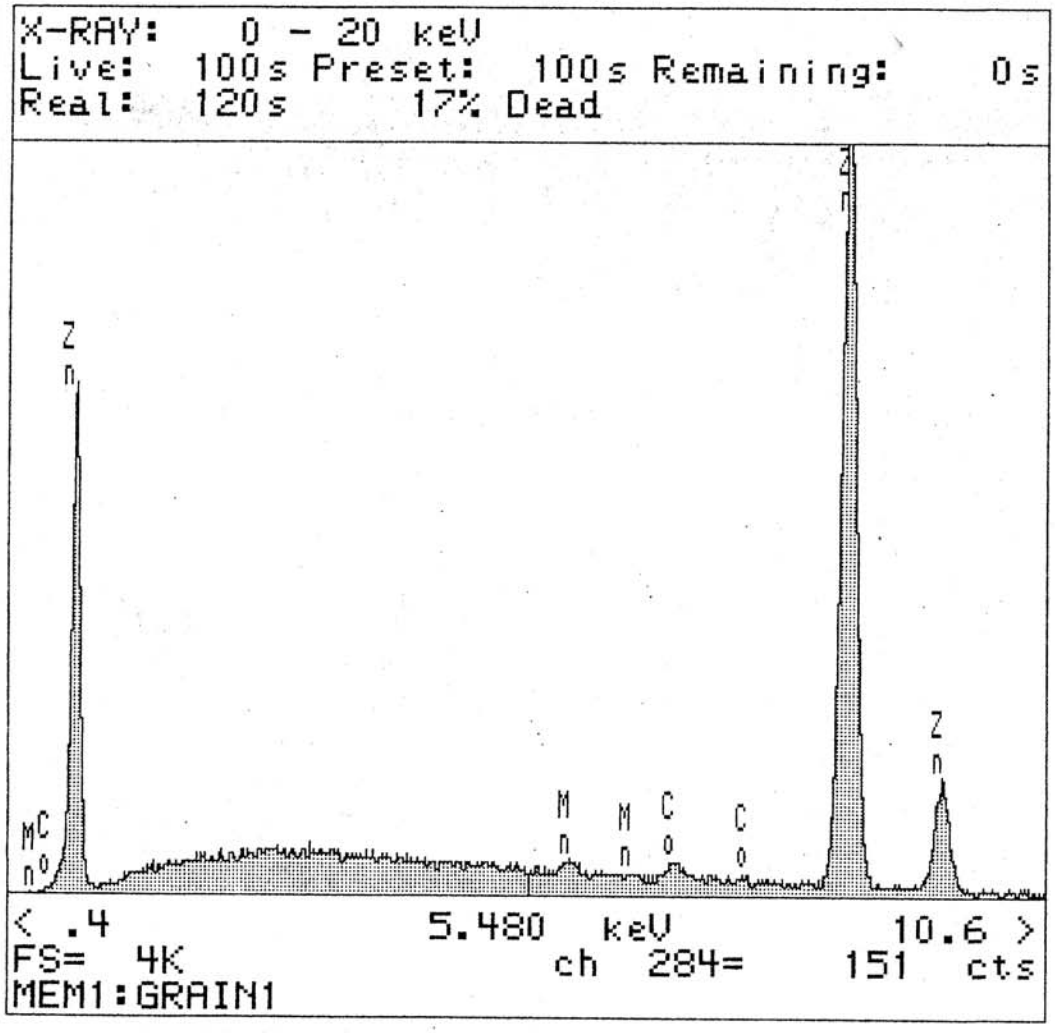

Figure 5.5: EDS spectrum of the prototype MOV, showing the elements in the grey grains in figure 5.4.

Again from EDS an areal scan analysis of the grain boundary material showed that the elements in the matrix were Zn, Bi, Te, Si., Cd, La, Mn and Co. This is as per characterisation. The Cd is an impurity from the as-supplied powders. This result is shown in figure 5.6.

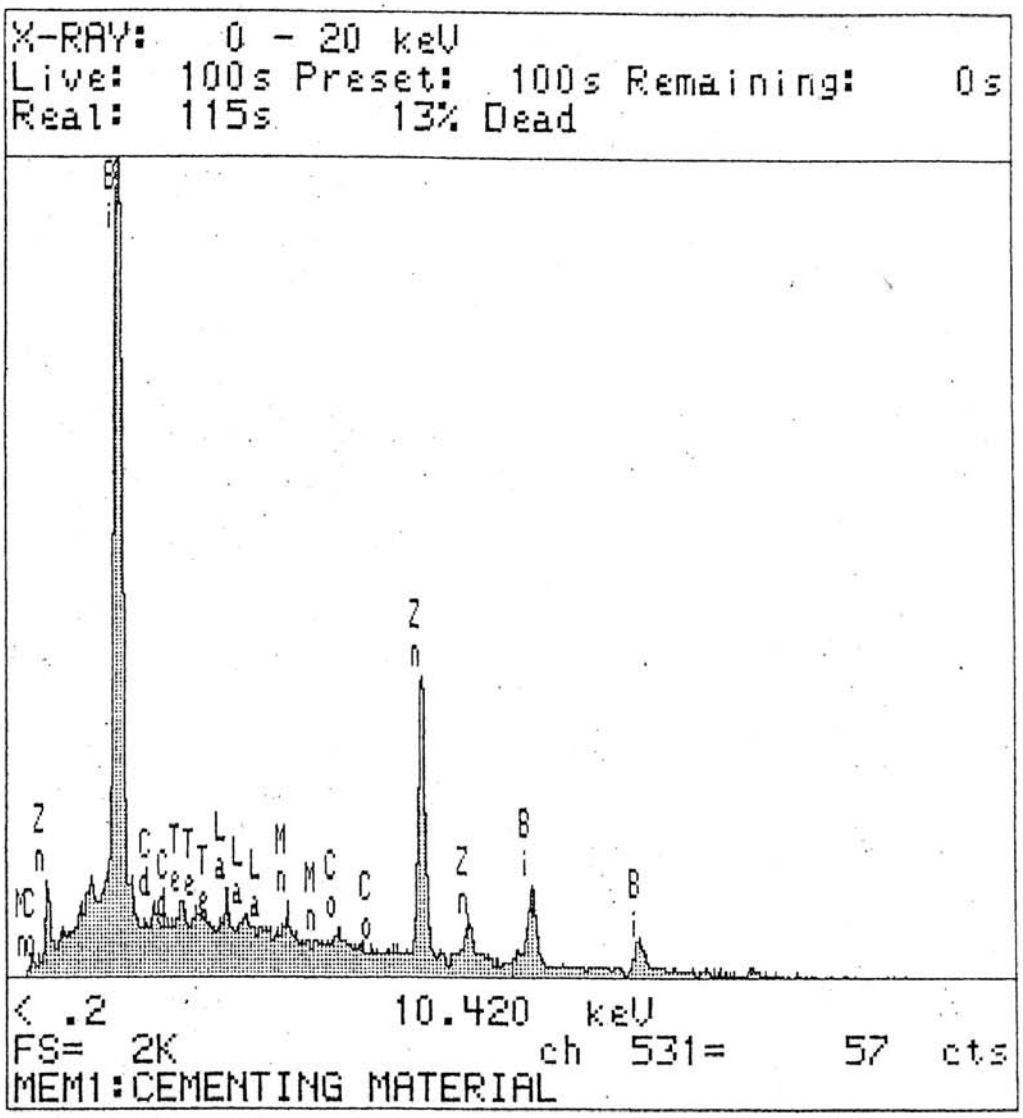

Figure 5.6: EDS spectrum of the grain boundary material in figure 5.4, showing the elements contained in it

In addition to the "rod-like" structure shown in figure 5.4, more of these structures are shown in figures 5.7-5.9. It is noteworthy that these rod-like structures are not found in commercial ZnO-based MOVs, and that they are not foreign organic fibres that accidentally entered the structure. More of this is presented in the "Discussion", section 6.3.1.

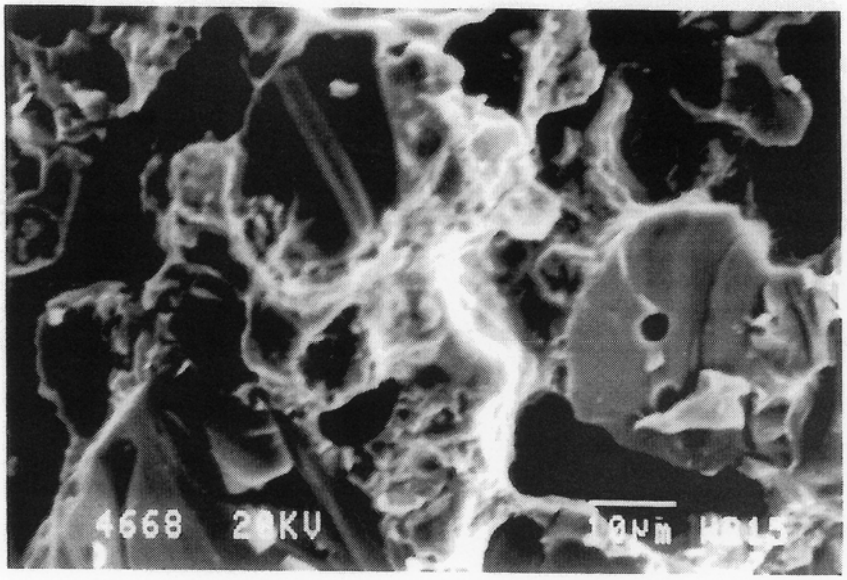

Figure 5.7: Fracture surface of the prototype MOV showing two "rod-like" structures

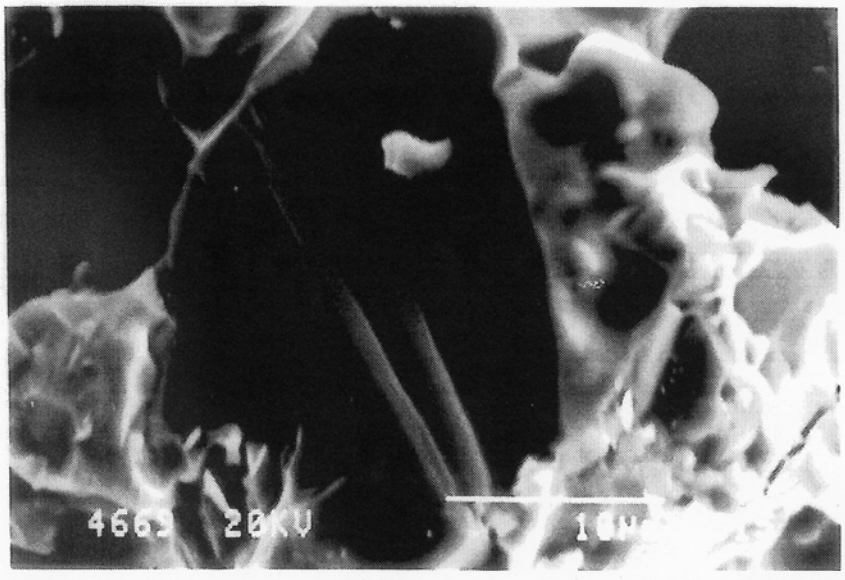

Figure 5.8: One of the "rod-like" structures in figure 5.7 at a higher magnification.

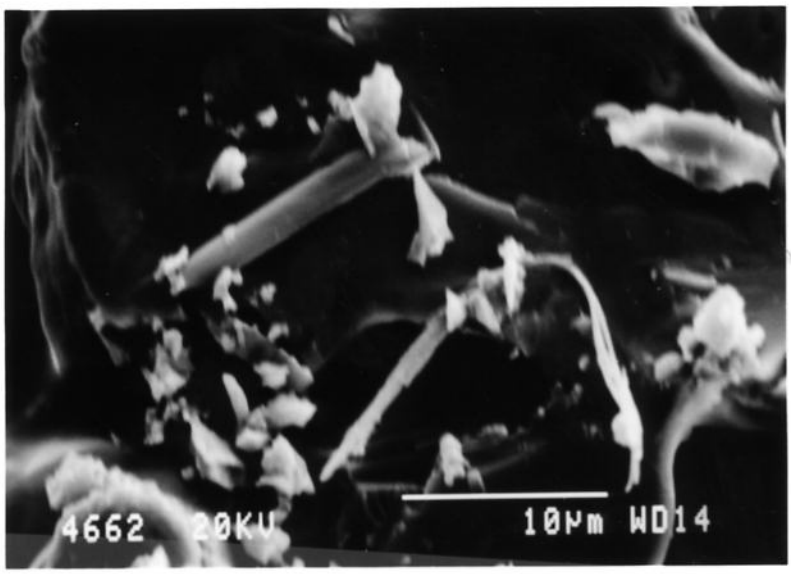

Figure 5.9: Fracture surface of the prototype MOV showing a free "rod-like" structure possibly snapped.

From EDS, a spot scan analysis of these "rod-like" structures revealed that they were composed of Zn, Bi, Te and Si, see figure 5.10. That is, the composition was identical to that of the grain boundary material! What was different was the concentration of the Zn as reflected by the area under the peaks of the EDS spectrum. The Zn concentration was found to be higher in the "rod-like" structures than in the grain boundary material.

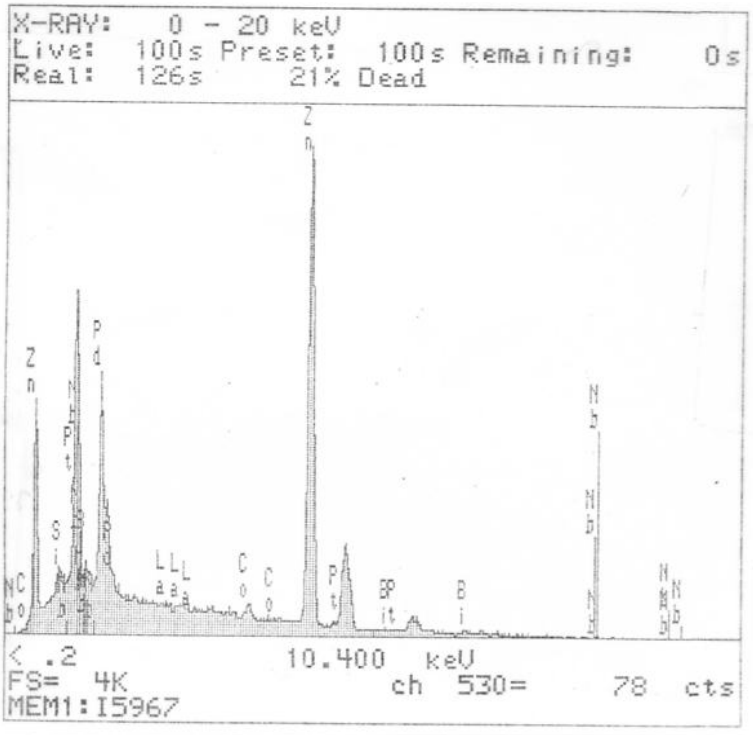

Figure 5.10: EDS spectrum of a typical "rod-like" structure

The prototype MOV also consisted of other structures as shown in figures 5.11-5.12.

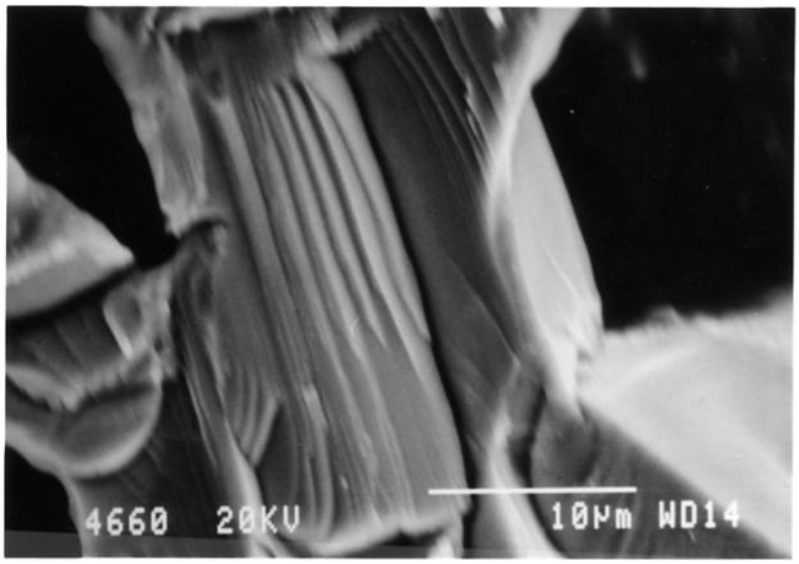

Figure 5.11: Fracture surface of the prototype MOV showing a "stub-like" structure.

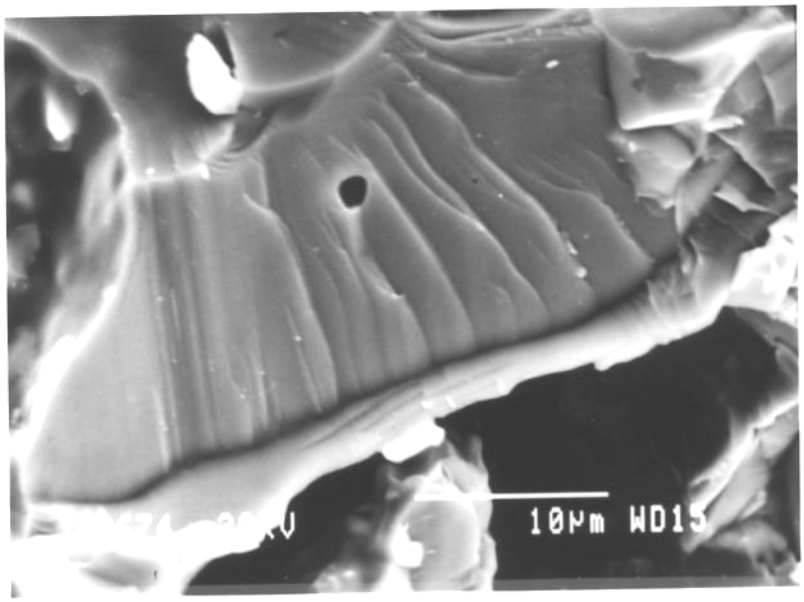

Figure 5.12: Fracture surface of the prototype MOV showing a layered phase.

5.3.2 Phases

The XRD pattern of the prototype MOV is shown in figure 5.13. The phases present in the pattern were determined from XRD studies by "peak matching" the xrd peaks of starting powders, whose xrd patterns were separately determined as mentioned in section 4.4. The identified phases were:

1. Hexagonal ZnO
2. Bismuth Oxide (Bi_2O_3) phases, seemingly α- and δ-phases
3. Zinc Platinum Oxide (Zn_2PtO_4)
4. Silicon Telluride ($SiTe_2$)

Each of these phases is identified by a tag in figure 5.13. It ought to be noted that platinum (Pt) was not directly added to the starting powders. It is the author's opinion that it went in as an impurity from the as-received starting powders, and the Zinc Platinum Oxide (Zn_2PtO_4) phase must have evolved as a result of chemical reactions that took during the sintering process.

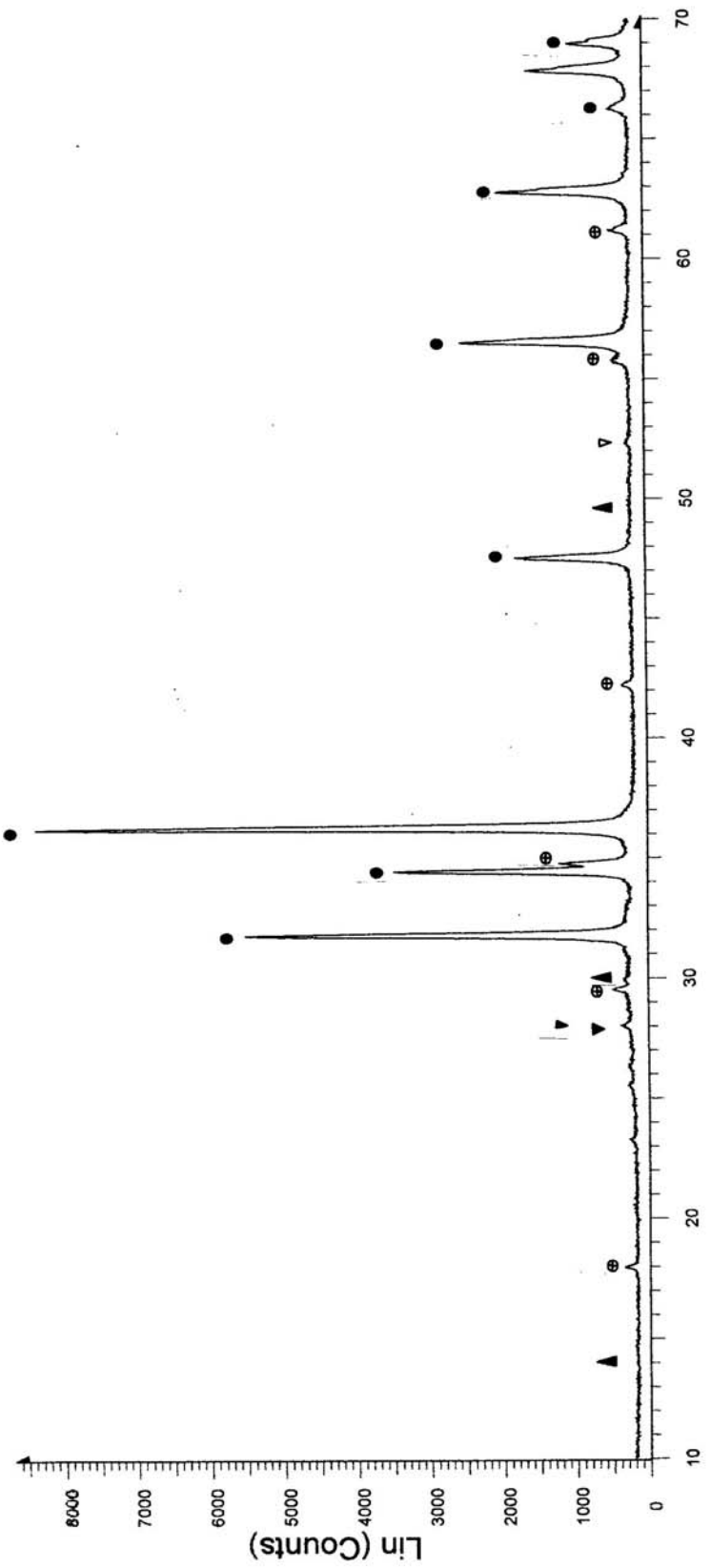

Figure 5.13: XRD pattern of the prototype MOV

(●) Hexagonal ZnO, (▼) α-Bi_2O_3 (▽) δ-Bi_2O_3 (▲) $SiTe_2$ (⊕) Zn_2PtO_4

Having presented the results of the experimental study carried out, the next chapter discusses and explains these findings.

6 DISCUSSION

In this chapter, the V-I characteristic of the developed prototype MOV is compared to that of a dimensionally comparable ZnO-based commercial MOV. The improvements and the benefits that accrue are presented. The reasons for the improvements are also discussed. Also discussed is the surge clamping action, the microstructure and phases of the prototype MOV. Finally the contribution is presented.

6.1 The V-I Characteristic of the Prototype MOV

This work sought to develop a ZnO-based prototype MOV whose V-I characteristic is ideal (Van Der Merwe, 1989). An ideal device has been defined in section 2.6. The V-I characteristic of the studied prototype MOV is compared to that of an ideal device as well as that of a typical commercial MOV that is ZnO-based so as to show the improvements achieved.

Figure 5.2 shows the V-I characteristic of the developed prototype MOV. This prototype MOV was fabricated according to the hypothesis, a model and theory as presented in chapter 3. The model predicted a result shown in figure 2.11. Clearly this result (figure 5.2) agrees well with the predicted V-I characteristic.

Since the V-I characteristic in figure 2.11 is an approximation of the of the ideal V-I curve, figure 2.10, it follows that the V-I characteristic of the developed prototype MOV is near ideal This is because of the new additive materials used as well as the processing method. This results in a ceramic with a microstructure of different breakdown instability from that of the commercial MOV. The new additive materials used are $SiTe_2$ and LaB_6. The process route was changed such that the main constituent powder used in the fabrication of the prototype MOV was characterised to be μ-MOVs instead of the plain ZnO as is the case in

commercial MOVs. How the new additives and the processing method influence the microstructure is presented later.

The prototype MOV is now compared to a dimensionally comparable commercial ZnO-based MOV, V275K20P. Figure 6.1 shows the V-I characteristics of the respective MOVs. On an overview, the prototype MOV shows no up-turn region. The improvements and benefits are presented below.

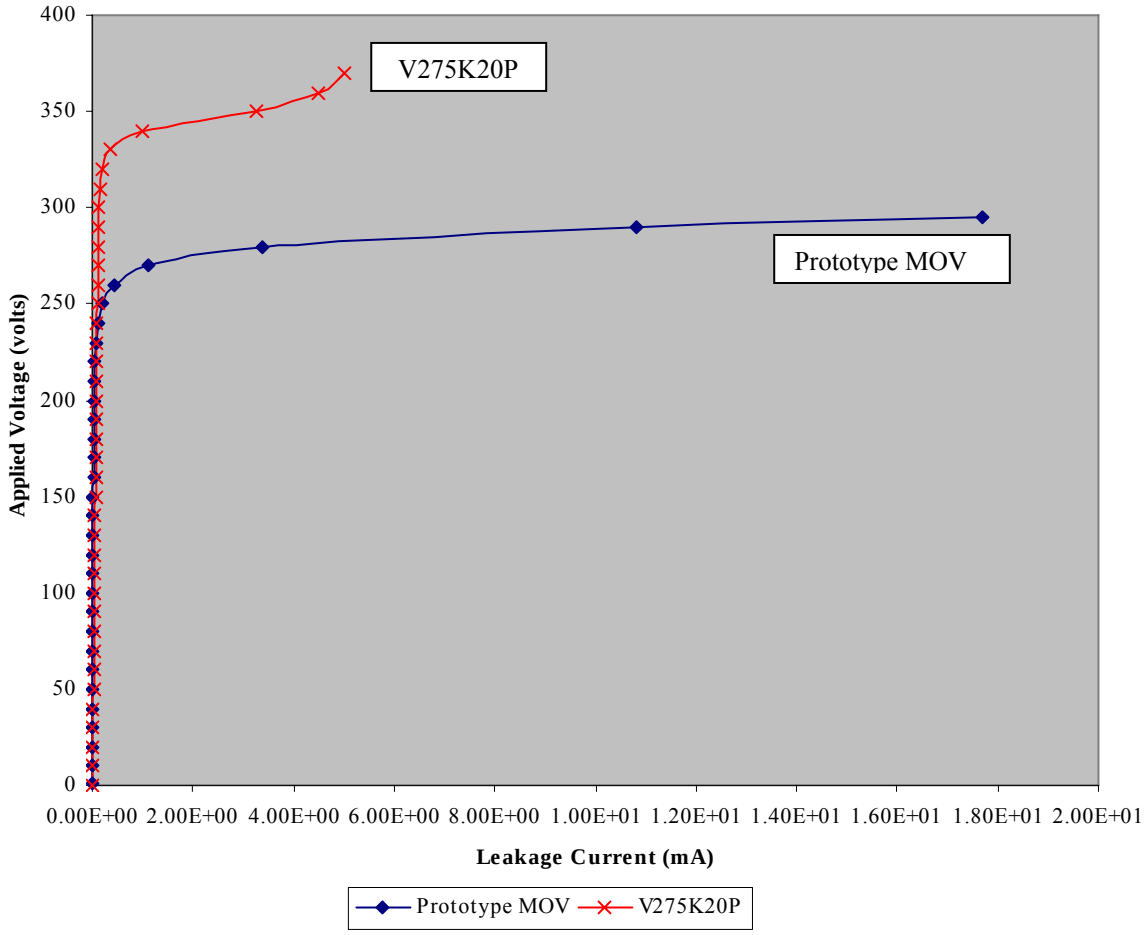

Figure 6.1: The V-I characteristic of the prototype MOV compared to that of a commercial MOV, V275K20P. The prototype MOV has no up-turn region.

6.1.1 The Improvements and Benefits

The various regions of the V-I characteristic of a ZnO-based commercial MOV have been presented in section 2.1. How these regions arise has also been presented in sections 2.4 and 2.5. The improvements made in these regions are presented below

1) Improvement in the leakage region

Figure 6.2 is a zoom of the above characteristics (figure 6.1) in the "low voltage" (L.V.) region, showing the leakage and active regions on an expanded scale. It is quite clear that the area of the leakage region for the prototype MOV is much lower than that of the commercial MOV. The reduction in area was computed to be 1.0 % lower than that of the commercial MOV, see Appendix A. Thus the improvement in the leakage region in numerical terms was determined to be 1.0%. All this goes to show that the V-I characteristic of a developed prototype MOV shows significant improvements over that of a commercial MOV of comparable dimensions. This was the objective of the work.

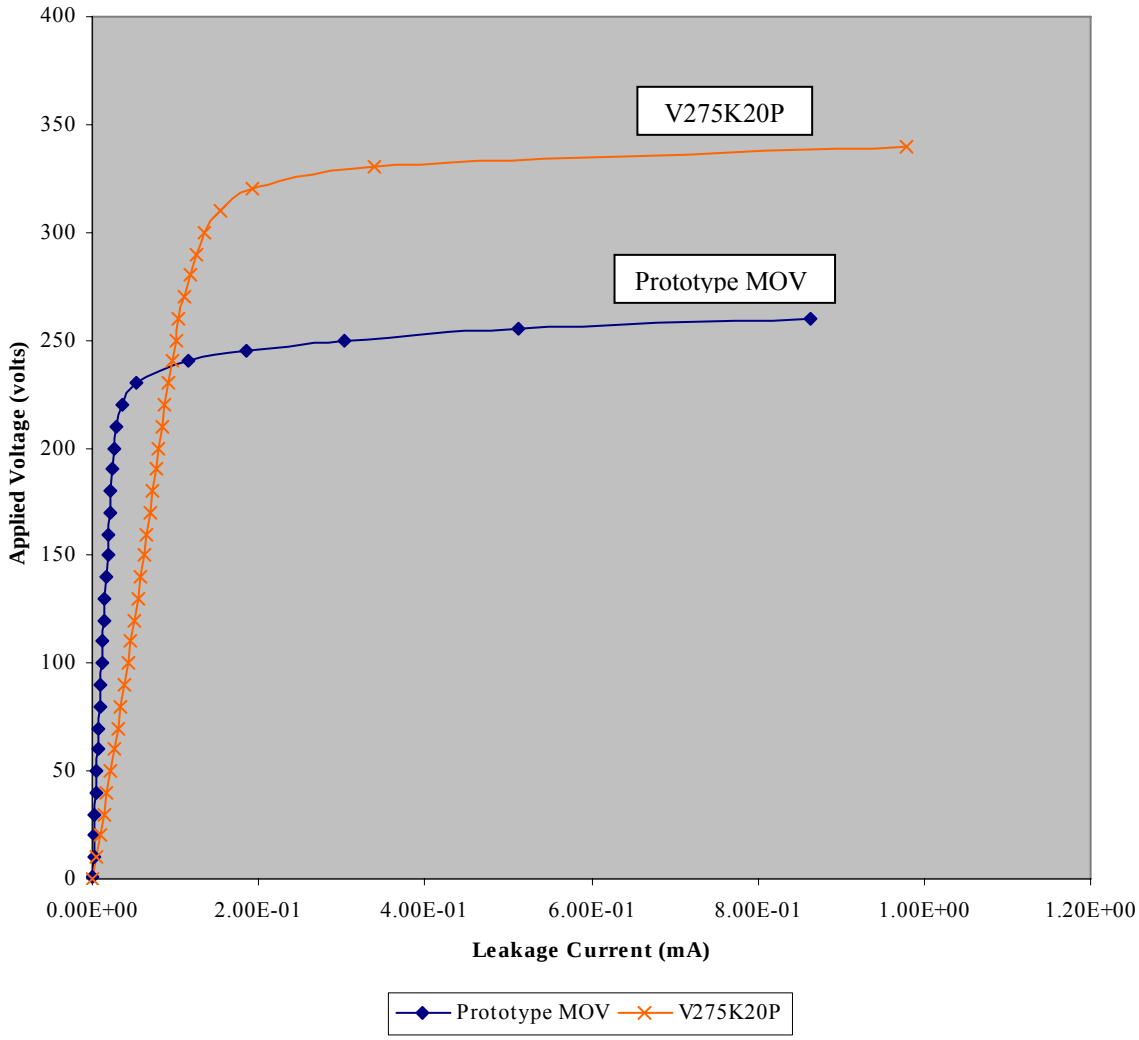

Figure 6.2: The V-I characteristic of prototype MOV compared to that of V275K20P in the L.V. region, showing that the prototype has lower leakage currents.

2) Improvement in the active region

In the active region, the prototype MOV has two-fold improvements, namely,

a) the rate of breakdown is on average 4 times that of the commercial MOV, see Table 6.1.

Table 6.1: Comparative rates of breakdown of prototype MOV and a commercial MOV

MOV	(V_1,I_1)	(V_2,I_2)	$\Delta I/\Delta V$ ΔV=10 volts(unit)
V275K20P	340, 0.979	350, 3.24	2.261
	350, 3.24	360, 4.49	1.25
Prototype MOV	275, 3.74	285, 9.38	5.64
	285, 9.38	295,17.70	8.32

The states (V_1,I_1) and (V_2,I_2) are typical points of the respective MOVs in the active region. These are part of the V-I data collected. The rate of breakdown is calculated as $\Delta I/\Delta V$.

The observed high rate of breakdown is because the prototype MOV has an instability, the Γ-instability, which is strongly **E**-field dependent upon breakdown. As mentioned earlier, this instability is a result of using i) new additive materials, $SiTe_2$ and LaB_6, ii) the characterised ***Q*** -powder, and (iii) the characterised ***M*** -powder together with the processing method. How this instability arises has been presented in Chapter 3. The ***M*** -powder provides the N-type instability; the $SiTe_2$ provides the S-type instability and is enhanced by the field-emission instability due to the LaB_6. The ***Q*** -additive provides the avalanche instability as well as the much needed energy handling capability. The overall instability is what I coined the Γ-type instability.

The commercial MOV on the other hand has a strong thermally assisted N-type instability, effectively avalanche, with a weaker **E**-field dependent instability superimposed. Because of this the rate of breakdown is slow, since the breakdown is thermal in nature and thermal processes are inherently time dependent. For the same reason, this explains why the commercial MOVs heat up too fast to temperatures typically in the range of 65° + C, before they fail. This was observed experimentally.

b) it has a higher α-value, which was calculated to be 30.20. The α-value of the commercial was found to be $\alpha = 19.00$. The difference in the α-values is tied up with aspects presented in a).

Since the α-value is a measure of the slopes (gradients) of V-I curves in the active regions, it follows that the V-I curve of prototype MOV is more flat than the commercial and hence is more towards the ideal active region ($\alpha = \infty$).

3) Improvement in the up-turn region

The characteristic for the prototype MOV has no up-turn region; the commercial one has.

From the foregoing it is quite clear that the V-I characteristic of the prototype MOV shows improvements in all the regions with the exception of the pre-breakdown, which is similar to that of the commercial MOV. Ii is also clear that by definition of an ideal device (section 2.6), the prototype MOV has a V-I characteristic which is near ideal. It can be argued therefore that the prototype MOV is a near ideal device. This is a significant improvement.

It is also noteworthy that the "knee" point (see section 2.1) of the prototype MOV could be shifted up to higher voltages or down to lower voltages by altering the additive levels.

To further test the hypothesis, the model, characterisation method, as well as the process method, a specimen MOV whose $\boldsymbol{M}$ -powder was produced from a commercial MOV block (V275K20P) was fabricated using a powder formulation as for the prototype MOV. It was code-named V275K20P-c. The V-I characteristic so obtained had much lower area in the leakage region than the as-received commercial MOV. The reduction in area of the leakage region and hence reduction in leakage current was computed to be 76.72 %. The old "knee" point was also exceeded. Figure 6.3 shows the characteristics for the voltage range that could be studied. Higher voltages were not used to avoid potential flashover, for the prototype MOV had no resin coating to increase the dielectric strength of surrounding air-MOV block interface.

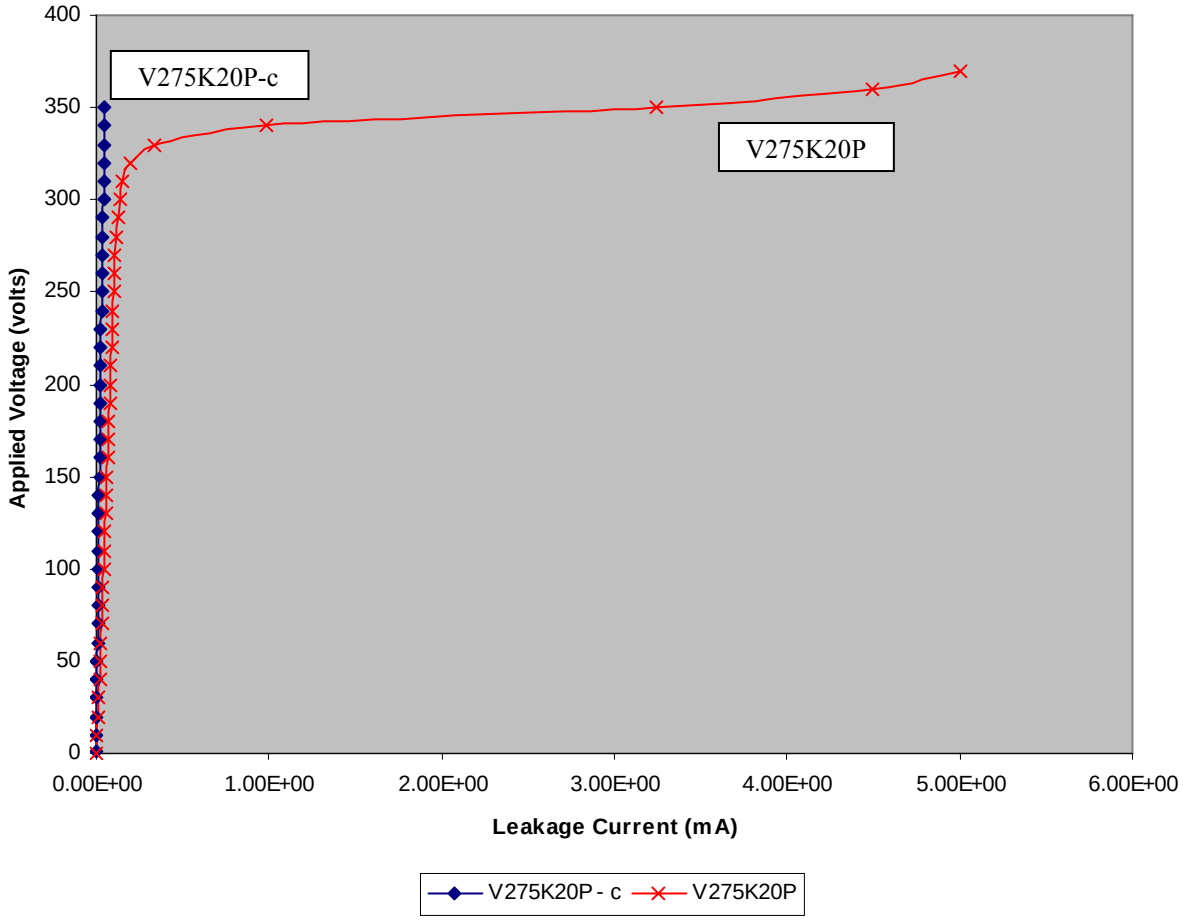

Figure 6.3: The V-I characteristic of specimen V275K20P-c compared to V275K20P, showing a significant improvement in the leakage region.

All this validates the model used and goes to show that the new additives used, and the process method, results in a ceramic whose microstructure gives an improved V-I characteristic over that of the commercial MOV.

Now that the improvements achieved have been presented, the benefits that accrue are presented below. These are

a) Extended Service Life

Improvement in the leakage region is important because high leakage currents when the MOV is in the OFF state lead to high watt (I^2R)-losses. This is undesirable because it leads to a higher rate of thermal degradation of the MOV mechanically and of the V-I characteristic. This in turn leads to premature device failure. Because the prototype MOV developed exhibit lower leakage currents, this seems to imply extended service life compared to commercial MOVs. This extended service life is further promoted by the breakdown mechanism which is non-thermal. That is, **E**-field dependent instability is preferred to thermal because the later promotes ageing effect in MOVs (Greuter *et al*, 1989) which is thermal in nature.

b) Higher energy handling capabilities

The studied commercial MOV failed at leakage current of about 5 mA. From figure 6.1 the prototype MOV was able to discharge 3.5 times this (5 mA) value without failure. This seems to suggest that the prototype MOV could be capable of handling higher energies than a commercial MOV of comparable dimensions. This was the reason of characterising $\boldsymbol{Q}$ -powder as mentioned before.

c) Higher Protective Range

No up-turn region: Figure 2.1 is the generalised V-I characteristic of ZnO-based commercial MOV. Figure 6.1 shows in part the V-I characteristic of a particular

ZnO-based commercial MOV, V275K20P, determined in this study. The V-I dependence in the up-turn regions of both characteristics is ohmic. This implies that if the surge current is in this range or region the MOV **no longer** offers the required protection, since then the MOV voltage rises with the surge current. This feature is not desirable. The developed prototype MOV does not have an up-turn region. This means higher or extended protective range as compared to the commercial MOV.

d) A near ideal SPD has been developed

The fact that the V-I characteristic of the developed prototype MOV has no up-turn region also implies that the prototype MOV is a near ideal device. That is, a near ideal ZnO-based surge protective device (SPD) was developed.

The pre-breakdown region of the prototype MOV could not be made sharper as that of the ideal device because of the additives used. This constitutes a deficiency in the studied prototype MOV. It is attributed to the fact that the ***O*** -additive did not give a strong *S*-type instability as was expected from works of previous researchers, like Ovshinsky (1968) and Deis *et a*l (1970). A possible reason for this could be argued thus: The ***O*** -additive has a very low melting temperature, which is in the region of 450-500 °C (Deis *et a*l, 1970). This temperature range is much lower than the process temperature (850 °C) used to fabricate the prototype MOV. This means that the characterisation is probably tampered with through melting by the time the process temperature is reached. It is most unlikely that the characterization is recoverable upon air quenching of the as-sintered prototype MOV blocks. What is needed is a glassy semiconductor additive with a higher melting temperature than the process temperature, and with strong *S*-type instability.

6.1.2 Explaining the Improvements in the V-I Characteristic of the Prototype MOV

The improvements made on the V-I characteristic of a ZnO-based commercial MOV hinge on the developed microstructure of the prototype MOV, see figure 5.4. The microstructure determines the electrical behaviour. It was hypothesised that the modelled microstructure shown in figure 3.3 would give a near ideal V-I characteristic shown in figure 2.11. Indeed the microstructure that evolved for the prototype MOV yielded a V-I curve as presented in figure 5.2. Clearly this characteristic is identical to the one predicted by the model, figure 2.11.

The V-I characteristic of the commercial MOV was explained using the equivalent circuit in sections 2.4 and 2.5. This is because the microstructure shown in figure 2.5 can be represented by an equivalent circuit shown in figure 2.6. Similarly the V-I characteristic and hence the improvements, of the prototype MOV can be explained using the equivalent circuit shown in figure 3.4. Figure 3.4 corresponds to the microstructure of the prototype MOV shown in figure 5.4.

The differences between the equivalent circuit of the ZnO-based commercial MOV (figure 2.6) and that of prototype MOV (figure 3.4) are in the following respects:

a) R_{OFF} in figure 3.4 is much larger than that in figure 2.6. This is due to the powders used to fabricate the prototype MOV as well as the processing method.
b) Switching element BCCZD - this is also introduced as a result of the type of additives used, together with the processing method used to fabricate the prototype MOV.

Since the magnitude of R_{OFF} is a measure of the leakage currents in the leakage region, it follows that the larger it is, the lower the leakage currents. R_{OFF} is much larger in figure 3.4 than in figure 2.6; this explains the lower leakage currents of the prototype MOV compared to the commercial MOV as shown in figure 6.2.

The major difference between figures 2.6 and 3.4 is the switching element I coined *bi-direction current controlled Zener diode* (BCCZD); it by-passes R_{ZnO}. R_{ZnO} is known to be responsible for the up-turn region in the ZnO-based commercial MOV (EPCOS, 2001). As highlighted in the model, in order to remove the up-turn region found in the V-I characteristic of commercial ZnO-based MOVs, what is required is to incorporate in the existing equivalent circuit a by-pass switching element to R_{ZnO}. From the foregoing, this has been done. The switching element BCCZD is responsible for the removal of the up-turn region in the prototype MOV. It does so by undergoing a reversible **E**-field dependent instability at breakdown. I coined the instability *Γ- instability*, for the resultant V-I curve is like the Greek letter Γ. This is just in the same way that the V-I curve of the commercial MOV is like the letter N, and the corresponding instability is called *N-type* instability, see section 2.7. The Γ-instability also accounts for the higher rate of breakdown in the active region of the prototype MOV than the commercial MOV.

It ought to be noted that the equivalent circuit of the commercial MOV has a switching element, R_{SE}, and at breakdown, $R_{SE} << R_{ZnO}$, and hence the up-turn region.

A quantum mechanical explanation for the V-I characteristic of the prototype MOV is given in section 6.1.3 below.

6.1.3 Charge Transport Mechanism in the Prototype MOV

To explain the transport mechanism in the prototype MOV and hence the observed electrical behaviour at microscopic level, the following energy band diagram (the model) is proposed. I have coined the arrangement a *semiconductor-insulator-metal-insulator-semiconductor (S-I-M-I-S)*. That is, the prototype MOV is a S-I-M-I-S device.

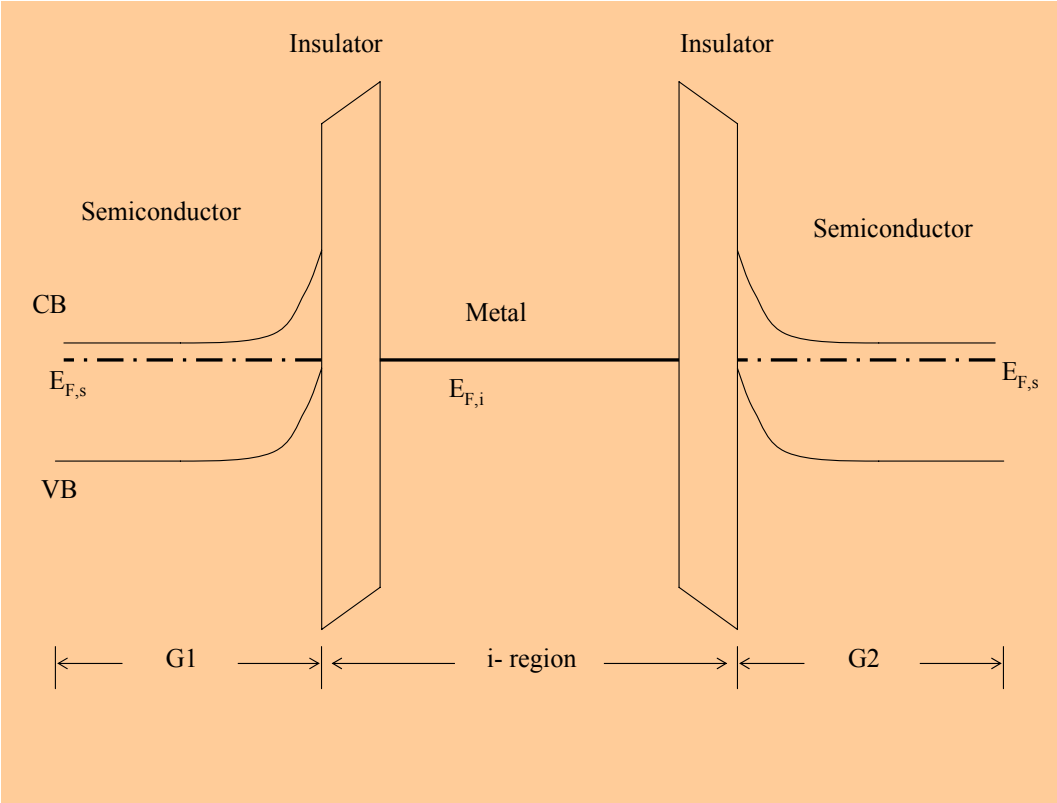

Figure 6.4: Energy band diagram for the prototype MOV modelled to be a S-I-M-I-S for zero bias (V = 0). $G_1 = G_2 =$ ***M*** -grains (n-type), i = intermediate region (insulating with a metallic background), E_{Fs} = Fermi Level for the semiconductor, E_{Fi} = Fermi Level for the i-region.

The energy band diagram in figure 6.4 results if one invokes the model, figure 3.3, and if one imagines that in the microstructure of prototype MOV, two adjacent ***M*** -grains with a grain boundary material in between them constitute an n-i-n heterojunction (Schwing, *et al*, 1985). The ***M*** -grains are characterised to be μ-MOVs and form non-degenerate n-regions, the grain boundary material forms the i-region. Because the ***M*** -grains are μ-MOVs, the energy band diagram for the grains is that of the ZnO doped with additives giving the current commercial ZnO-based MOV (Schwing *et al*, 1985). The i-region is highly insulating with a metallic background, whereas the grains are n-type semiconductive. The i-region is highly insulating because it is essentially composed of α -Bi_2O_3 - based phase,

with a dispersion of $SiTe_2$ phase, both of which have insulating properties. It is assumed that at grain surfaces of α -Bi_2O_3 - based phase, sparsely populated LaB_6 particles are found. This material (LaB_6) has metallic properties and is field-emissive (f-emissive) (Oyez, 1985). Thus the i-region is partitioned into an insulator-metal-insulator (I-M-I) system. This makes the overall system to be a semiconductor-insulator-metal-insulator-semiconductor (S-I-M-I-S) system, and the prototype MOV block then is just a series-parallel arrangement of these n-i-n devices connected together (Schwing, *et al*., 1985).

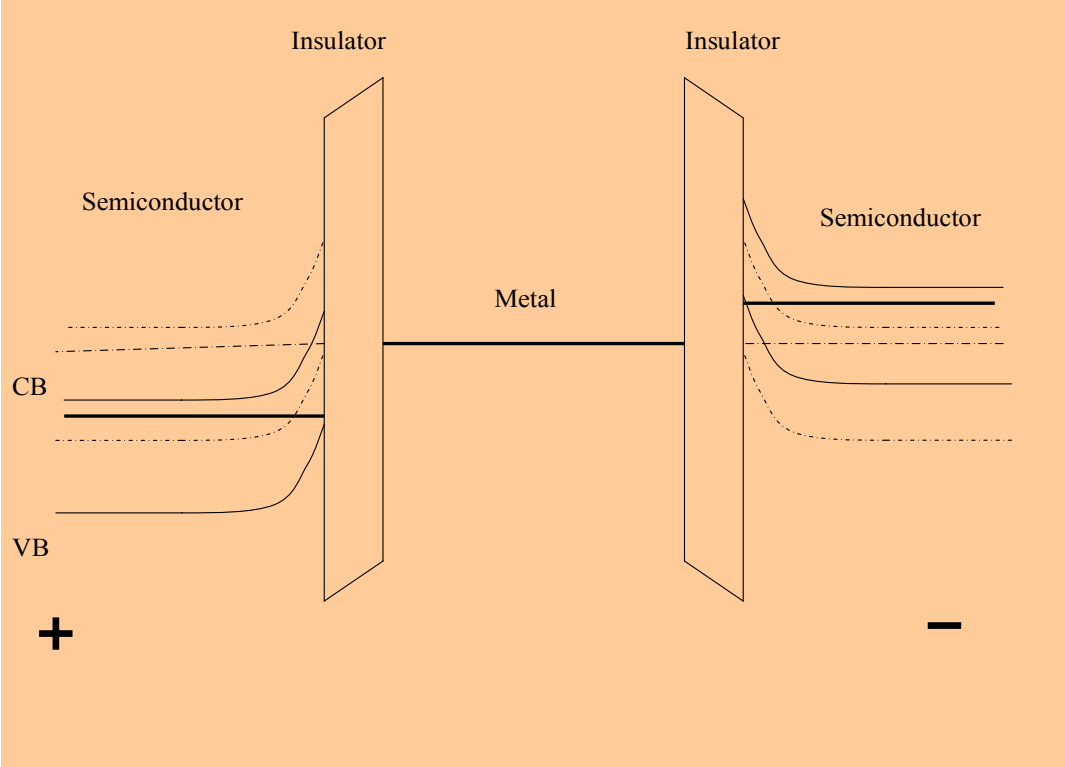

Figure 6.5: Energy band diagram for the prototype MOV modelled to be a S-I-M-I-S device with bias (V > 0), showing a shift the Fermi-Levels in the 2 adjacent grains. The dotted lines refer to the situation for zero bias (V = 0)

For zero bias (V=0), the S-I-M-I-S system is in equilibrium and therefore the Fermi Levels in the various regions coincide as shown in figure 6.4.

Consider now the heterojunction device under voltage bias (V>0), figure 6.5. For low **E**-fields corresponding to low voltages, the prototype MOV block is insulating due to i-region. This is because the i-region has a high density of traps and hence traps charge carriers and hence negligible current flow. The traps arise from a number of sources. $SiTe_2$, one of the grain boundary phases is an amorphous material and amorphous materials are known to contain a high density traps with an exponential energy distribution (Ovshinsky, 1968), (Kao *et a*l, 1981). The grain boundary is also Bi-rich, with an α-Bi_2O_3-based phase as the predominant phase present. This material is an insulator, and insulators by their nature have traps. The overall effect of these materials is the creation of the two double Schottky potential barriers (DSPBs). It was reported in section 2.5 that these potential barriers control the transfer of charge, and hence the electrical current from one grain to another. A similar process occurs here. The only difference is the presence here of a f-emissive zone in the energy band (E-B) diagram.

It is assumed that two types of charge carriers, electrons and holes, are involved in the charge transport process. The electrons are trapped by both shallow and deep trap levels, and holes by deep trap levels.

Because of the blocking potential barriers, there is negligible current flowing. That is, had it been not of the DSBs (insulator barriers) it would have been very easy for electrons to tunnel under bias from G2 into the i-region, and transit to the i-region under field emission and further tunnel into G1 with very little scattering. Because of the two (2) insulator barriers (implying traps), the electrons get trapped, and those that make it to G2 constitute the small discharge current. This explains why there is very low leakage current in the ohmic region of the V-I characteristic of the prototype MOV, see figures 6.2. Note that leakage region = ohmic region + pre-breakdown region.

The I-V dependence in this (ohmic) region obeys the Varistor Equation,

$$I = \kappa V^{\alpha} \quad \text{..... (6.1)}$$

where symbols used have usual meanings. Here $\kappa << 1$ by characterisation and $\alpha = 1$.

For intermediate voltages, corresponding to the pre-breakdown region, charge transport is still effectively the same. The DSPBs are still too high and relatively too thick for excited charge carriers to surmount or tunnel the potential barriers. However, there is a small increase in the tunnel current. This is because the charge carriers are bosons and as such they will obey the Boltzmann distribution. As such there will be some few carriers with high energy sufficient enough to either surmount or tunnel the DSPBs. This explains why in the pre-breakdown, the leakage current is slightly higher than the ohmic region. The I-V dependence seemed to obey Childs square law, namely

$$I = \kappa V^{2} \quad \text{..... (6.2)}$$

thus again obeying the Varistor Equation with $\alpha = 2$.

For high voltages, corresponding to the active or breakdown region, three instabilities are in force: a) avalanche breakdown, b) field-dependent breakdown, and c) field emission (f-e), with f-emission as the predominant mechanism. That is at breakdown, G_1 and G_2 undergo thermally assisted avalanche breakdown (implying N-type instability as they are μ-MOVs). The i-region undergoes two kinds of field-dependent breakdown 1) in the α-Bi_2O_3-based phase which is insulating with an energy gap of the order of 5 eV - it undergoes a field-dependent breakdown as is typical of insulators, 2) in the $SiTe_2$: This material is glassy, and as such it too is insulating. It undergoes field-dependent breakdown as it inherently has S-type instability. These two breakdown modes are enhanced by 3) f-e breakdown from the metallic region represented by the Lab_6 particles. Lab_6 has a low work function (ϕ) which stands at 2.6 eV (Oyez, 1985), (Storms *et al*, 1979), and is inherently field emissive at some threshold voltage. Thermal breakdown is very low here due to the very high potential barriers presented by the insulating materials. Because all regions are under breakdown, there is a "sea"

of electrons available for conduction and hence the leakage current diverges. This explains why the leakage current is so high at breakdown in the V-I characteristic.

Field-emission (f- emission) is a quantum mechanical process and is electronic in nature. This explains why in the active region of the V-I characteristic of the prototype MOV the instability is **E**-dependent. It is due to the LaB_6 phase.

To the breakdown processes which are found at the grain boundaries (predominantly S-type instability), is superimposed the thermally assisted avalanche breakdown mechanism (N-type instability) coming from the $\boldsymbol{M}$ -grains which are μ-MOVs by characterisation. The combined effect by the Superposition Principle is the Γ-instability. This was the hypothesis.

Because the main instability is electronic in nature, there is no imbalance in equation (2.6). Hence there is no marked increase in phonon generation, hence no scattering. This also explains why there is no up-turn region in the V-I characteristic of the prototype MOV and why the rate of breakdown is high for the prototype MOV as compared to the commercial MOV.

In the active region, the I-V relation is again described by equation 6.1 with $\alpha \geq 30$, and $\kappa >> 1$. The corresponding electrical conductivity,σ, I believe, is of the form (Adler, *et al*, 1971)

$$\sigma = \sigma_0 \exp\left(-\Delta/\kappa_\beta T\right).\exp\left(E/E_0\right) \quad \ldots\ldots\ldots\ldots\ldots\ldots \quad (6.3)$$

where the relations

$$I = \sigma E\,, \quad \ldots\ldots\ldots\ldots\ldots\ldots\ldots\ldots\ldots\ldots \quad (6.4)$$

and

$$\sigma_0 = ne^2\tau/m^* = ne\mu\,, \quad \ldots\ldots\ldots\ldots\ldots\ldots\ldots\ldots \quad (6.5)$$

have been used. Δ is the activation energy for electrical conduction, E is the applied electric field, T is the absolute temperature, κ_β is the Boltzmann constant, n is the number of electrons, e is the charge of an electron, τ is the relaxation time, m^* is the effective mass of an electron, and μ is the electron mobility. This assumption is justified because instability was experimentally found to be strongly

E-dependent and weakly dependent on T, as expressed by equation (6.3). Thus the **E**-term overrides the T-term. The current flowing, I, then becomes a function of the conductivity, keeping the **E**-field and hence voltage essentially constant. That is, the supplied electromagnetic energy goes into the generation of electrons (n) and not to raise the voltage. This is the meaning of the relation in equation (6.4). The conductivity phenomenally increases due to the large number of electrons created by the breakdown mechanisms, hence relation in equation (6.5).

Having discussed the V-I characteristic of the studied prototype MOV, its surge clamping action is discussed next, for the two are inter-related

6.2 The Surge Clamping Action of the Prototype MOV

The surge response action of the prototype MOV for the two types of electrode systems is shown in figures 5.3 (a1) - (e1) and 5.3 (a2) - (e2). Whether it is surge clamping or not is argued below.

To establish whether the prototype MOV is surge clamping or not, it was necessary to set the studied commercial MOV to the same conditions as the prototype MOV, that is "acclimation". It was then tested under these conditions. Both electrode systems were used. Figure 6.6 compares the surge response action of the prototype MOV to the acclimatised commercial MOV using type (i) electrode system, whilst figure 6.7 compares them using type (ii) electrode system. Tables 6.2 and 6.3 show the corresponding data. In each case the data is compared to that of the commercial MOV when tested in the as-received state.

Table 6.2: Surge response data of the prototype MOV and acclimatised commercial MOV tested using type (i) electrode system compared to the commercial MOV tested in the as-received state

	Prototype MOV		V275K20P (aclima.)		V275K20P (As-received)	
Va (kV)	Vc (kV)	Is (A)	Vcl (kV)	Is (A)	Vcl (kV)	Is (A)
0.50	0.48	0	0.48	0	0.50	0
0.80	0.71	16.00	0.75	0	0.66	76
1.00	0.80	28.00	0.92	0	0.70	140
1.25	1.05	52.00	1.12	9.20	0.76	230
1.50	1.21	82.00	1.28	41.20	0.80	340
1.80	-	-	1.43	102.00	0.85	450
2.00	-	-	-	-	0.88	540

In both Tables 6.2 and 6.3, the "-"implies that surface discharges were experienced hence there was a limitation on the voltage range used. V_a, V_c and I_s stand for applied voltage, clamped voltage and surge current respectively.

In figure 6.6 (a), both MOVs show an open circuit condition. The prototype MOV starts to conduct at an applied surge voltage of 0.8 kV, whereas the acclimatised commercial MOV still in the OFF state, see figure 6.6 (b). The same trend persists for higher applied voltages until at 1.25 kV, when the acclimatised commercial MOV starts to conduct, see figure 6.6 (d). For higher applied surge voltages, both MOVs conduct and the discharge currents are relatively high. For both MOVs, the voltage waveforms are characterised by a voltage "hump", whose amplitude increases with increase in the applied surge voltage. These waveforms are not of the type normally associated with surge voltage clamping action.

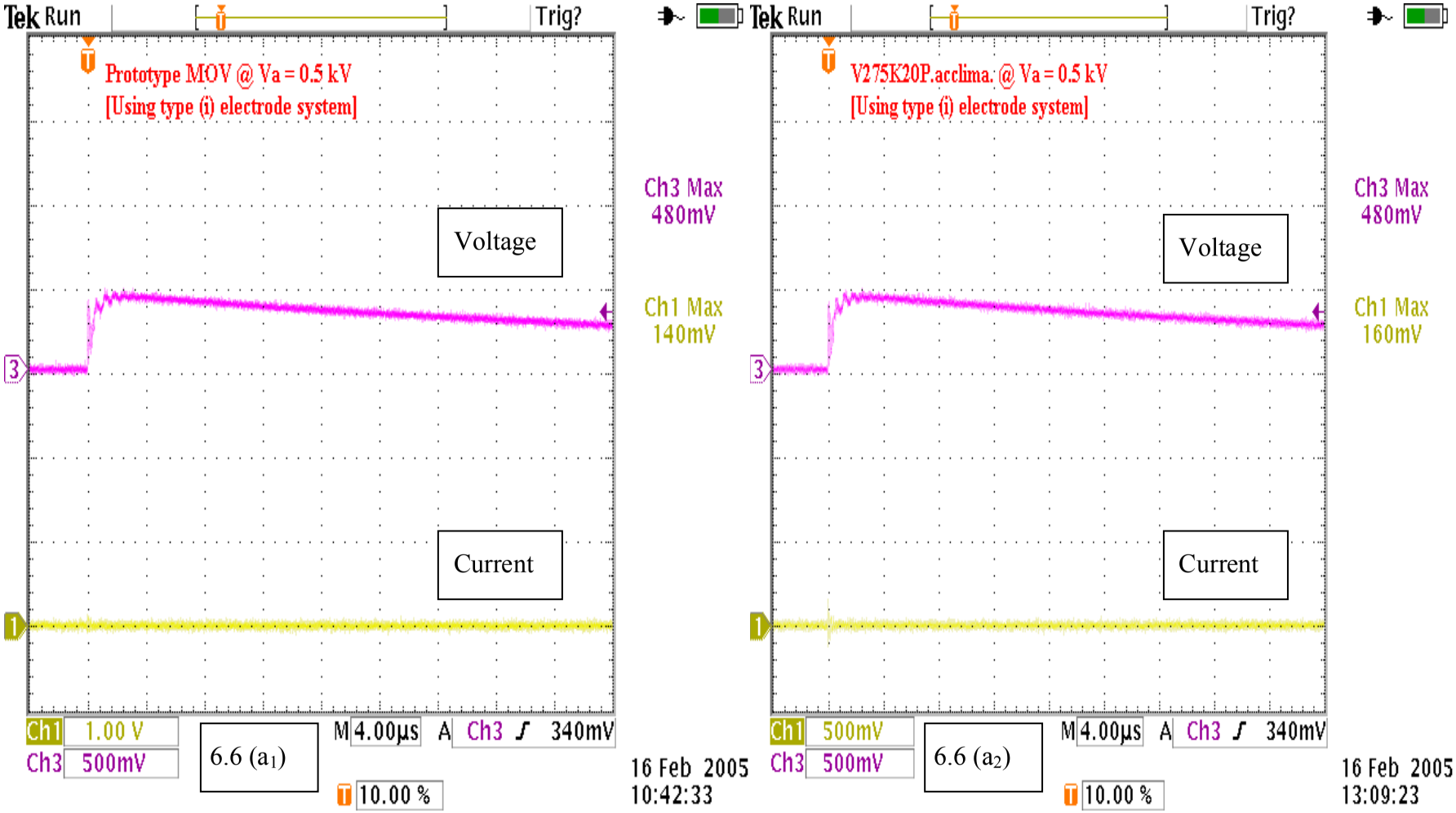

Figure 6.6 (a): Comparative surge clamping action of the prototype MOV to the acclimatized V275K20P @ V_a =0.5 kV

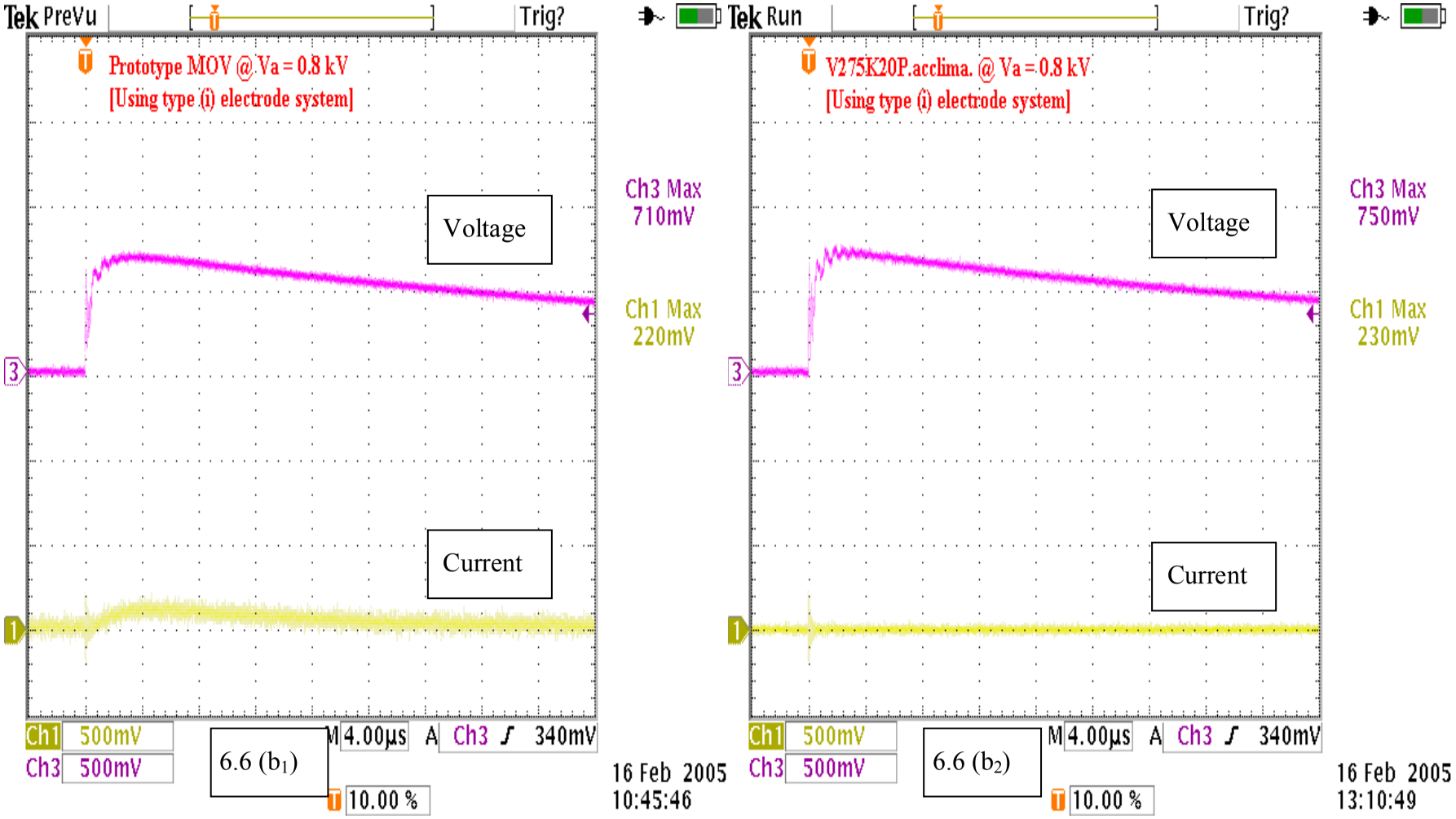

Figure 6.6 (b): Comparative surge clamping action of the prototype MOV to the acclimatized V275K20P @ V_a=0.8 kV

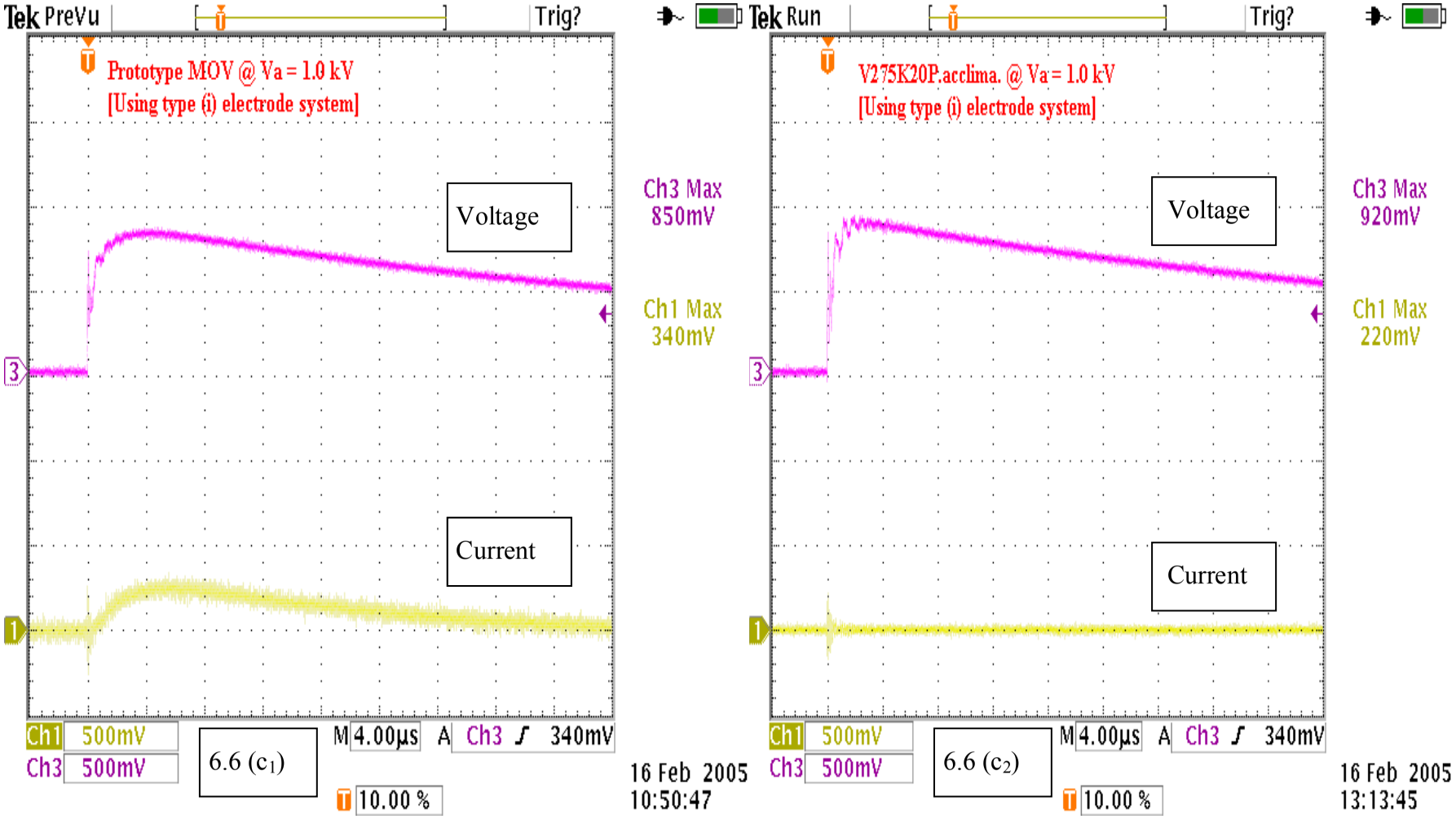

Figure 6.6 (c): Comparative surge clamping action of the prototype MOV to the acclimatized V275K20P @ V_a =1.0 kV

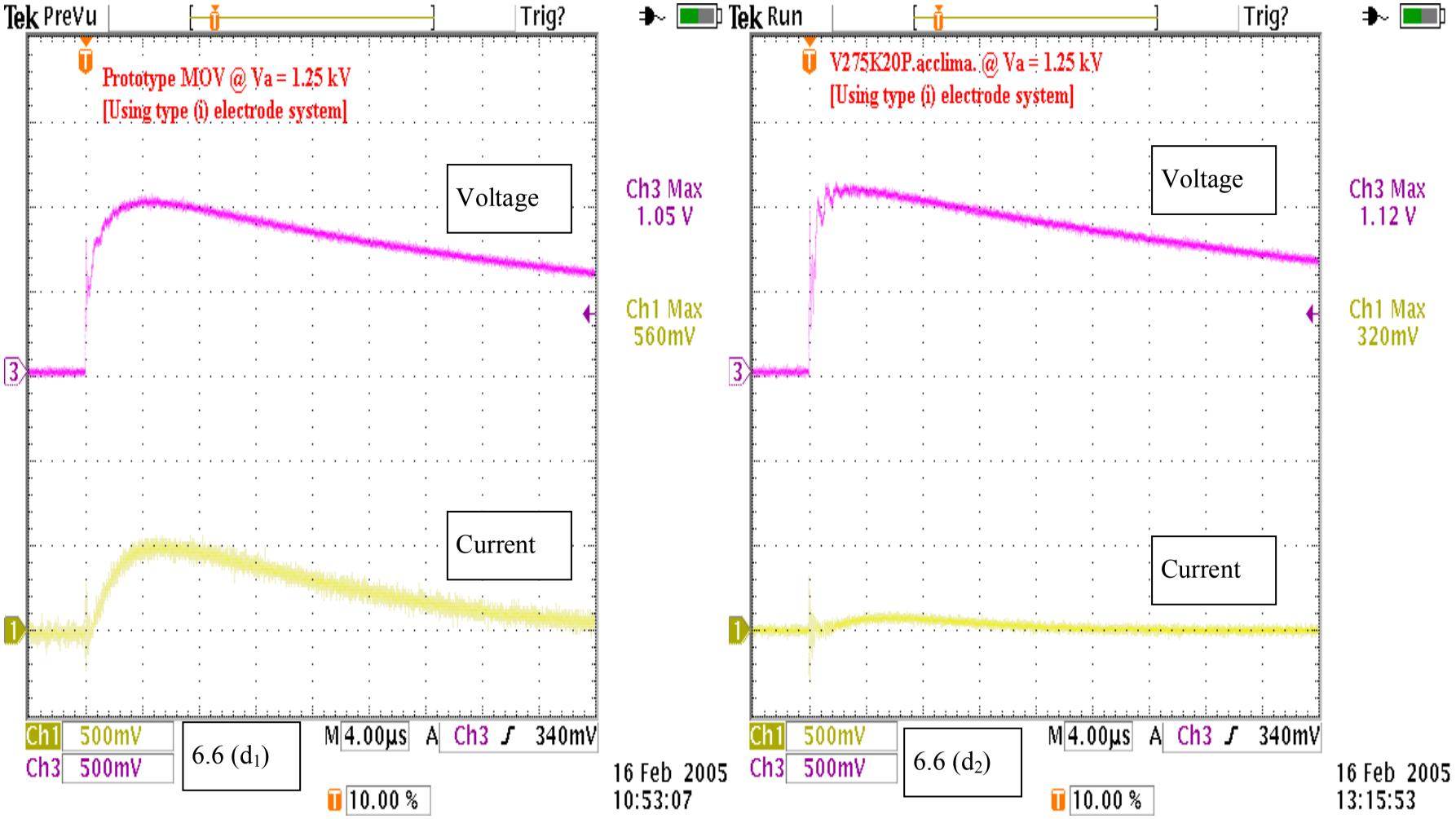

Figure 6.6 (d): Comparative surge clamping action of the prototype MOV to the acclimatized V275K20P @ V_a=1.25 kV

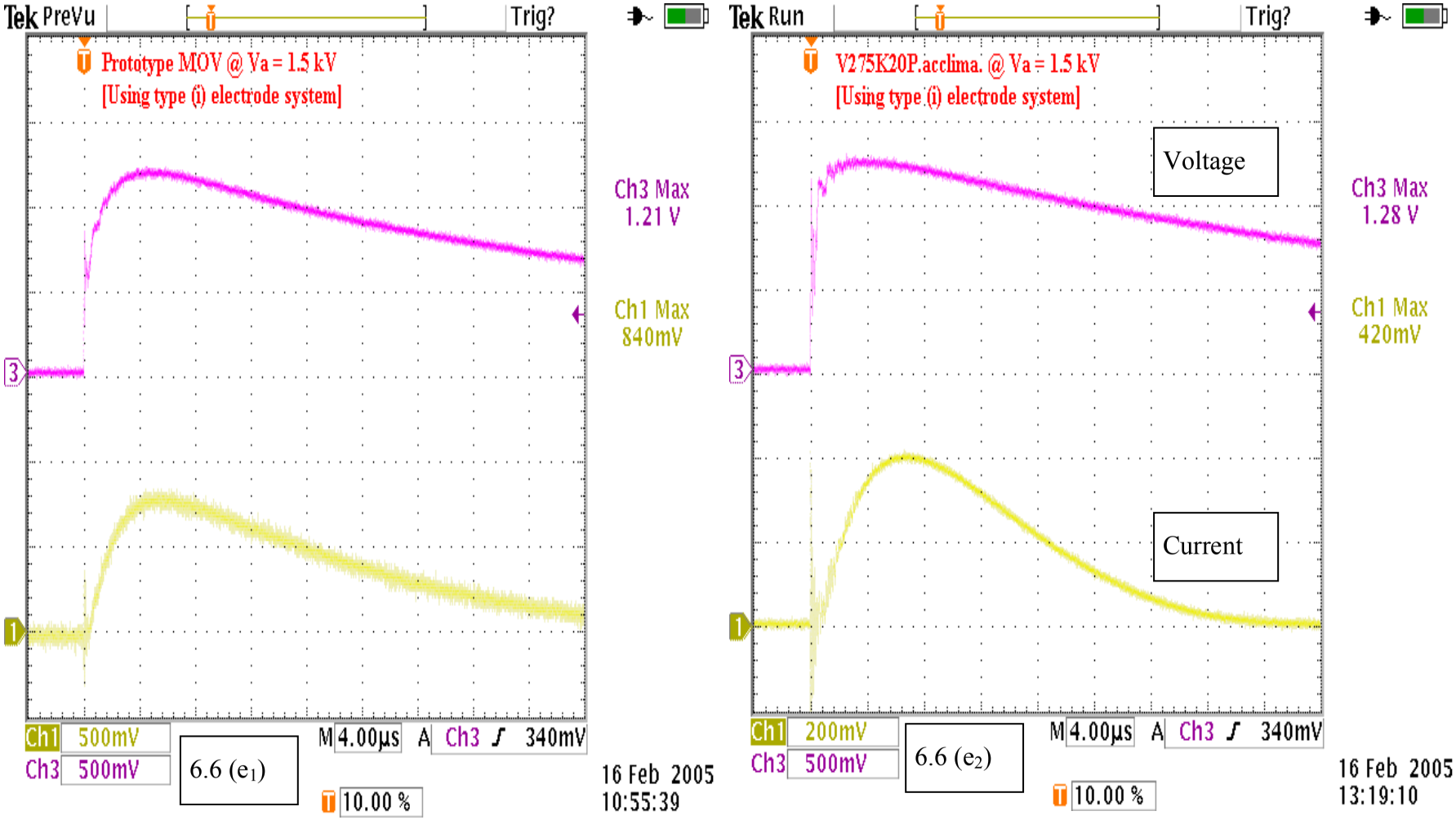

Figure 6.6 (e): Comparative surge clamping action of the prototype MOV to the acclimatized V275K20P @ V_a =1.5 kV

The above result shows that the prototype MOV and the acclimatised commercial MOV did not classically surge clamp at all. By "classically" is meant traditionally as in figure 2.2. The prototype MOV started to conduct at 0.8 kV; the acclimatised commercial MOV, V275K20P (acclima.) did not conduct until at 1.25 kV and yet the as-received V275K20P starts to conduct and simultaneously surge clamps at 0.8 kV, see figure 6.8 b) below. This result implies that the **type** of electrode system has a strong influence on the surge clamping action of the MOV blocks.

The surge response waveforms are also characterised by a voltage "hump", a kind of a voltage overshoot. Similar voltage overshoot was also reported by Eda (1979). The amplitude of this voltage overshoot is identical for both the prototype MOV and the acclimatised commercial MOV. I think that this overshoot is caused by what I coined the "**electrode effect**", see Appendix B, and possibly by the large lead separation area. This is discussed in more detail later.

As mentioned earlier the prototype MOV block and the commercial MOV block were also tested using type (ii) electrode system. The results were compared to those of the commercial MOV in the as-received state. The data is presented in Table 6.3, and the surge response waveforms are shown in figure 6.7.

Table 6.3: Surge response data of the prototype MOV and acclimatised commercial MOV tested using type (ii) electrode system compared to the commercial MOV tested in the as-received state

	Prototype MOV(coated) (In.Ga) (u.p.e.)		V275K20P (coated) (In.Ga) (u.p.e.)		V275K20P (As-received)	
Va (kV)	Vc (kV)	Is (A)	Vcl (kV)	Is (A)	Vcl (kV)	Is (A)
0.50	0.46	0	0.47	0	0.50	0
0.80	0.70	26.40	0.69	28.00	0.66	76
1.00	0.85	60.40	0.85	84.00	0.70	140
1.25	1.04	110.00	1.03	170.00	0.76	230
1.50	1.23	166.00	1.18	260.00	0.80	340
1.80	-	-	-	-	0.85	450
2.00	-	-	-	-	0.88	540

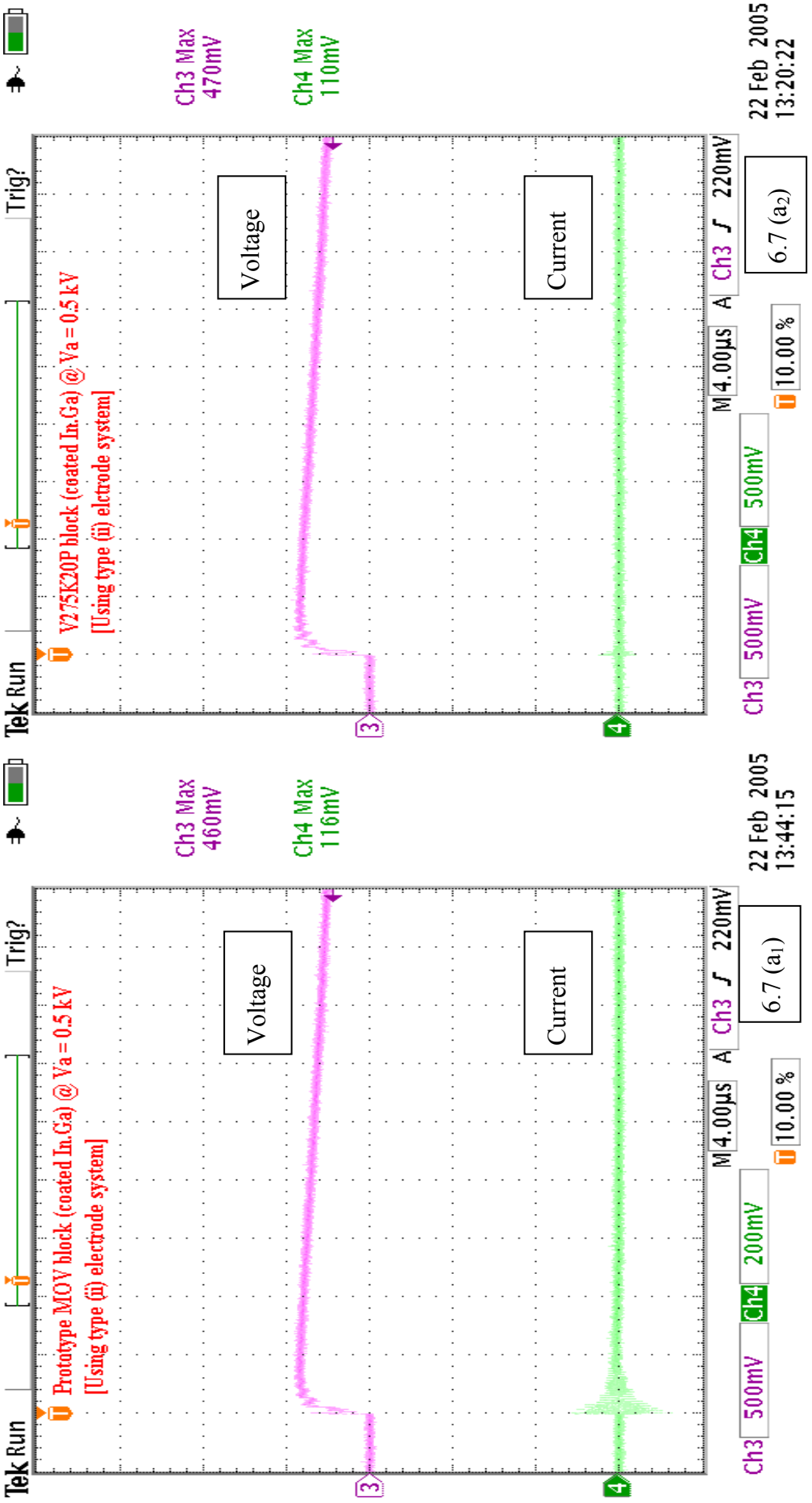

Figure 6.7 (a): Comparative surge clamping action of the prototype MOV to the acclimatised V275K20P @ V_a= 0.5 kV

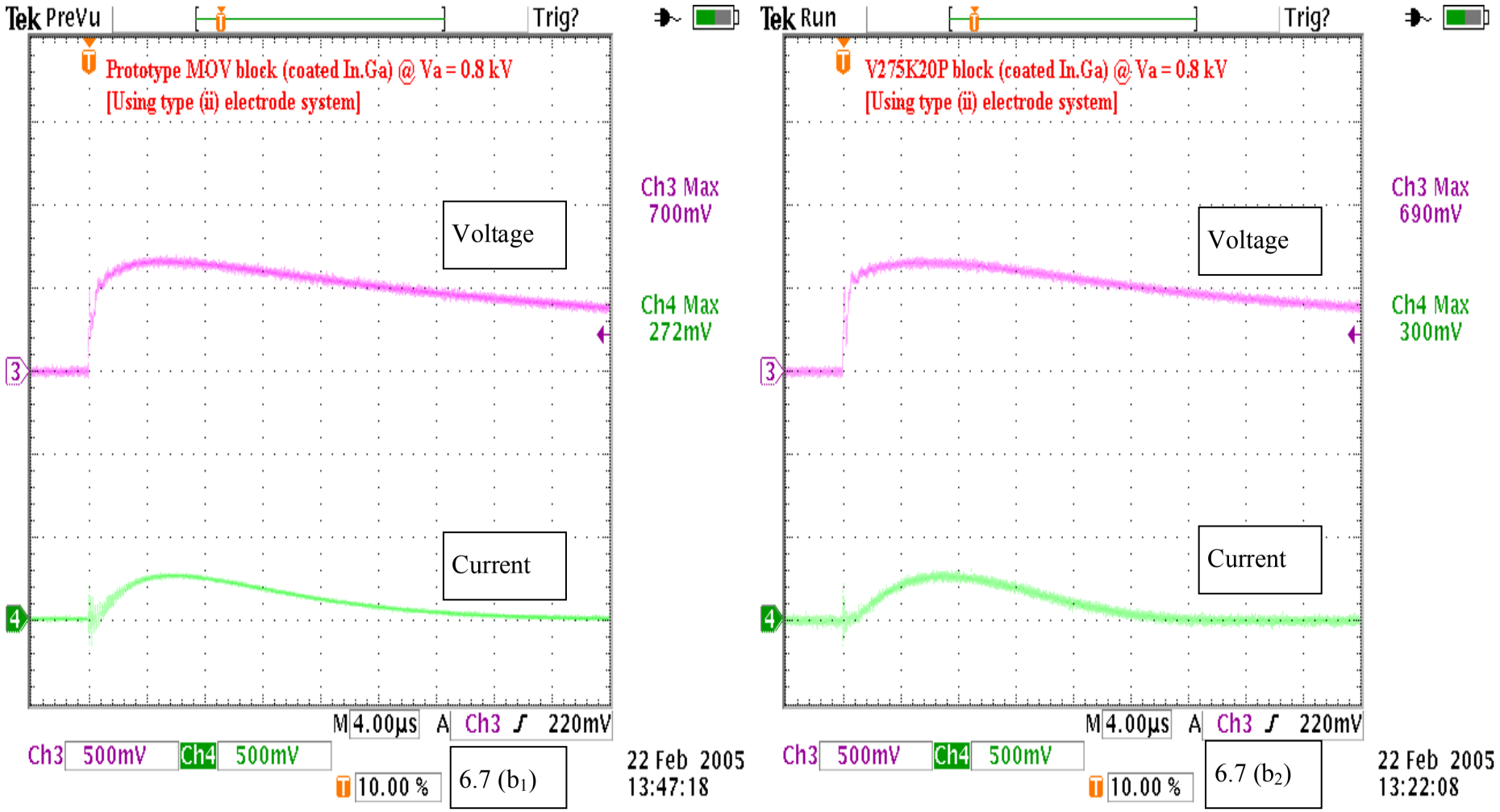

Figure 6.7 (b): Comparative surge clamping action of the prototype MOV to the acclimatised V275K20P @ V_a=0.8 kV

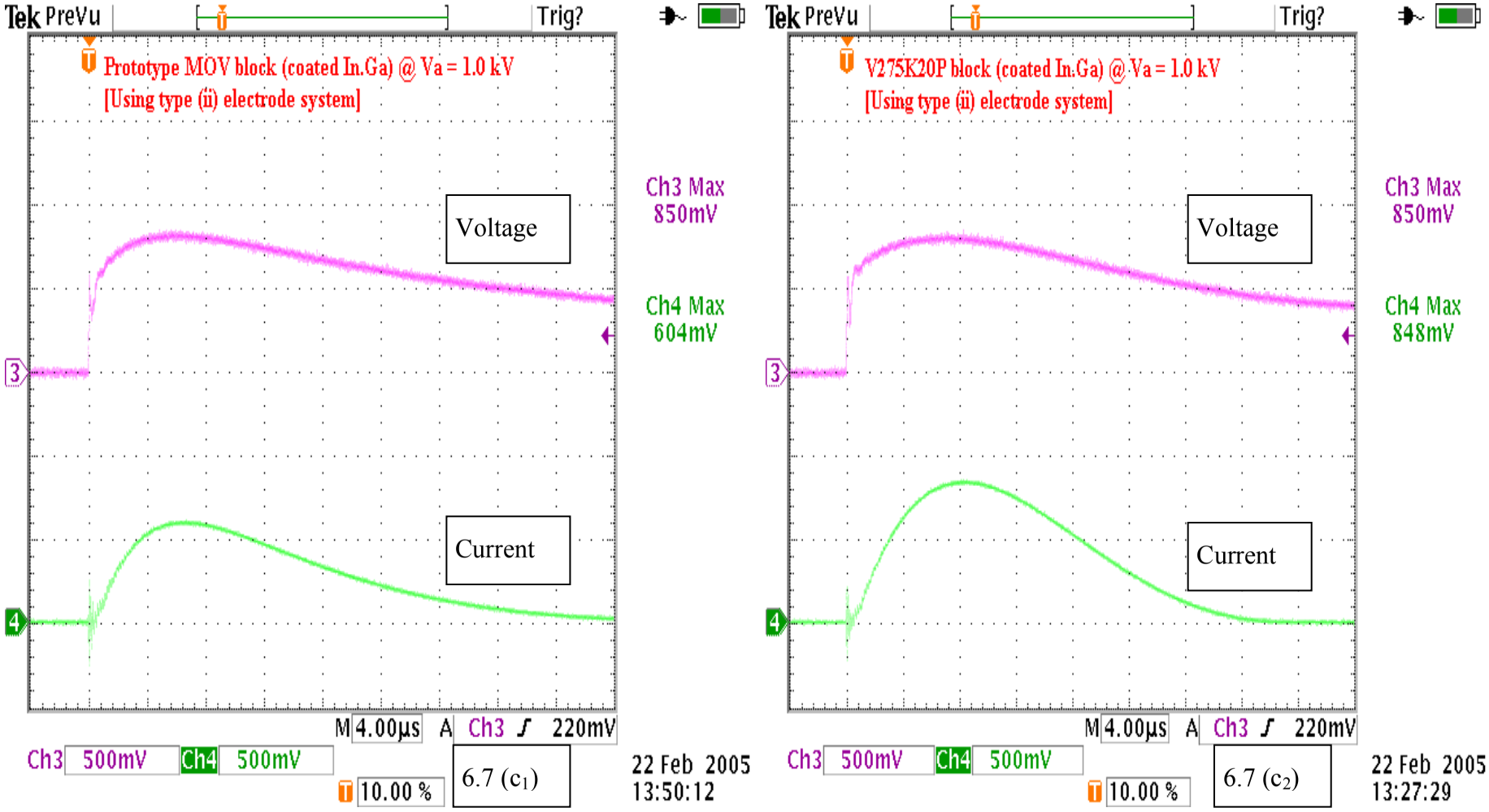

Figure 6.7 (c): Comparative surge clamping action of the prototype MOV to the acclimatised V275K20P @ V_a=1.0 kV

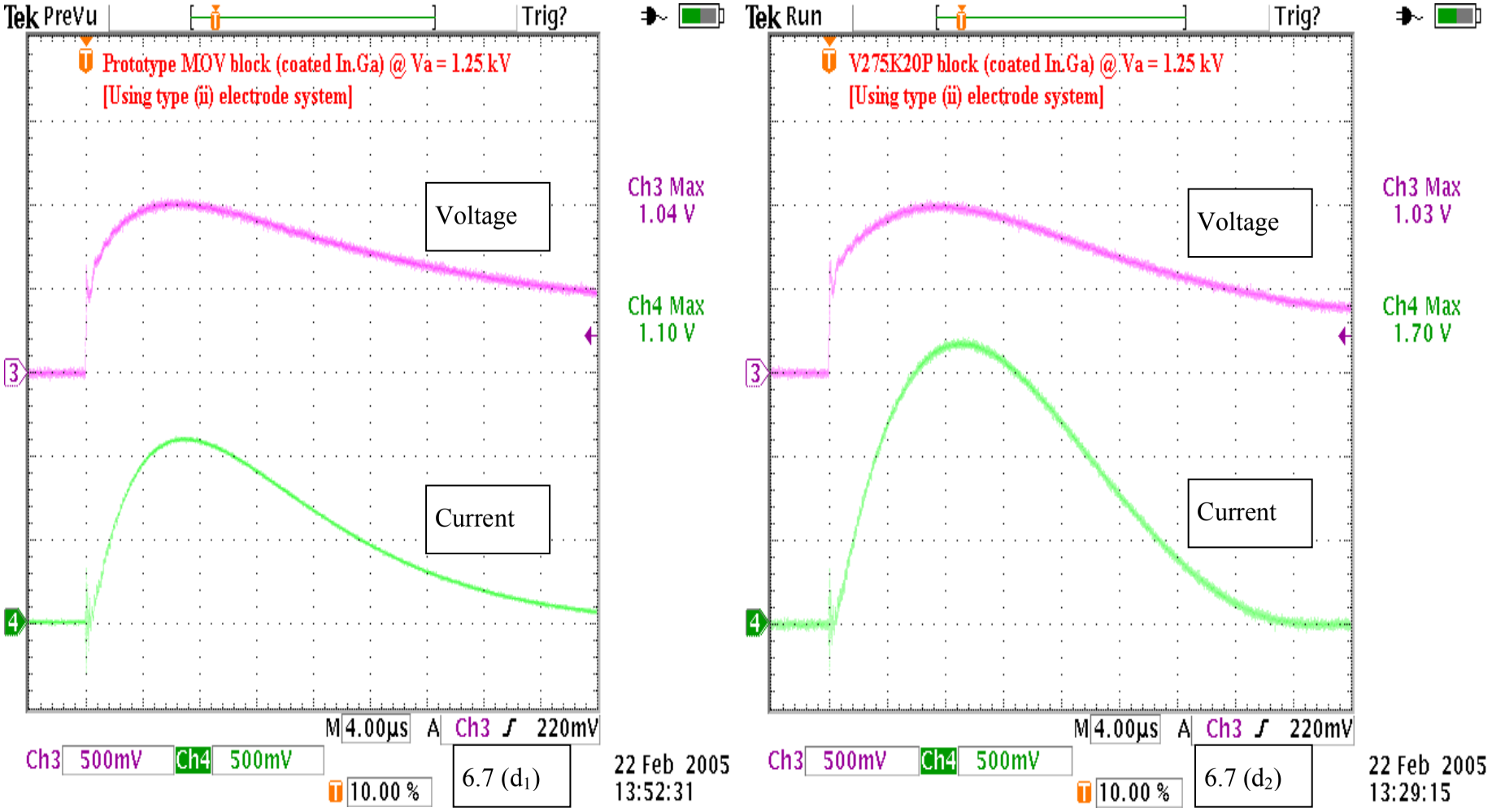

Figure 6.7 (d): Comparative surge clamping action of the prototype MOV to the acclimatised V275K20P @ V_a=1.25 kV

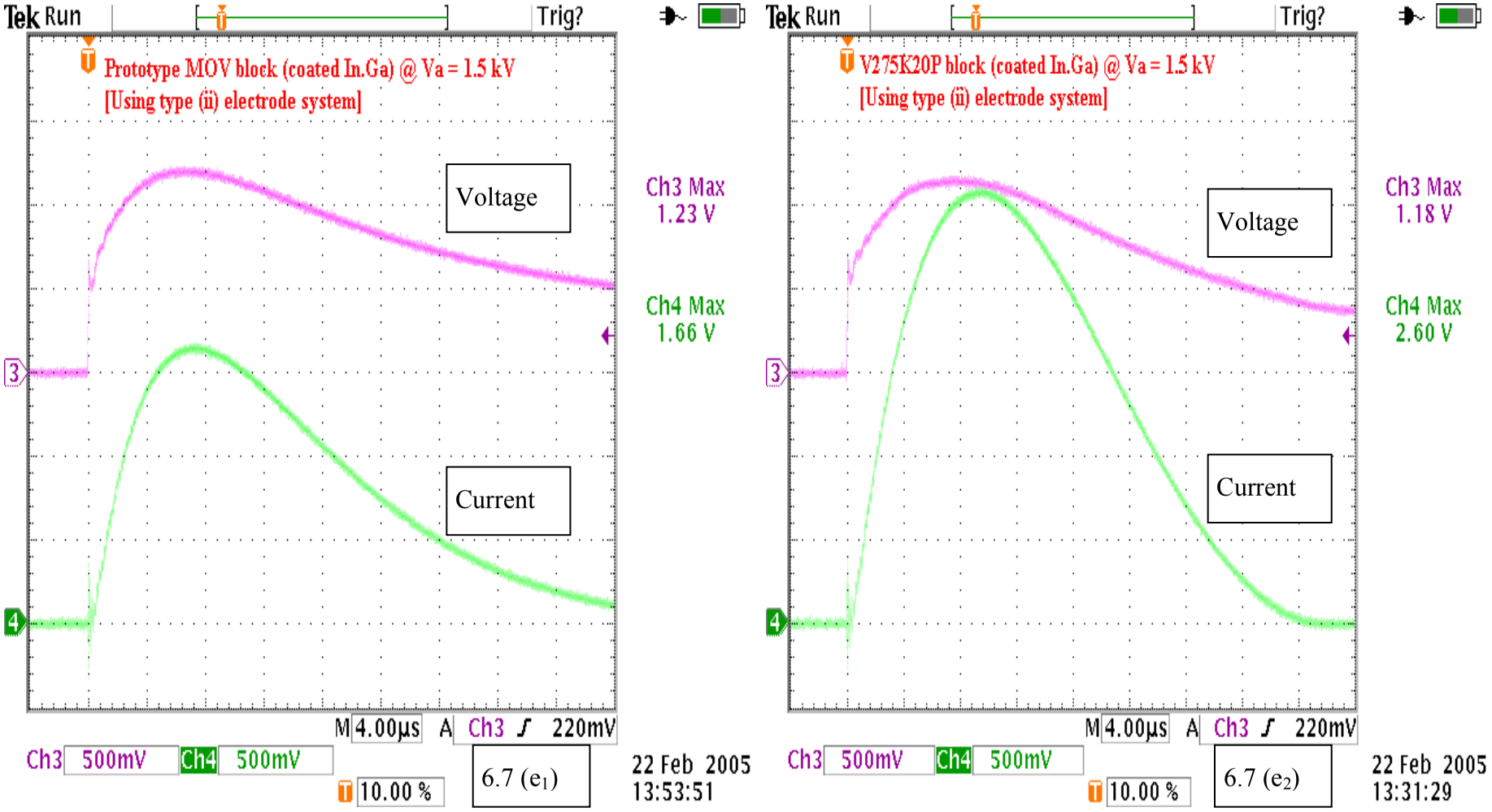

Figure 6.7 (e): Comparative surge clamping action of the prototype MOV to the acclimatised V275K20P @ V_a=1.5 kV

In figure 6.7 (a), both MOVs are in the open circuit condition. In figure 6.7 (b), both MOVs are conducting and show surge clamping action, with the voltage waveform characterised by a voltage "hump". The discharge currents are comparable. However in figure 6.7 (c), they show the same behaviour, but the prototype MOV has lower discharge current compared to the acclimatised commercial MOV. The same trend continues at higher applied surge voltages, see figures 6.7 (d) and 6.7 (e). The voltage "hump" too increases in magnitude with increase in applied surge voltage for both MOVs.

This result (figure 6.7) shows that by changing the type of electrode system and coating the MOV block surfaces to some area, the surge response behaviour is also affected. This became what was coined the **"Electrode Effect"**, see Appendix B. This is further substantiated by the fact that the commercial MOV when impulse tested in the as-received state for the same voltage range as above, see figures 6.8 (a)-(e) below, its surge response action is quite different from that in the acclimatised state as reported above. Thus the behaviour is dependent on the type of electrode system, the type of block coating material as well as coating the MOV block surfaces to some area.

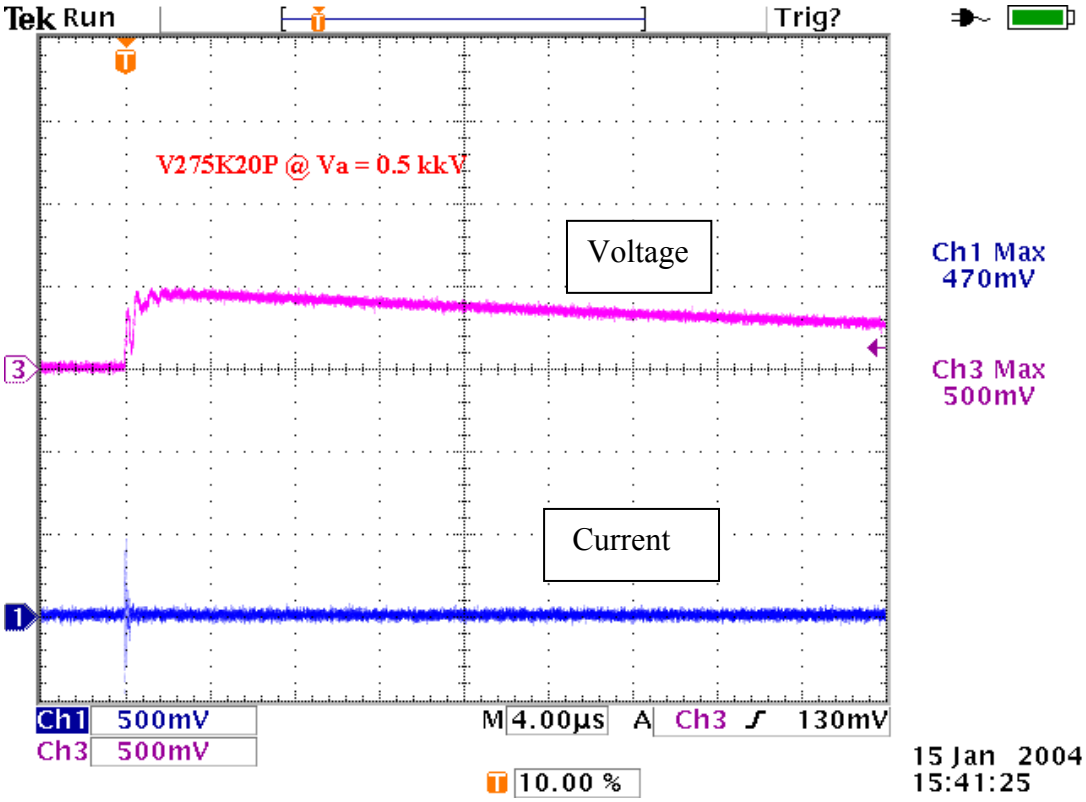

Figure 6.8 (a): Surge clamping action of the as-received V275K20P at 0.5 kV

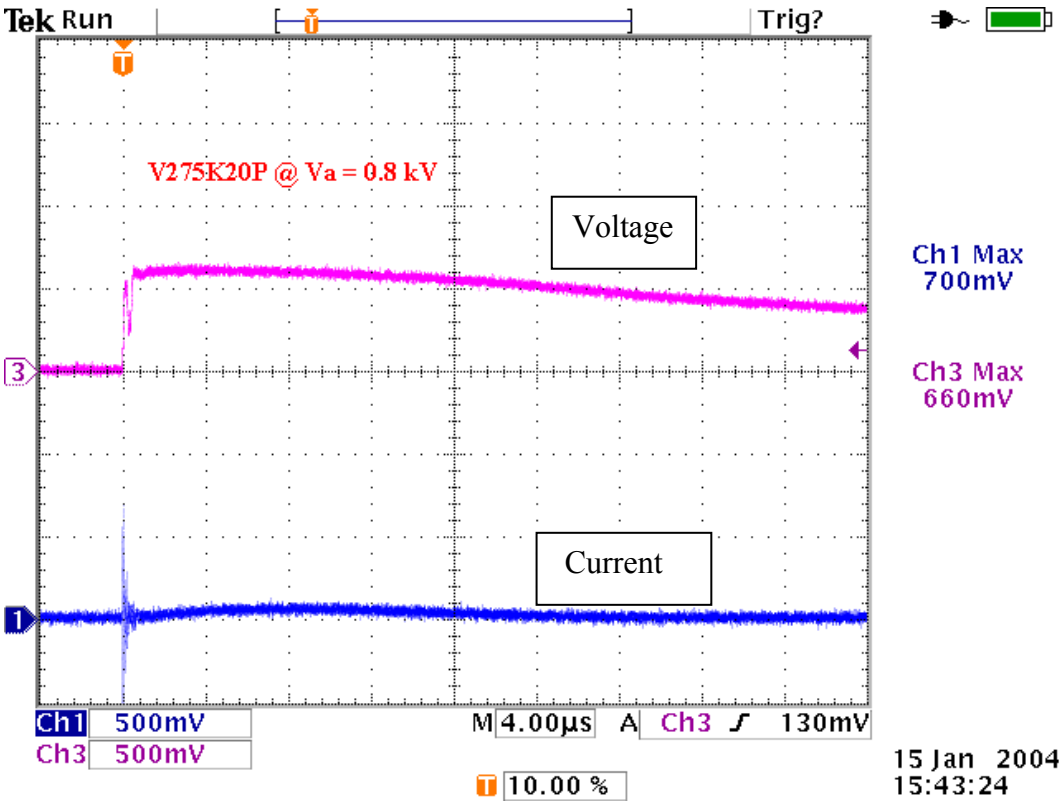

Figure 6.8 (b): Surge clamping action of the as-received V275K20P at 0.8 kV

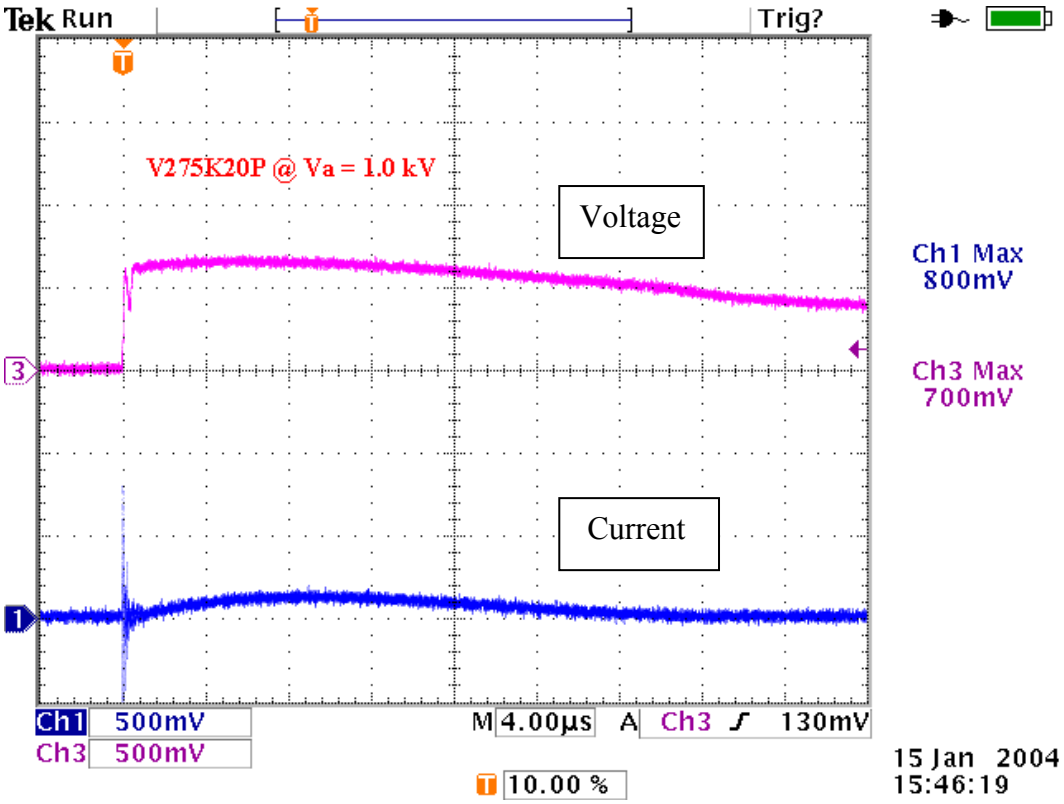

Figure 6.8 (c): Surge clamping action of the as-received V275K20P at 1.0 kV

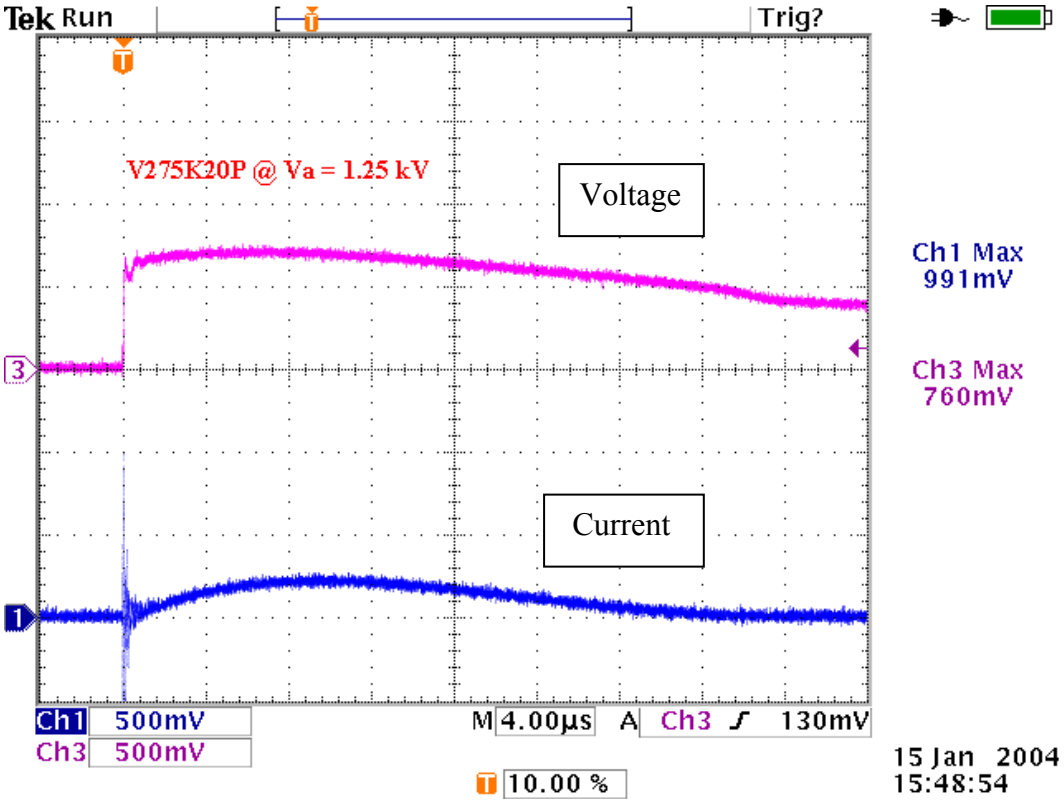

Figure 6.8 (d): Surge clamping action of the as-received V275K20P at 1.25 kV

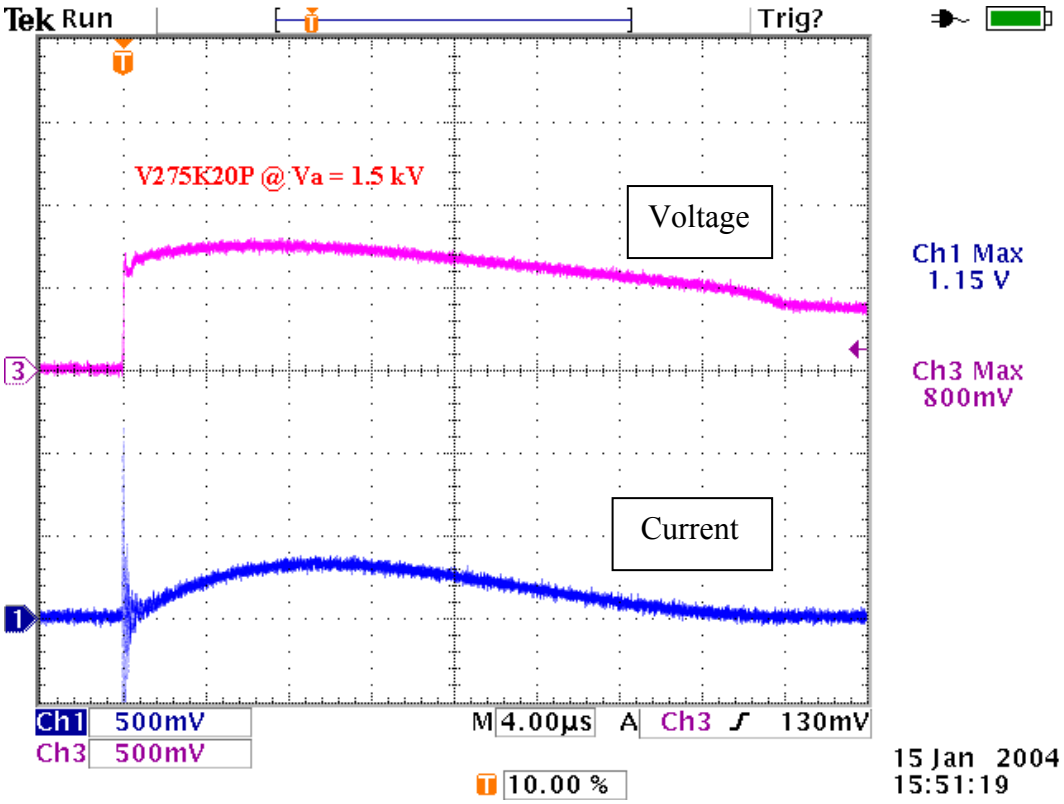

Figure 6.8 (e): Surge clamping action of the as-received V275K20P at 1.5 kV

The above results when taken in aggregate show the following:

a) Depending on the type of electrode system used, the prototype MOV and the commercial MOV can exhibit surge clamping action or they can not. For example, the commercial MOV when tested using type (ii) electrode system, it showed potential surge clamping capabilities, and yet when tested in the as-received it showed full clamping action.

b) The prototype MOV block has a surge clamping action that is almost identical to that of the commercial MOV block when tested under identical conditions. However, the magnitude of the surge current of the prototype MOV is lower than that of the commercial MOV, and the surge current waveform is an 5.6 x 20µs. The surge current waveform for the commercial MOV tested in the as- received state is an 8 x 20µs.

c) When using type (i) electrode system the clamped surge voltage waveform of the acclimatized commercial MOV "tails off" at different levels which are higher than those of the prototype MOV. The "tail off" level increases

with increase in the applied surge voltage. When using type (ii) electrode system the reverse scenario occurs. However, the difference is so small such that the "tail off" levels may be regarded as identical. This small difference could be accounted to be due to differences in the applied pressure on the MOV blocks. Further the amount of drifting in the "tail off" levels is so small in both MOVs. Thus the surge clamping of the prototype MOV block is comparable to that of the commercial MOV block when tested under the same conditions. The drifting in the "tail off" level is not observed in the commercial MOV when tested in the as-received state.

d) The surge clamping level (V_c) of the acclimatized commercial MOV shifts a little more up, i.e., it drifts upwards, with increase in the applied surge voltage than the prototype MOV when tested using type (i) electrode system, see Table 6.2. When both are tested using type (ii) electrode system the surge clamping levels are identical. The clamping levels are higher than those of the commercial MOV when tested in the as- received state. It ought to be noted that the clamping level of the commercial MOV when tested in the as- received state drifts too, however the amount of drift is small.
e) The amplitude of the voltage "hump" is higher when impulse testing using type (ii) electrodes than type (i). It is least in the commercial MOV when tested in the as-received state.
f) The commercial MOV when tested in the as-received state shows a voltage "step" which is not observed when tested using type (i) and type (ii) electrode systems.

For a)-e), the author is of the opinion that this is partly caused by the aforesaid "electrode effect", and partly due to the large lead separation area.

Why the prototype MOV has lower surge current than the acclimatised commercial MOV, is as explained as in section 6.1.3. The same model used to explain why leakage currents were lower in V-I characteristic of the prototype

MOV than that of the commercial MOV is used also to explain why surge currents are lower here.

The surge response action of the prototype MOV as well that of the commercial MOV when tested using type (i) and type (ii) electrode systems showed a voltage "hump", and no voltage "step" - the so-called "current ($I_{8/20}$) zero crossing". The commercial MOV in the as-received on the other hand showed a weaker voltage "hump" and a voltage "step. The cause of this voltage "hump" can be explained by the aforesaid "electrode effect", together with the effect of lead separation area (Harris Manual, 1995), (Beutel, 2000). Other contributing factors are the dynamic resistance of the MOV blocks at surge (Harris Manual, 1995). The concept of the "electrode effect" is given in Appendix B. How the lead separation area influences the voltage "hump" is seen in the following.

The larger the lead separation area, that is, the area encompassed by the leads from the test piece to the output terminals of the impulse generator, the larger the stray magnetic flux, φ. And from Faraday-Neumann Law, the induced voltage, ε, into the circuit is

$$\varepsilon = -\boldsymbol{L}_s \frac{\partial \varphi}{\partial \boldsymbol{t}}, \quad \ldots\ldots\ldots\ldots\ldots\ldots \quad (6.6)$$

with

$$\varphi = \boldsymbol{BA} \qquad \ldots\ldots\ldots\ldots\ldots\ldots \quad (6.7)$$

where L_s is the stray inductance, B is the magnetic flux density, and A is the cross-sectional area. The "-" in equation (6.6) expresses Lenz's Law. It can be seen from equations (6.6) and (6.7) that the larger the lead separation area, also called loop area, the larger the stray flux and the larger the induced voltage. This induced voltage appears as additional volt-drop onto the residual voltage across the MOV. That is, ε is superimposed onto the clamped voltage, and because the rate of change is highest at the front of wave of the surge wave, there will be a larger ε during this period than any other, and hence the observed voltage "hump".

It is for the same reason that the larger the applied surge voltage, the more pronounced the voltage "hump", for then ε becomes larger.

In view of the above effects, namely the "electrode effect" and the lead separation area, the question that arises is: Is the prototype MOV surge clamping or not? The arguments presented below answers this question. It must be born in mind that the need for these arguments was necessitated by the fact that the developed prototype MOV could not be electrode mounted using the same material as the commercial MOV as it is not readily available. An indication of its surge clamping action could only be ascertained by testing it using types (i) and (ii) electrode systems and then compare its behaviour with that of the commercial MOV when tested in the same state. This limited the voltage range of testing to which the investigation would go to 1.5 kV. Higher applied impulse voltages could not be used because of surface discharges that set in, which then masked the true surge clamping action of the MOV blocks.

In the absence of proper electrode mounting and coating material as is used in commercial MOVs, the observed surge clamping action of the studied prototype MOV can be described as comparable to that of the commercial MOV, and it surge clamps with lower surge currents. This has been discussed above. Further, if scientific arguments are taken into account, then it can be shown that by inference, the prototype MOV does in fact surge clamp. The argument put forward, which is in form of a mathematical equivalent statement (Group Theory), is: **If** for the commercial MOV the surge response waveform shown in figure 6.9 implies ($\Rightarrow$) the surge response waveform shown in figure 6.10 (as-received and with clamping action), **then,** for the studied prototype MOV, the surge response waveform shown in figure 6.11 implies ($\Rightarrow$) a surge response waveform with clamping action if the correct electrode system is used **plus** if the correct type of electrode mounting and coating material is used. Thus one can write:

If (for the commercial MOV)

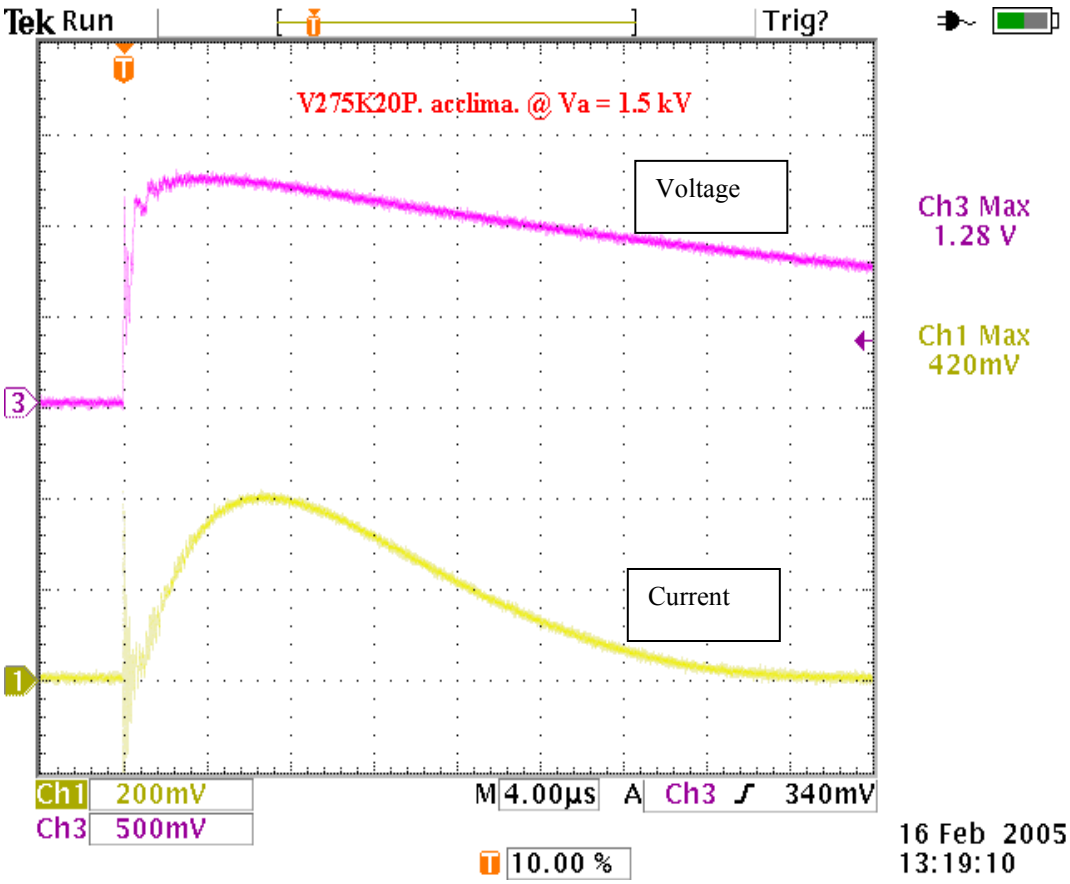

Figure 6.9: Surge clamping action of the acclimatised commercial MOV tested (using type (i) electrode system)

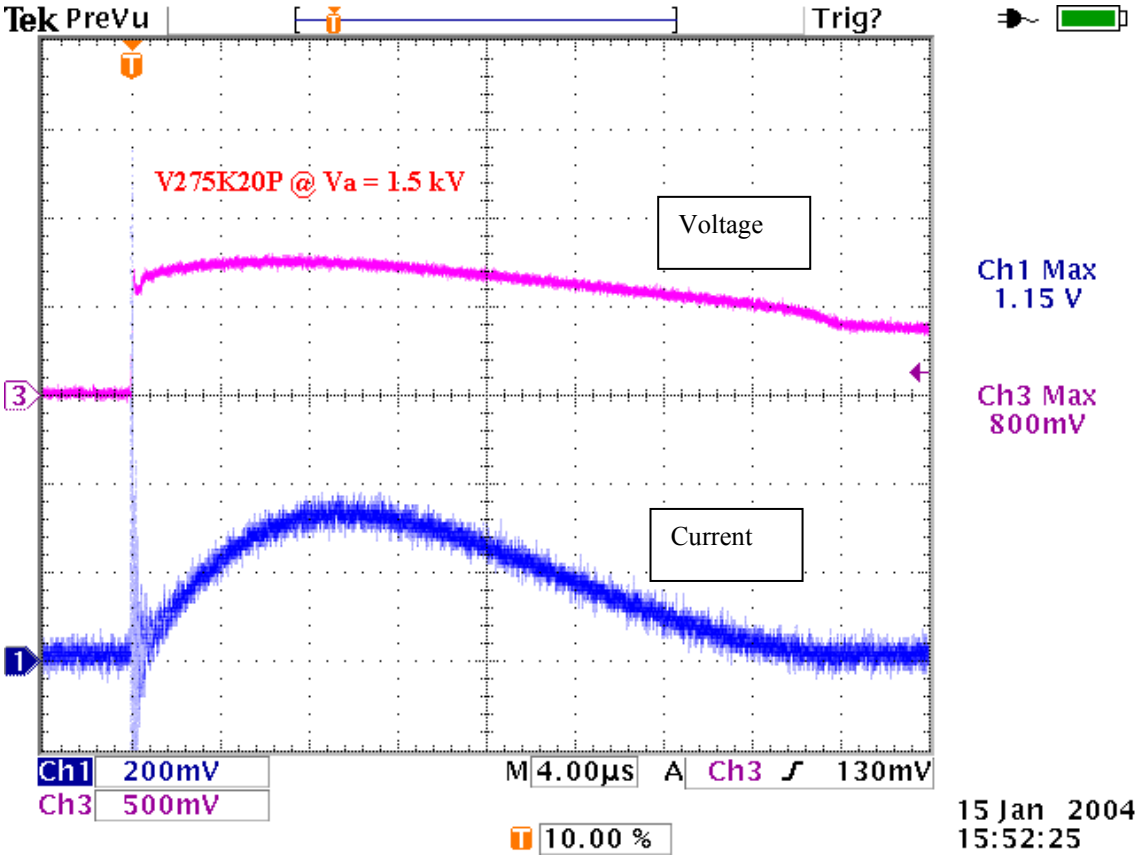

Figure 6.10: Surge clamping action of the commercial MOV tested in the as-received state, showing (classical) clamping action

then, (for the prototype MOV)

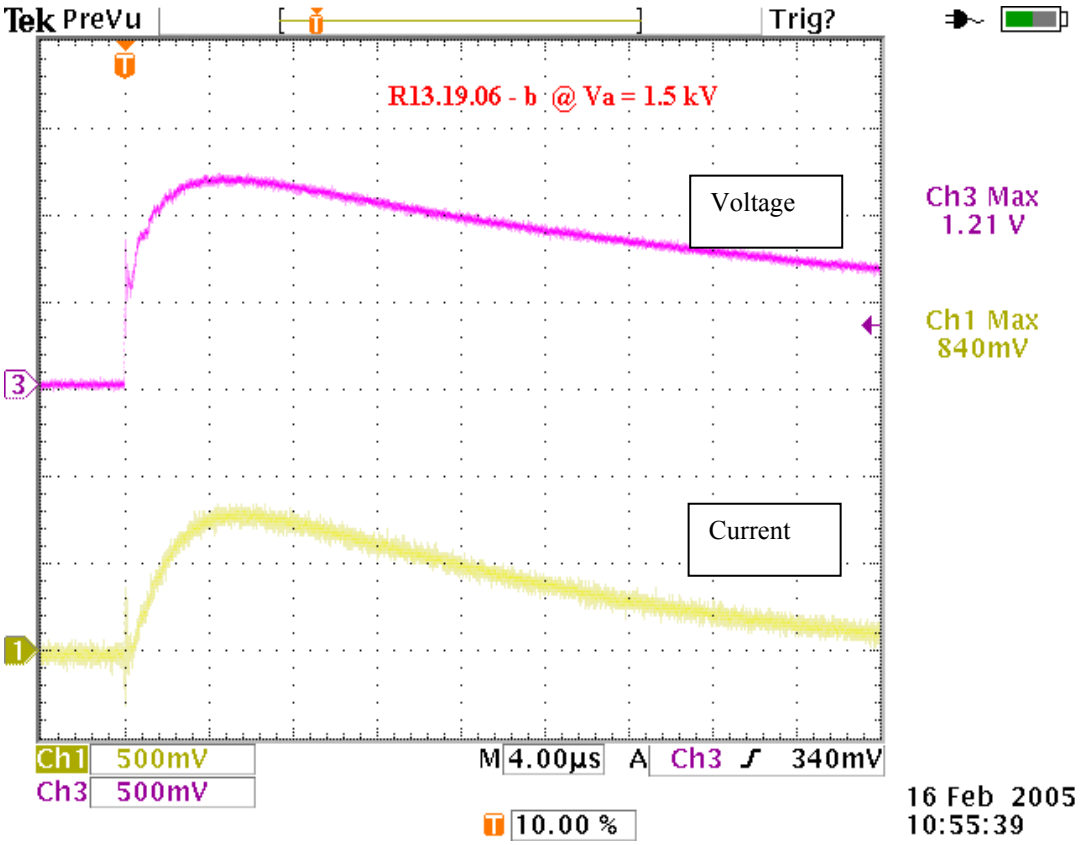

Figure 6.11: Surge clamping action of the prototype MOV tested (using type (i) electrode system)

⇓

Surge response waveform with clamping action if proper electrodes + correct electrode and coating material are used

Further, the phases of the prototype MOV are similar to those of the commercial MOV, see figure 6.16. Thus it can be argued that if it is accepted that the microstructure and hence phases determine the electrical behaviour of a material, then the electrical behaviour of the prototype MOV must be comparable to that of the commercial. Surely if the MOV block of the acclimatised commercial MOV is

re-coated and encapsulated according to commercial standards, it will surge clamp as in the as-received state. Thus it can be inferred that the studied prototype MOV surge clamps classically, with lower surge currents than a dimensionally comparable commercial MOV.

In order to show that the above argument holds water, the commercial MOV was re-tested in the as-received state at applied impulse voltages much higher than those reported in figures 5.6 and 6.7. It was re-tested in the voltage range 0.5 kV - 5.0 kV. The results of this test at applied impulse voltages 1.5 kV and 5.0 kV are shown in figures 6.12 and 6.13. The corresponding discharge currents are shown in the insert. A more attenuating current probe was used in this test so as to protect the digital storage oscilloscope from possible damage.

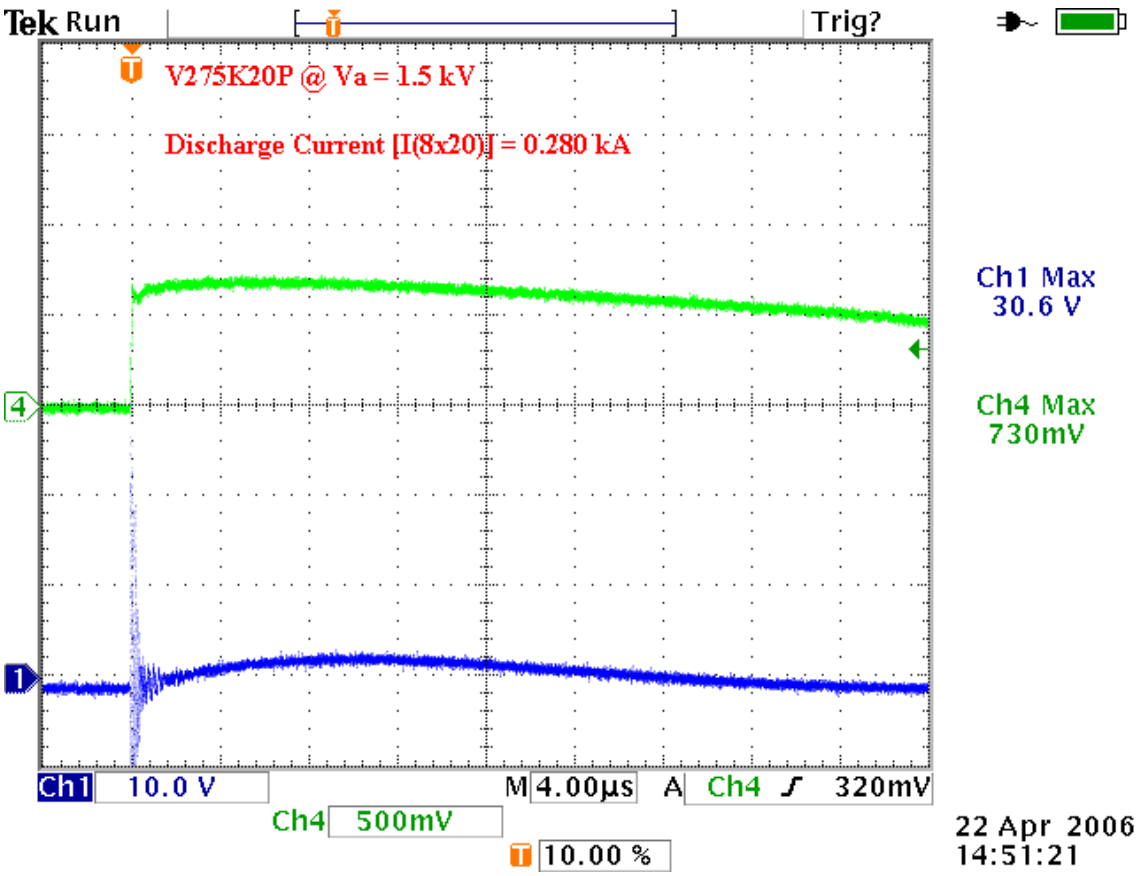

Figure 6.12: Surge clamping action of the as received V275K20P at 1.5 kV tested using a more attenuating current probe

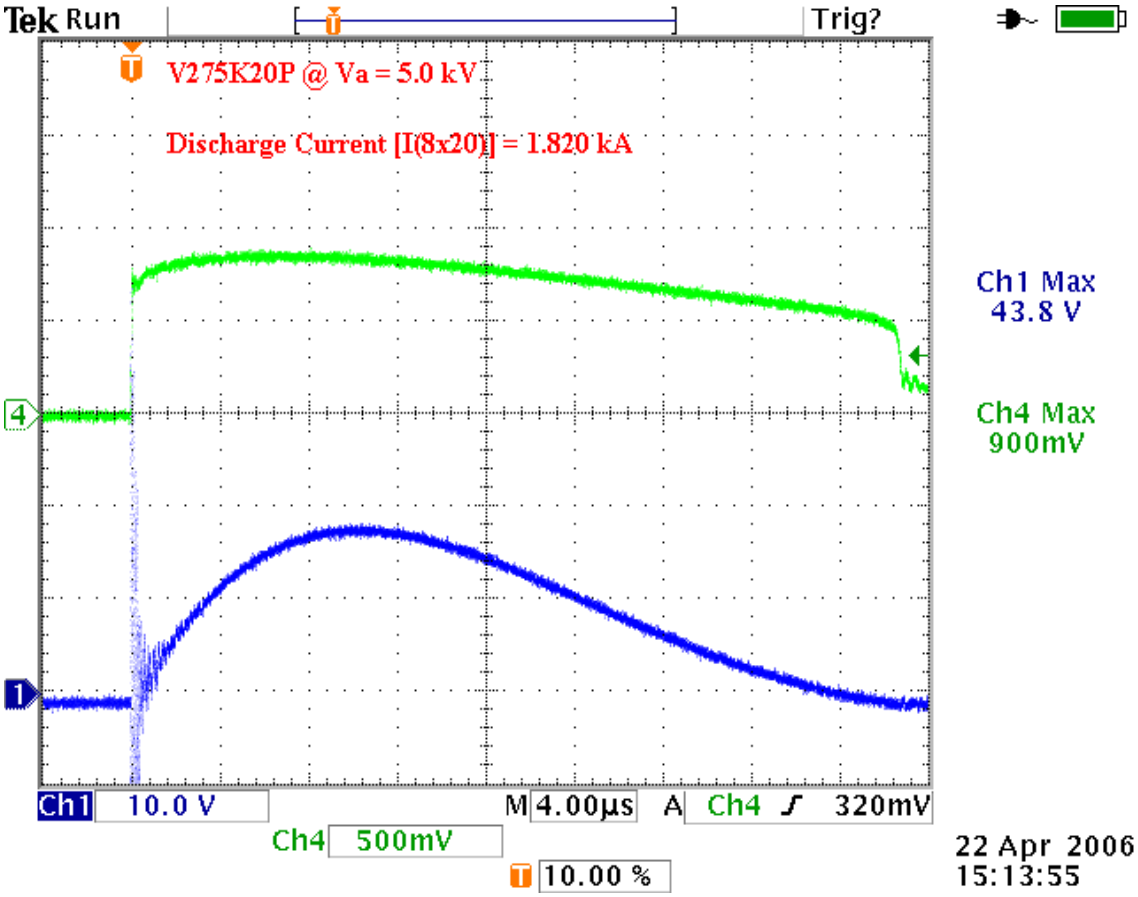

Figure 6.13: Surge clamping action of the as received V275K20P at 5.0 kV tested using a more attenuating current probe

Now compare figure 6.8 (e) with figure 6.12; which are waveforms obtained for the same applied impulse voltage of 1.5 kV but different current probes. It is clear that the clamping level is practically the same. The discharge current in the former was 0.115 kA and in the latter 0.280 kA. The difference in the discharge currents could be due to different current probes used in two tests. Despite this, the fact still remains, that the clamping level is practically the same.

If now the clamping level for an applied impulse voltage of 5.0 kV, see figure 6.13, is compared to that at 1.5 kV, it is seen that the clamping level has shifted from 0.8 kV at 1.5 kV to 0.9 kV at 5.0 kV, but the discharge current has gone up nearly seven (7) times, from 0.280 kA at 1.5 kV to 1.820 kA at 5.0 kV. Surely the commercial MOV is surge clamping at both voltages 1.5 kV and 5.0 kV. And the

clamped surge voltage waveform is practically the same with the exception of the "voltage step" at 5.0 kV.

If now it is accepted that the clamping action of the commercial MOV at 1.5 kV and 5.0 kV when impulse tested in the as-received state is the same, then it surge clamps also at 1.5 kV when in the acclimatised state, see figures 6.6 (e_2) and 6.7 (e_2). What is different between the waveforms in figures 6.8 and 6.12 and those in figures 6.6 (e_2) and 6.7 (e_2) are the voltage "humps". But this difference is partly due to the "electrode effect" and partly due to the large lead separation area as presented before.

Now that the commercial MOV has been shown to be surge clamping at lower applied surge voltages as presented in figures 6.6 and 6.7, and the prototype MOV was found to behave likewise, it follows that the developed prototype MOV does indeed surge clamp, and does so with lower discharge currents.

6.3 Microstructure and Phase Analysis of the Prototype MOV

6.3.1 Microstructure Analysis

In this section, the microstructure of the prototype MOV is discussed and compared to that of the studied commercial MOV. The influence of the microstructure to the observed V-I characteristic and surge clamping action is also presented.

Figures 2.5 (a) and 2.5 (b) show typical microstructure of a ZnO-based commercial MOV, with the later highlighting the grain-boundary layer. This structure was discussed in section 2.2.2.

The microstructure of the prototype MOV is shown in figure 5.4. It was found to be poly-phase. Of significance is that the grey grains were as characterised. They were found to consist of Zn, Bi, Co and Mn. This ties well with characterisation process, namely that the $\boldsymbol{M}$ -grains be μ-MOVs, and the identified elements are known to be typical oxides found in a ZnO-based commercial MOV (Matsuoka, 1971), (Clarke, 1978), (Greuter *et al*, 1989).

The grain boundary material of the prototype MOV was found to consist of Zn, Bi, Mn, Co, Te, Si, La and Cd. Again this is as per characterisation, namely that the inter-granular material should contain phases that give the required instabilities. The Cd is an impurity from the as-supplied powders. This is unlike the commercial MOV, which contains Zn, Bi, Mn, Co, Cr and Sb. There is therefore a difference in microstructures.

From the above it is reasonable to conclude that the Si and Te constitute the $SiTe_2$, and the Bi to be tied to one of its natural phases, typically α-Bi_2O_3. The latter makes sense since α-Bi_2O_3 was the main constituent additive powder. The Zn is then present in the inter-granular material as a dopant. This analysis would tie well with the energy band (E-B) diagram given in figures 6.4. This (E-B) diagram was used to explain the reported V-I characteristic and surge voltage clamping action of the prototype MOV. Thus there is a correlation between the microstructure and the electrical behaviour.

A point of observation needs to be made at this point. It was mentioned in section 5.3.1 that a spot scan analysis of the grey grains did not detect the presence of Bi as was the case with an areal scan. This is explained as follows: According to the model used for the characterisation process, the grey grains scanned were $\boldsymbol{M}$ -grains, see figure 3.3, section 3.2. The sub-structure of these grains is shown in figure 3.2. At sintering the Co^{2+} and Mn^{2+} dissolve into the Zn-lattice, i.e. substitutional dopants, hence can be detected by the spot scan. The Bi^{3+} does not dissolve into the Zn-lattice by virtue of its ionic radius; it is confined to the grain

boundary regions. Hence its probability of detected in a spot scan is low unless a large number of spot scans are done.

The microstructure also consists of "rod-like" structures as well pores. Figure 5.4 shows such a typical structure. It is clear that it is part of the microstructure.

To rule out the possibility that the observed "rod-like" structures were not organic fibres coming from outside, microstructure studies on a number of preliminary prototype MOV blocks of similar composition were studied. Similar such structures were observed. What differed was their morphology which was found to be composition dependent. Figure 6.14 shows a "rod-like" structure in **one** such MOV block. One end of the same structure is shown at a higher magnification in figure 6.15. It is clear that the rod-like structure is anchored, meaning that it is an integral part of the microstructure.

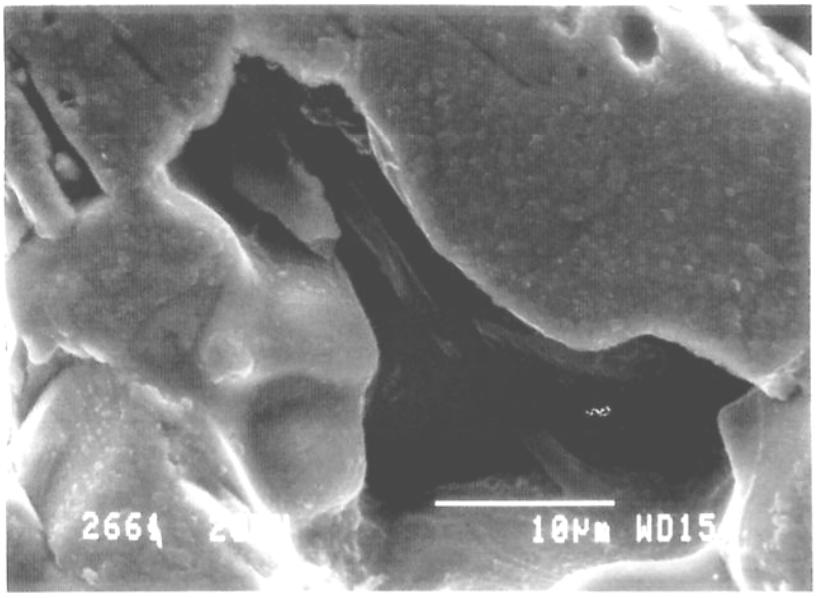

Figure 6.14: Microstructure of a MOV block, showing a "rod- like" structure inside and running across a pit

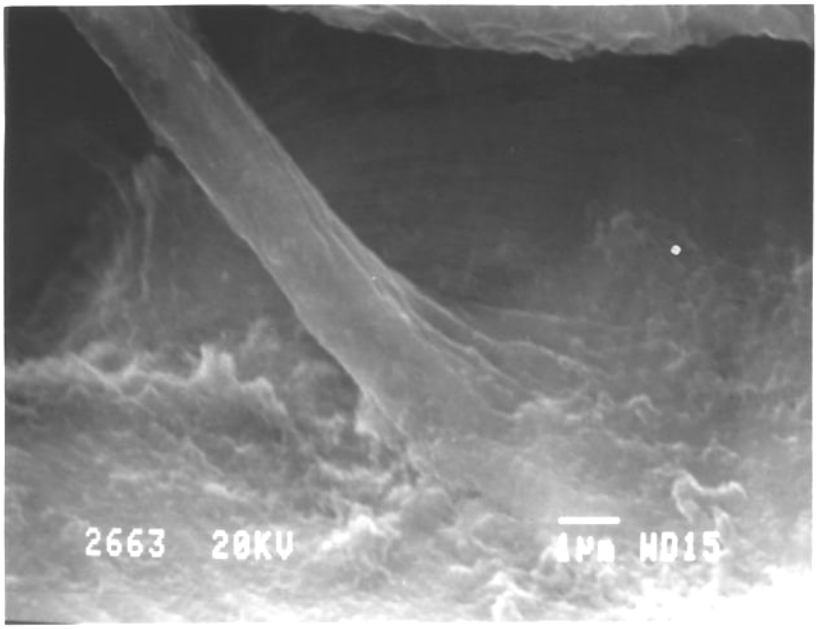

Figure 6.15: The "rod-like" structure in figure 6.15 at a higher magnification showing that it is anchored.

To further substantiate that the fibres were not organic coming from outside, fractured samples of prototype MOV blocks were also studied. The results of this study confirmed the existence of "rod-like" structures, see figures 5.7-5.9. It was further observed that the microstructure of the prototype MOV had in addition to the "rod-like" structures other unique sub-structures which were not observed in polished samples. Typical such structures are shown in figures 5.11-5.12.

The evolution of these inorganic fibres can possibly be explained as follows: The prototype MOV blocks were fabricated from powder mixtures of which the main powder was a characterised powder termed the ***M*** -powder. The grain size of this powder was ≤ 53 μm. Thus they are large grains. The microstructure of the as-sintered prototype MOV blocks was found to be porous. Now the process temperature for the prototype MOV blocks was 850 °C. Two of the additives used to fabricate these blocks melt at lower temperatures. These are the $SiTe_2$ which

melts around 450 °C, and Bi_2O_3 which melts at 825°C. Thus we have a two-stage liquid phase sintering process. At the above process temperature the liquid phase will be viscous and as such it can flow. The as-sintered prototype MOV blocks were air quenched at 850 °C. It is plausible therefore that upon air quenching, the viscous phase running in and across the pores is quenched too in stu.

Having discussed the microstructure of the studied prototype MOV, this microstructure is now compared to that of the studied commercial MOV.

The microstructure of the studied prototype MOV differs from that of the studied commercial MOV in a number of respects. The grains of the commercial MOV contain ZnO doped with Co^{2+} ands Mn^{2+} (Greuter *et al*, 1989). Those of the prototype MOV contain ZnO doped with Co^{2+} ands Mn^{2+} **plus** all additives that go in the making of a commercial MOV. This was the model, see figure 3.3.

The grain boundary material in a commercial MOVs is made of two phases, a pyrochlore phase, $Bi_2Zn(Zn_{4/3}Sb_{2/3})O_6$, and a spinel phase, $Zn(Zn_{4/3}Sb_{2/3})O_4$ (Clarke, 1978), (Asokan *et al*, 1990), (Cho *et a*l, 1997), (Greuter *et al*, 1989). The grain boundary material is responsible for the varistor action observed in ZnO-based commercial MOVs, and the above-mentioned phases are said to be responsible. Now in the studied prototype MOV, the grain boundary material had neither the pyrochlore phase nor the spinel phase and yet it exhibited varistor action with improvements in the three regions of the V-I characteristic over that of the commercial MOV. This is an important and significant difference. It is important because it means that the pyrochlore phase, $Bi_2Zn(Zn_{4/3}\ Sb_{2/3})O_6$, and the spinel phase, $Zn(Zn_{4/3}\ Sb_{2/3})O_4$ are not the only phases responsible for the varistor property which gives rise to the non-linear V-I characteristic in ZnO-based commercial MOVs. It is significant because the varistor property was obtained using new materials previously not reported.

Further, and of major significance also, is the fact the microstructure of the prototype MOV had "rod-like" structures which were not observed in the microstructure of the commercial MOV. Again this is yet another important and significant difference. It is important and significant because it is new information and therefore forms a significant contribution in MOV technology. The role(s) played by these "rod-like" structures in the electrical behaviour of the prototype MOV is not known yet. However, I think they participate in the conduction mechanism of the MOV, by acting as conduction paths, see also section 6.3.3.

It was mentioned in Chapter 1 that an ideal microstructure of an ideal device is not known yet and is unheard of. The microstructure of a material determines the electrical behaviour of that material. Because the microstructure of the developed prototype MOV yielded a near ideal V-I characteristic, it can be argued that this microstructure forms the basis for the development of an ideal ZnO-based commercial MOV.

6.3.2 Phase Analysis

In this section, the phases of the prototype MOV are discussed and correlated to the reported microstructure. These phases are compared to those of the studied commercial MOV.

The XRD pattern of a material shows the phases present in that material. It is a plot of the intensity (I) of diffracted x-rays versus the 2θ-values, the angles of diffraction. The peaks in XRD pattern are the intensity lines of a particular material in its elemental or pure form, and are thus unique. This identifies the phases present in a material.

From XRD studies, the XRD pattern of the prototype MOV is shown in figure 5.13, and the phases determined as described in section 4.4 are shown. The identified phases were:

1. Hexagonal ZnO
2. Bismuth related phases, seemingly α-Bi_2O_3 and δ-Bi_2O_3 phases
3. Zinc Platinum Oxide (Zn_2PtO_4)
4. Silicon Telluride ($SiTe_2$)

The main phase in the microstructure of the prototype MOV was found to be ZnO, see figure 5.13. This was also confirmed by EDS studies, see figures 5.5 and 5.6. The as-received ZnO powder was found to be hexagonal ZnO $P6_{3mc}$ (186), with d-spacings of the first three main peaks as 2.48_x 2.82_{58} 2.60_{44}, and with lattice parameters a = 3.2539(1), b = -, and c = 5.2098 (3). The corresponding Miller indices are (1 0 1), (1 0 0) and (0 0 2). The d-spacings of ZnO phase found in the prototype MOV were found to be identical to those of the as-received powder, and hence it was concluded that the other crystallographic parameters were accordingly the same.

One of the main additives used in the fabrication of the prototype MOV was α-Bi_2O_3. It is almost invariably found in all ZnO-based commercial MOVs. The as-received α-Bi_2O_3 had d-spacings of the first three strongest lines (main peaks) as 3.25_x 2.71_{40} 3.31_{40} and with lattice parameters a = 5.850, b = 8.166, c = 7.51. A phase with these d-spacings was found in the figure 5.13, and accordingly it was concluded that it was the α-Bi_2O_3. From the unaccounted d-spacings, the other Bi-related phase was determined, and that is, the δ-Bi_2O_3.

Of the new additive powders, $SiTe_2$ was one of them. The other one was LaB_6. The $SiTe_2$ was the s-phase prepared as reported in section 4.1. Also as reported in that section, this material was silvery and brittle. Its XRD pattern was characterised by broad and diffuse peaks. Such is the xrd pattern of a disordered or amorphous material. That it was $SiTe_2$ was determined as described in section 4.4. It was determined to be hexagonal $SiTe_2$, space group P$\underline{3}$m1 (164), with d-

spacings of the first three main peaks as 3.2521_x 2.4944_{23} 2.1443_{22} and with the following lattice parameters: a = 4.2887, b = -, c = 6.7330. A phase with these d-spacings was also found in the XRD data of the prototype MOV and accordingly it was concluded that it was the $SiTe_2$.

The LaB_6.was sourced from commercial outlets. Its crystallographic parameters were determined from the PDF database. It was found to be cubic, space group Pm-3m (221), with lattice parameters lattice parameters a = b = c = 4.1566, and d-spacings of the first three main peaks as 2.94_x 4.16_{66} 1.86_{41}. This phase was not found in the experimentally determined XRD data. However, from EDS studies it was found to be in the grain boundary material as well as in the "rod-like" structures, see figures 5.6 and 5.10.

Of interest is the presence of the Zinc Platinum Oxide (Zn_2PtO_4) phase in the prototype MOV. Platinum was **not** added directly in the starting powders used to fabricate the prototype MOV. I think it came about as an impurity from the as-received powders. Hence the Zinc Platinum Oxide (Zn_2PtO_4) must have evolved as a result of chemical reactions that took during the sintering process. It too was determined as described in section 4.4 when trying to account for the unknown or unaccounted for phases in the XRD data. It was found to be face-centred cubic, space group Fd-3m (227), with lattice parameters a = b = c = 8.5490, and d-spacings of the first three main peaks as 2.5770_x 1.5110_{50} 1.8450_{40}. Its influence on the V-I characteristic and surge clamping action of the prototype MOV is not known as yet. However, from figure 6.16, the influence seems to be strong, for its presence makes the xrd pattern, and hence the phases, of the prototype MOV to be very similar to that of the studied commercial MOV. And as such similar electrical behaviour is expected, in particular surge clamping action, see section 6.2.

To account for the differences and similarities in the electrical behaviour of the prototype MOV from that of the commercial MOV, the phases of the commercial MOV, V275K20P, were also studied. It was found to consist of the following phases:

a) Hexagonal ZnO
b) Bismuth-related phases; seemingly the α-Bi_2O_3, β-Bi_2O_3 and δ-Bi_2O_3
c) Pyrochlore phase, $Bi_3Zn_2Sb_3O_{14}$
d) Spinel phases, both the α-$Zn_7Sb_2O_{12}$ and β-$Zn_7Sb_2O_{12}$.

Cho *et al* (1997) reported similar results in ZnO-based MOV compositions.

The XRD pattern of V275K20P is compared to that of prototype MOV in figure 6.16. It is clear that the main phase in the prototype MOV is identical to that in the commercial MOV. However the secondary phases are different. The difference in the secondary phases is attributed to the additives used in the prototype MOV. Table 6.4 compares the secondary phases of the prototype MOV and those of the commercial MOV. From this table it is clear that the prototype MOV has similar phases to those of the commercial MOV. Further, they are phases in both the prototype MOV as well as the commercial MOV that could not be uniquely identified, for advanced techniques to do so were required.

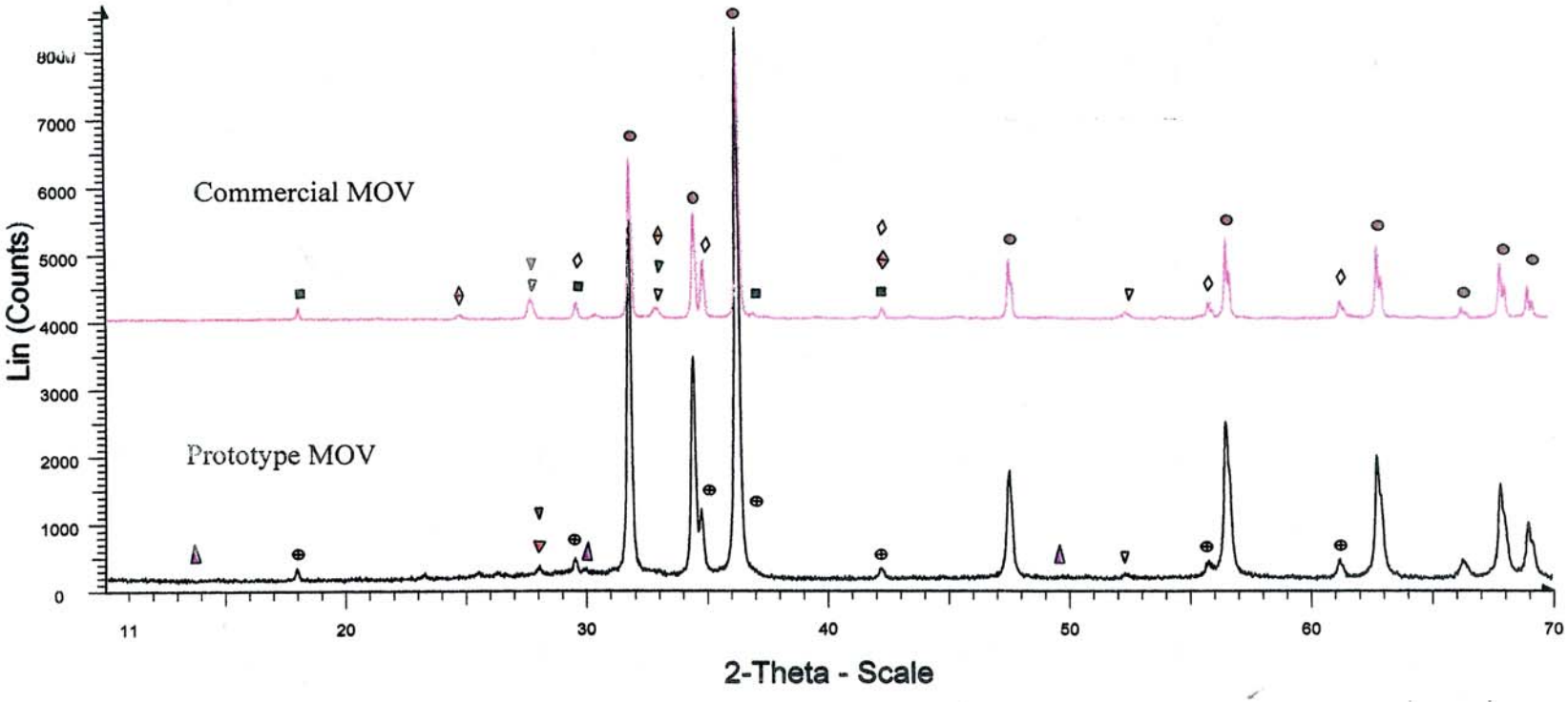

Figure 6.16: XRD pattern of the prototype MOV compared to that of the studied commercial MOV.
(⊙) Hexagonal ZnO, (▽) α-Bi_2O_3 (▽) β- Bi_2O_3 (▽) δ-Bi_2O_3 (△) $SiTe_2$ (⊕) Zn_2PtO_4 (▪) Pyrochlore
(◊) α-Spinel(◊) β-Spinel

Table 6.4: Secondary phases of the prototype MOV and the studied commercial MOV compared

Prototype MOV		V275K20P	
2θ - values (°)	d-spacings	2θ - values (°)	d-spacings
10.121	8.7328	10.130	8.7249
17.933	4.9424	17.955	4.9362
21.839	4.0664	21.345	4.1593
23.4	3.7986	24.715	3.5993
25.4599	3.4957	27.685	3.2195
26.1727	3.4021	29.540	3.0214
28.0472	3.1788	30.380	2.9398
29.5155	3.0240	32.865	2.7229
29.8933	2.9866	34.775	2.5776
32.837	2.7253	39.580	2.2751
34.7544	2.5792	42.265	2.1365
39.5584	2.2763	43.465	2.0803
42.2242	2.1386	45.495	1.9921
43.721	2.0688	49.245	1.8488
45.6098	1.9874	52.435	1.7436
49.4231	1.8426	54.020	1.6961
52.4238	1.7440	55.840	1.6451
54.4267	1.6844	61.320	1.5105
55.8237	1.6546	61.495	1.5066
61.2407	1.5123	64.520	1.4431
61.6043	1.5043		
64.6977	1.4396		

The main difference in secondary phases of the prototype MOV and the commercial MOV is that the prototype MOV had $SiTe_2$ and Zn_2PtO_4 which were not found in the commercial MOV. The commercial MOV on the other hand had β- Bi_2O_3, the pyrochlore phase, $Bi_3ZnSb_3O_{14}$, the spinel phases, α-$Zn_7Sb_2O_{12}$ and β-$Zn_7Sb_2O_{12}$ which were not found in the prototype MOV. It is these similarities and differences in the phase composition of the prototype MOV and the commercial MOV that explain the similarities and differences in the V-I characteristics and surge clamping action of these two.

What needs to be highlighted however, is the role played or significance of Zinc Platinum Oxide (Zn_2PtO_4) in the prototype MOV. Zinc Platinum Oxide (Zn_2PtO_4) seems to bring forward the close similarity in secondary phases with respect to location in the xrd patterns in terms of 2θ-values, and yet different in composition between those found in the studied commercial MOV and those found in the prototype MOV. Figure 6.16 shows this. In brown are phases that are very similar. I believe they play similar roles electrically. In green are phases that are "out of synchronism". I believe this is what causes the two to differ in their electrical behaviour This observation is significant because it explains why the surge clamping actions of the two MOVs are similar. It is the difference in the composition, and difference in the morphology of the microstructures that gives rise to the observed differences. For example, the surge clamping action of the prototype MOV was characterised by lower discharge currents compared to that of the commercial MOV. Similar arguments apply when it comes to explaining the differences in the V-I characteristics between the two MOVs.

Zinc Platinum Oxide, Zn_2PtO_4, is cubic, space group $F_{d\text{-}3m}$ (227), and has the following lattice parameters a = b = c = 8.54900. Zn_2PtO_4 seems to be isomorphous with $ZnCr_2O_4$, a phase reported in other ZnO-based prototype MOVs (Choo *et a*l, 1997). It is therefore not surprising that the surge clamping action of these two devices is very similar.

Now that the electrical results, the microstructures and phases have been discussed, the correlation between the reported electrical results and microstructures is discussed.

6.3.3 Microstructure-Electrical Properties Relationship

The problem in this investigation is to do with the microstructure. This work sought what may be called an *ideal microstructure*. An ideal microstructure is not yet known and is unheard of in current literature. What is known though is the desired electrical behaviour that results from such an unknown microstructure, in particular the V-I behaviour must be ideal as shown in figure 2.10, and the surge clamping action must be ideal too as shown in figure 2.12. As reported before the microstructure determines the electrical behaviour. In this sub-section, the inter-relationship between the microstructures and the electrical results reported above are discussed.

The microstructure of the prototype MOV was found to consist of "rod-like" structures. The role played by the "rod-like" structures is not known yet. I believe they act as conduction paths and thereby promote the instability (breakdown process) in force. Their contribution to the transport mechanism in addition to that due to the grains which are μ-MOVs, as well as that due to $SiTe_2$ and LaB_6 phases present in the inter-granular material, may explain the near ideal V-I characteristic. The surge clamping action is assured in the prototype MOV by the presence of the $\boldsymbol{M}$ -grains, which are μ-MOVs by characterisation. This has been proved.

The prototype MOV had a main phase that was identical to that of the studied commercial MOV. The secondary phases were different in chemical form but were of similar crystal structures. This is because the peak positions (2θ-values) in the XRD pattern of the prototype MOV were almost identical to those of the commercial MOV. It is this similarity in the secondary phases that makes the surge clamping action of the prototype MOV to be similar to that of the studied commercial MOV. It is the difference in the chemical form of the secondary phases as well as the topology and morphology of these phases (the microstructure) that makes the V-I characteristic of the prototype MOV different from that of the commercial, and hence the improvements that go with it. It also explains why the surge voltage clamping action was characterised by lower surge current. The author is of the opinion that if the "electrode effect" is taken care of by using the same electrode mounting and coating material as well as proper ohmic electrodes as per current commercial procedures, and if the prototype MOV block is resin coated/encapsulated, then the prototype MOV may exhibit even better electrical behaviour. With it will also fall away the aspect of lead separation area, which seems to be the most contributing factor to the presence of voltage "humps".

The microstructure-electrical properties have also been linked via the equivalent circuit as explained above.

Since the objective of the investigation was to "improve" the existing electrical behaviour in ZnO-based commercial MOVs with special focus on the V-I characteristic, from the foregoing it is clear that the objective was met.

6.4 The Contribution

This work constitutes a contribution in the field of MOV technology in the following respects:

a) Use of characterised powders, new additives, and new processing method to get an improved V-I characteristic

There are marked improvements in the V-I characteristic of the studied prototype MOV over that of the studied commercial MOV. The improvements were achieved in the leakage, active (breakdown) and the up-turn regions. These improvements and the benefits that accrue were discussed in section 6.1.2. These improvements were made possible due to the use of characterised powders, new additives and a new processing method.

The use of characterised powder in the form of $\boldsymbol{M}$ -powder in the manufacture of ZnO-based MOVs is a new concept. The grains of this powder are μ-varistors. It is also a new concept to use $SiTe_2$, and LaB_6 as additives in the manufacture of ZnO-based MOVs. The same goes for characterised $\boldsymbol{Q}$ -powder, which is a Bi-Co-Mn-Ni based compound. There is nowhere in literature where the use of $SiTe_2$ and LaB_6 as additives in the manufacture of ZnO based MOVs has been reported. This constitutes a significant contribution.

b) An *ideal microstructure*

A prototype MOV with a unique microstructure has been developed. Because near ideal V-I behaviour was obtained without sacrificing the surge clamping action, this forms the basis for the development of an *ideal microstructure*. An ideal microstructure gives an ideal SPD. The concept of an ideal microstructure in current commercial MOVs is unheard of in current literature. ZnO-based MOVs with microstructures that contain rod-like structures have not been reported to the best of my knowledge. This opens a new window of study in this field.

c) Equivalent circuit of a near ideal MOV

An equivalent circuit of a ZnO-based SPD with near ideal V-I characteristic was hypothesised and verified. The V-I behaviour of studied prototype MOV was predicted on the basis of a hypothesised equivalent circuit shown in figure 3.4 and this characteristic was experimentally found to be near ideal. Thus the equivalent circuit becomes that of a near ideal ZnO-based SPD. This equivalent circuit is an improvement over that of the commercial MOV, see figure 2.6. Further, ideal surge clamping action was reported in related work (Hove, 2002), (Hove, 2003). Thus the equivalent circuit shown in figure 3.4 forms a basis for the development of an ideal ZnO-based SPD.

d) Pyrochlore and spinel phases not a pre-requisite for the VP

The insulating pyrochlore phase, $Bi_2Zn(Zn_{4/3}Sb_{2/3})O_6$, and the spinel phase, $Zn(Zn_{4/3}Sb_{2/3})O_4$, are two major accessory phases in the microstructure of current commercial MOVs (Asokan, 1990). They are both located at the grain boundary and triple point regions separating ZnO-ZnO grains. These phases are said to be responsible for the varistor property (Clarke, 1978), (Asokan *et al*, 1990), (Cho *et a*l, 1997) as is found in current commercial MOVs. The developed prototype MOV did not use Sb_2O_3 as an additive, and therefore does not have the above phases. Thus, it is not necessary to have these phases; they are not the only ones that can produce the varistor action. One can do without them! This also forms a significant contribution.

CONCLUSIONS AND RECOMMENDATIONS

Conclusion

A study to improve the V-I characteristic of ZnO-based commercial MOVs has been conducted. Improvements were achieved in the leakage, active (breakdown) and up-turn regions. In the leakage region, leakage currents were reduced by 1.0 %. In the active region, the rate of breakdown was increased and discharge currents were increased by on average 4 times that of a comparable commercial MOV. The instability responsible for the breakdown was found to be **E**-field dependent. The up-turn region was removed. The improvements were achieved because of the characterised powders and new additives used as well as the processing method. The corresponding surge clamping action of the prototype MOV was identical to that that of the studied commercial, but with lower surge current.

The pyrochlore phase, $Bi_2Zn(Zn_{4/3}\ Sb_{2/3})O_6$, and the spinel phase, $Zn(Zn_{4/3}\ Sb_{2/3})O_4$ are not the only phases that are responsible for the VP, which gives rise to the non-linear V-I characteristic in a commercial MOV.

Recommendations for Future Work

- Ideal microstructure: What constitutes an ideal microstructure and an ideal MOV needs to be explored further. The prototype MOV had a V-I characteristic that was near ideal. This means that the microstructure responsible can be regarded as near ideal. Is this microstructure unique or it has some polymorphs?

- Unidentified phases: There were some phases not identified in the prototype MOV. Their composition, and the role they play in the V-I behaviour is not known yet.

- The role played by the "rod-like structures" in the conduction mechanism needs further study.

- The "**Electrode Effect**": The best electrode mounting and coating material needs to be established. This would minimise the "electrode effect", and hence reduce the observed voltage "hump" in the surge voltage response behaviour of the prototype MOV. This would give a perfect ASPD that is ZnO-based. Interface with current procedures and practice in commercial concerns will be necessary.

  It was established that a **minimum surface** area of the MOV blocks need to coated by electrode mounting material. What this "minimum" is, is not yet known. Two methods are current practice: one involves coating the rest of the MOV block and leave about 2 mm strip towards the edge uncoated; the other involves coating a strip of set dimensions that run across the block surface along the diameter, and again a clearance of about 2 mm at the edges is left. What criteria is used, and whether these practices are empirical, the so called "Rule of the Thumb", or they are scientific justifications is not known.

APPENDIX A

CALCULATION OF THE AREA UNDER THE LEAKAGE REGION OF THE V-I CHARACTERSTIC

This section shows how the areas of the leakage regions under the V-I characteristics of the prototype MOV and the commercial MOV, V275K20P, were computed and therefore the improvement

The V- I characteristics are shown in figure A1.1

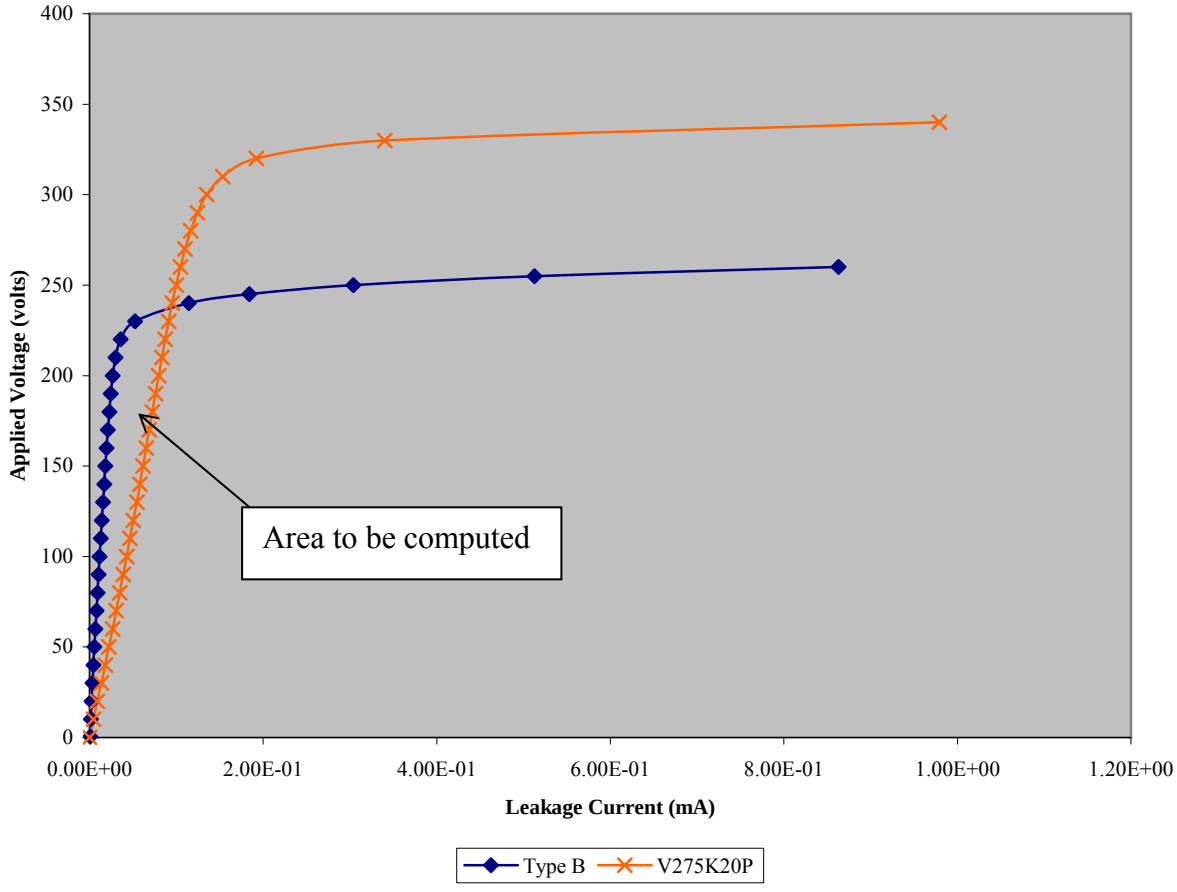

Figure A1.1: V-I characteristic of prototype MOV compared to the commercial MOV-Calculation of the area under the leakage regions

To determine the improvement numerically, we need to calculate the area bounded by the 2 V-I curves in the leakage region. This is done as follows:

a) Compute the area under the V-I curves in the ohmic region. Call it S11. Since the V-I relation in this region is ohmic, the Varistor Equation hold with α = 1, and therefore equation (2.1) becomes

$$I = \kappa V \qquad \text{…….. (A 1)}$$

For the ohmic region, the area under the curve is given by

$$S_{11} = \int_{I1}^{I2} V dI = \tfrac{1}{2}\frac{1}{\kappa'} I^2 + C \Big|_{I11}^{I21} \qquad \text{…….. (A 2)}$$

The area calculated using (A2) should be equal to the area of right-angled Δ

$$S_{11} = \tfrac{1}{2} ab \qquad \text{…….... (A 3)}$$

b) Compute the area under the V-I curves in the pre-breakdown region. Call it S12

$$S_{12} = \int_{I12}^{I22} V dI = \tfrac{2}{3}\frac{1}{\kappa'} I^{3/2} + C \Big|_{I12}^{I22} \qquad \text{…….... (A 4)}$$

At intersection point Vi ≈238 volts, Ii = 0.095 mA: Areas are calculated from Table A1, which gives the co-ordinates of points in the respective characteristics.

Table A1: Computed areas in the leakage regions of the prototype MOV and commercial MOV

MOV	(V2i, I2i) (V, mA)	I21 (A)	(V1i, I1i) (V, mA)	I1i (A)	S1i (W)
Type B					
S1o	200, 0.0267	0.0000267	0,0	0	
S12i	238, 0.095	0.000095	200, 0.0267	0.0000267	
V275K20P					
S1i = S1o	238, 0.095	0.000095	0,0	0	1.1305×10^{-2}

S1o: Area of ohmic region

S12i: area of pre-breakdown up to intersection point. This is computed as in section 4.3.1.1, using equation (4.2).

Type B: Area below curve up to intersection point, S1i, is

$$\text{S1i} = S_{11} = \int_{I1}^{I2} VdI = \tfrac{1}{2}\frac{1}{\kappa'}I^2 + C \Big|_{I11}^{I21} + S_{12} = \int_{I12}^{I22} VdI = \tfrac{2}{3}\frac{1}{\kappa'}I^{3/2} + C \Big|_{I12}^{I22}$$

= S1o + S12i

S1o = 3.56445 x10^{-10} - (350 - 200) (0.0000267 - 0)

= 3.56445 x10^{-10} - 0.004005

= 4.004999643555 x 10^{-3} W

This should be = area of right-angled Δ

= 0.5 x 0.0000356 x 200

= 3.56 x 10^{-3} W

S12i = 5.2532x 10^{-7} - (350-238) (0.000095 - 0.0000267)

= 5.2532x 10^{-7} - 0.0076496

= 7.64907468 x 10^{-3} W

= 7.65 x 10^{-3} W

∴ S1i = 3.56 x 10^{-3} + 7.65 x 10^{-3}

S1i = 1.121 x 10^{-2} W …… (A5)

V275K20P: Area below curve up to intersection point, S1i, is

$$\text{S1i} = S_{11} = \int_{I1}^{I2} VdI = \tfrac{1}{2}\frac{1}{\kappa'}I^2 + C \Big|_{I11}^{I21}$$

= 4.5125 x 10^{-9} - (350-238) (0.000095 - 0)

= 4.5125 x 10^{-9} - 112 x 0.000095

= 4.5125 x 10^{-9} - 0.01064

= 1.06399954875 x 10^{-2} W

This should be = area of right-angled Δ

= 0.5 x 0.000095 x 238

S1i = 1.1305 x 10^{-2} W …… (A6)

The reduction in area in the leakage region, ΔS1, is

$\Delta S1 = (A6) - (A5)$

$= (1.131 - 1.121) \times 10^{-2}$

$= 0.010 \times 10^{-2}$

$\therefore \Delta S1 = 1.000 \times 10^{-4}$ W

$\therefore \% \Delta S1 = (1.000 \times 10^{-4} / 1.121 \times 10^{-2}) \times 100\%$

$= 8.47 \times 10^{-1}\%$

$= 8.9206 \times 10^{-1}\%$

$\therefore \% \Delta S1 \approx 1.0\ \%$

This is the improvement!!

APPENDIX B

THE "ELECTRODE EFFECT"

This section explains the "electrode effect".

From section 6.2, it was mentioned that the type of electrode mounting and coating material, and the type of electrode system used in determining the surge response behaviour of the bulk material of the MOV block to an applied surge voltage is very critical. In addition, it was pointed out that it is imperative to coat the MOV block surfaces by the electrode mounting material to a certain minimum surface area. Failure to meet these requirements results in the MOV either not clamping completely, or if it does, it does so inefficiently. This phenomenon is what the author coined the "*electrode effect*" The author believes that it is related to the nature of potential barriers that exist at the MOV block - electrode interface. By "nature" is meant whether the type of electrical contact that results due to these potential barriers is blocking or injecting (Kao *et al*, 1981).

To affirm the fact that the MOV block surfaces need to be coated to a certain minimum surface area, the following experiment was done. Two as-received V275K20P MOVs were taken. Both had the resin stripped, electrode wires pulled off. Thereafter one was left coated with the as-received coating material. This one was code-named "V275K20P block (coated) (u.p.e.)". The other one had the coating material ground so that it was just like the as-sintered prototype MOV blocks. This block was code-named "V275K20P block (uncoated) (u.p.e.)". These two were in turn impulse tested both using pressure electrodes (u.p.e.). Their surge clamping action was studied at two applied surge voltage levels, 0.8 kV and 1.00 kV. The results are shown in figure B1.1. From this result it is clear that the uncoated block did not show any surge clamping capabilities as expected. V275K20P normally starts to surge clamp at 0.8kV and clamps to 0.66 kV. But because of improper electrodes and absence of coating material, it conducts weakly and does not surge clamp at both voltages either.

The coated one showed surge clamping capabilities due to the coating material, but because of improper electrodes, it clamps poorly. This goes to show that a certain minimum surface area of the MOV block surfaces needs to be coated, and coated by the correct material to ensure proper surge clamping action. This agrees with the aspects covered in section 2.5, typically, “Twice the area of the MOV block produces twice the current handling capability because then twice the numbers of current paths are arranged in parallel”.

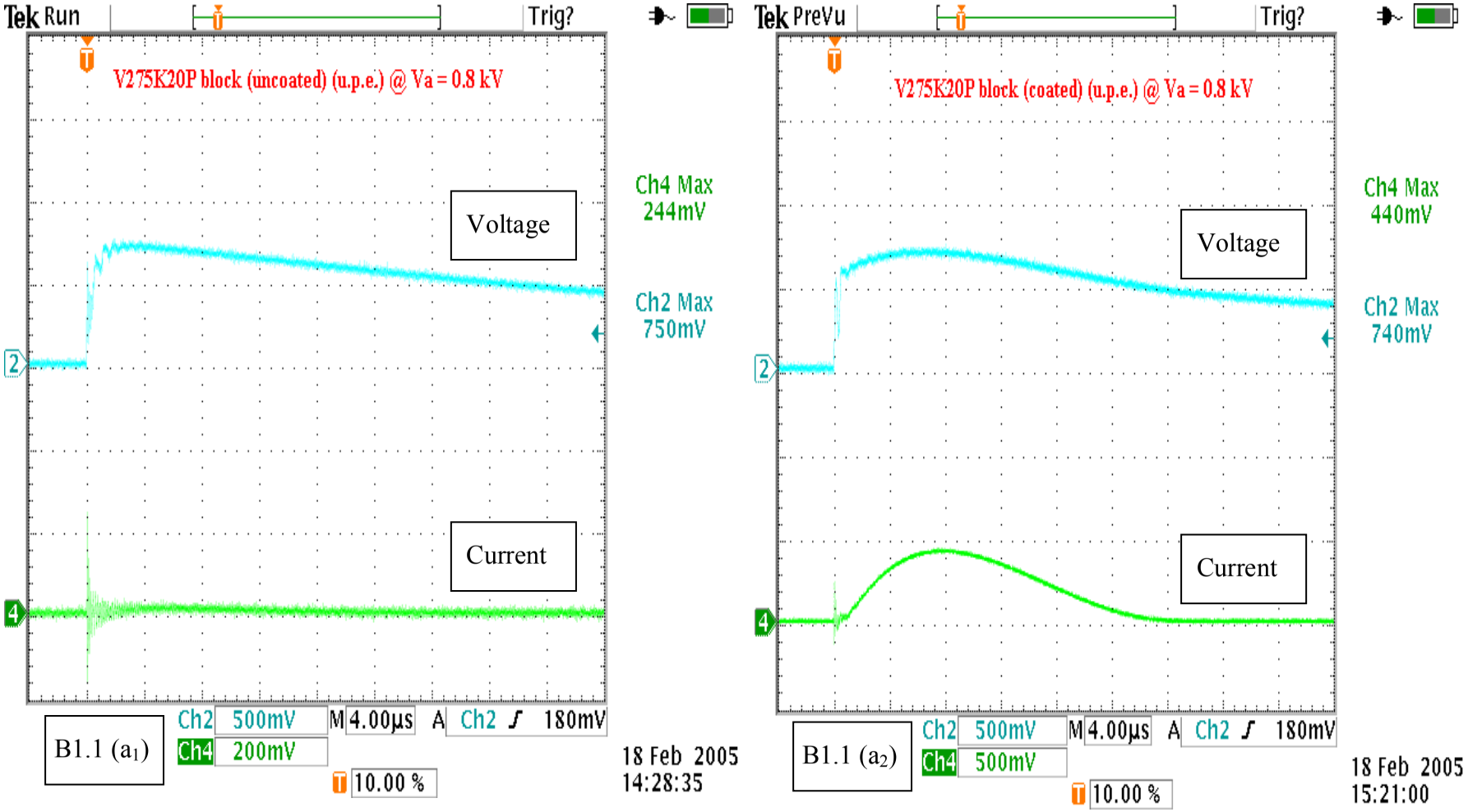

Figure B1.1 (a): Surge clamping action of V275K20P block (uncoated) (u.p.e.) compared to V275K20P (coated) (u.p.e.) @ V_a =0.8 kV

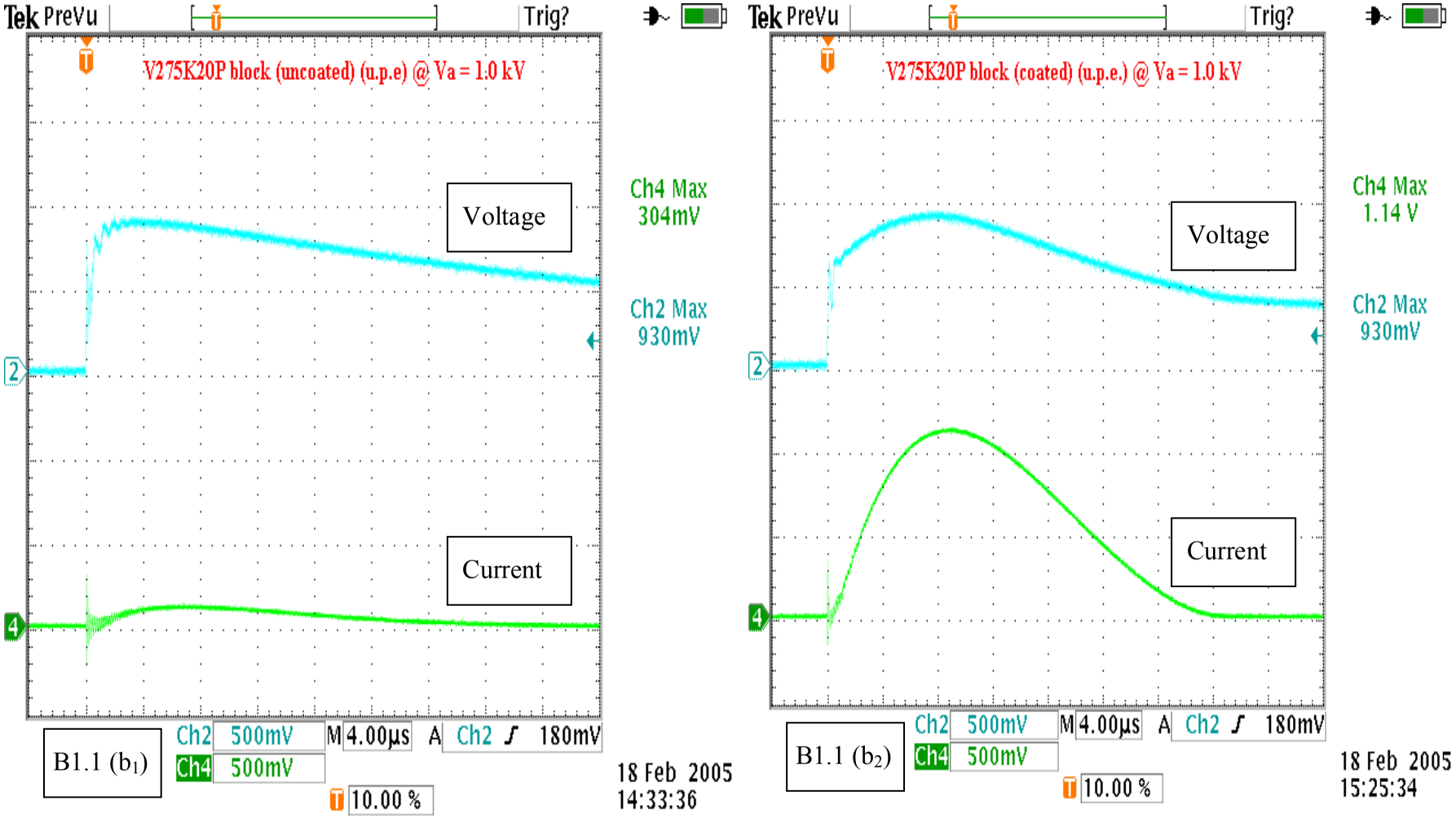

Figure B1.1 (b): Surge clamping action of V275K20P block (uncoated) (u.p.e.) compared to V275K20P (coated)(u.p.e.) @ V_a =1.0

REFERENCE LIST

[1] Adler, D., Kaplan, T. (1971) Thermal Effects in Amorphous-Semiconductor Switching, Applied Physics Letters, vol. 19, no. 10, pp. 418-419

[2] Asokan, T. and Freer, R. (1990) Characterization of Spinel Particles in ZnO Varistors, Journal of Material Science, vol. 25, pp. 2447 - 2453

[3] Beutel, A.A. (2000): M. Sc. Thesis The Application of Silicon Avalanche Devices for the Protection of Low Voltage Equipment from Dangerous Transients, University of Witwatersrand pp. 129 - 133

[4] Blatter, G. and Greuter, F. (1986) Carrier Transport through Grain Boundaries in Semiconductors, Physical Review B, Vol. 33, No. 66, pp. 3953

[5] Cho, S.G., Lee, H. and Kim, H.S (1997) Effect of Chromium on the Phase Evolution and Microstructure of ZnO-doped with Bismuth and Antimony, Journal of Material Science, vol. 32, pp. 4283 – 4287

[6] Clarke, D.R. (1978) The Microstructural Location of the Intergranular Metal – Oxide Phase in a Zinc Oxide Varistor, Journal of Applied Physics, vol. 49, no. 4, pp. 2407 - 2411

[7] Cordaro, J.F. and Shim, M. (1986) Bulk electron traps in zinc oxide varistors, Journal of Applied Physics, vol. 60, no. 12, pp. 4186 – 4190

[8] Deis, D.W., Dancy, E.A., and Patterson, A. (1970) On the switching characteristics and the bulk properties of chalcogenide glasses, Journal of Non – Crystalline Solids, vol. 2, pp. 141 – 147

[9] Eda, K. (1979) Transient Conduction Phenomena in non-Ohmic Zinc Oxide Ceramics, Journal of Applied Physics, vol. 50, no. 6, pp. 4436 - 4442

[10] EPCOS Manual (2001): SIOV Metal Oxide Varistors, p. 20

[11] Gibson, A.F., Burgess, R.E., and Kroger, F.A. (1960) Progress in Semiconductors, vol.4, New York: Wiley, p.104

[12] Greuter F.,Perkins R., Rossinelli M., Schmuckle F.: The Metal-Oxide Resistor – at the Heart of Modern Surge Arresters, ABB Review, Vol. 1 1989, pp.35 - 42

[13] Harris Manual (1995): Transient Voltage Suppression Devices, pp.3 – 6

[14] Harnden, J.D. Jnr,. Martzloff, F.D., Morris, W.G. and Golden, F.G. (1972) A new way to Suppress Transients, Electronics, no. 2, pp. 91 – 95.

[15] Hove, M, Jandrell, I.R., Koursaris, A. (2003) South African Universities Power Engineering Conference (SAUPEC) The Electrical Behaviour of Hot Pressed Elemental Metal Oxide Varistors (MOVs) pp 1 - 4

[16] Hove, M, Jandrell, I.R., Koursaris, A. (2004) South African Universities Power Engineering Conference (SAUPEC), Towards Absolute Voltage Clamping of Prototype Metal Oxide Varistors (MOVs) pp 1 - 4

[17] Hove, M. (1999) M.Phil Thesis, Improving Non-Linear Surge Arresters Using Re-Inforced Ceramics (Composites), pp. 19-20

[18] Kao, K.C., Hwang, W. (1981) Electrical Transport in Solids 1 st ed. Pergamon Press, p 303

[19] Kingery, W.D., Sande V.J.B., Mitamura T (1979) A Scanning Transmission Electron Microscopy Investigation of the Grain Boundary Segregation in ZnO-Bi_2O_3 Varistors, Journal of American Ceramic Society, vol. 62, no. 3 - 4, pp. 221

[20] Levinson, L.M., Philip, H.R. (1975) The Physics of Metal Oxide Varistors, Journal of Applied Physics vol. 46, no.3, pp. 1332 – 1341.

[21] Lide, D.R. (2001 – 2002), CRC Handbook of Chemistry and Physics, 82nd ed., p. 12.105

[22] Lou L.F. (1979) Current-Voltage Characteristics of ZnO-Bi_2O_3 heterojunction, Journal of Applied Physics, vol. 50, no. 1, pp. 555 - 558

[23] Mahan G.D., Bartkowiak M., Modine F.A., and Alim, M.A. (1996) Influence of Ohmic Grain Boundaries in ZnO Varistors, Journal of Applied Physics, vol. 79, no. 1 pp. 273 - 281

[24] Mahan G.D., Lionel M.L., Phillip H.R. (1979) Theory of Conduction in ZnO Varistors, Journal of Applied Physics, vol. 50 no. 4, pp. 2799 - 2812

[25] Matsuoka, M. (1971) Non-Ohmic Properties of Zinc Oxide Ceramics, Japanese Journal of Applied Physics, vol. 10, no. 6, pp. 736 – 746

[26] Matsuoka, M., Masuyama, T., and Iida, Y. (1970) Non-Linear Electrical Properties of Zinc Oxide Ceramics, Supplement to the Journal of the Society of Applied Physics, vol. 39, pp. 94 - 101

[27] Morris W.G.(1973) Electrical Properties of ZnO-Bi_2O_3 Ceramics, JACS vol.56, no.7, July 1973, pp. 360 - 364

[28] Mukae, K. Tsuda, and Nagasawa, I. (1971) .Non-Ohmic Properties of ZnO – Rare Earth Metal - Co_3O_4 Ceramics, Japanese Journal of Applied Physics, vol. 10, no. 6, pp. 736 – 746

[29] Omar, M.A. (1975) Elementary Solid State Physics, Principles and Applications, Addison – Wesley, pp. 586 – 579

[30] Ovshinsky, S.R. (1968) Reversible Electrical Switching Phenomena in Disordered Structures, Physical Review Letters, vol. 21, no. 20, pp. 1450 – 1453

[31] Oyez, IBC (1985) Engineering Ceramics; Proceedings of the First European Symposium and Advances on Engineering Ceramics, Applications, Availability, and in High Performance Technology, Oyez Scientific and Technical Services Ltd., London, pp. 45 – 60

[32] Pearson, A.D., Northover, W.R., Dewald, J.F., and Peck, Jr., W.F. (1962) in :Advances in Glass Technology, New York, Plenum Press, pp. 357

[33] Roy, D.K.(1976): Tunnelling and Negative Resistance Phenomena in Semiconductors, Pergamon Press, pp. 122-125

[34] SABS: NRS 039: 1995, p. 11

[35] Santhanam, A.T., Gupta, T.K., Carlson, W.G. (1979) Microstructural Evaluation of Multicomponent ZnO Ceramics, Journal of Applied Physics vol. 50, no.2, p. 853

[36] Seeger, K. (1973) Semiconductor Physics, New York, Springer-Verlag, Wien, p. 463

[37] Schöll, E. (1987): Nonequilibrium Phase Transitions in Semiconductors, Springer-Verlag, pp.4-5

[38] Schwing, U, and Hoffmann, B. (1985) Model Experiments Describing the Microcontact of ZnO Varistors, Journal of Applied Physics vol. 57, no.12, pp. 5372 – 5379

[39] Storms, E.K. and Mueller, B.A. (1979) A study of surface stoichiometry and thermionic emission using LaB_6, Journal of Applied Physics vol. 50, no.5, pp. 3691 – 3698

[40] Van Der Merwe, V.C., (1989) Lightning Arresters, Spark Gaps and Over - voltage Protection in "Seminar on the Lightning Protection of Distribution Lines", S.A.IEE and CSIR, pp. 35 - 39

[41] Walther, G.C., Hench, L.L. (1971) "Dielectric Breakdown of Solids" in Physics of Electronic Ceramics, edited by L.L. Hench and D.B. Dove, Marcel Dekker, pp 539 - 564

[42] Wong, J.(1980): Sintering and varistor characteristics of ZnO-Bi_2O_3 ceramics, Journal of Applied Physics, vol. 51 no. 8, pp. 4453 - 4459

[43] Wong, J. (1975) Microstructure and Phase Transformation in a Highly Non-Ohmic Metal Oxide Varistor Ceramic, Journal of Applied Physics, vol. 46, no. 4, pp. 1653 - 1659

[44] Wong, J. and Morris, W.G. (1974) Microstructure and Phases in Non-ohmic ZnO - Bi_2O_3 Ceramics, American Ceramic Bulletin, vol.53, no.11, pp. 816-820